A TRIDENT SCHOLAR PROJECT REPORT

NO. 452

Mathematical Modeling: Immune System Dynamics in the Presence of Cancer and Immunodeficiency in vivo

by

Midshipman 1/C Thomas J. Wester, USN

UNITED STATES NAVAL ACADEMY
ANNAPOLIS, MARYLAND

USNA-1531-2

U.S.N.A. --- Trident Scholar project report; no. 452 (2016)

Mathematical Modeling: Immune System Dynamics in the Presence of Cancer and Immunodeficiency in vivo

by

Midshipman 1/C Thomas J. Wester
United States Naval Academy
Annapolis, Maryland

Certification of Advisers Approval

Associate Professor Sonia M. F. Garcia
Mathematics Department

Acceptance for the Trident Scholar Committee

Professor Maria J. Schroeder
Associate Director of Midshipman Research

USNA-1531-2

REPORT DOCUMENTATION PAGE

Form Approved
OMB No. 0704-0188

1. REPORT DATE *(DD-MM-YYYY)*	**2. REPORT TYPE**	**3. DATES COVERED** *(From - To)*
05-11-2016		

4. TITLE AND SUBTITLE

Mathematical Modeling: Immune System Dynamics in the Presence of Cancer and Immunodeficiency in vivo

5a. CONTRACT NUMBER

5b. GRANT NUMBER

5c. PROGRAM ELEMENT NUMBER

6. AUTHOR(S)
Wester, Thomas J.

5d. PROJECT NUMBER

5e. TASK NUMBER

5f. WORK UNIT NUMBER

7. PERFORMING ORGANIZATION NAME(S) AND ADDRESS(ES)

8. PERFORMING ORGANIZATION REPORT NUMBER

9. SPONSORING / MONITORING AGENCY NAME(S) AND ADDRESS(ES)
U.S. Naval Academy
Annapolis, MD 21402

10. SPONSOR/MONITOR'S ACRONYM(S)

11. SPONSOR/MONITOR'S REPORT NUMBER(S)
Trident Scholar Report no. 452 (2016)

12. DISTRIBUTION / AVAILABILITY STATEMENT

This document has been approved for public release; its distribution is UNLIMITED.

13. SUPPLEMENTARY NOTES

14. ABSTRACT

The Human Immunodeficiency Virus (HIV) targets CD4 T-cells which are crucial in regulating the immune system's response to foreign pathogens and cancerous cell development. Furthermore, several studies link HIV infection with the proliferation of specific forms of cancer such as Kaposi Sarcoma and Non-Hodgkin's Lymphoma; HIV infected individuals can be several thousand times more likely to be diagnosed with cancer. In this project, we seek to apply systems of nonlinear ordinary differential equations to analyze how the dynamics of primary infection affect the proliferation of cancer. We first begin by characterizing the dynamics of HIV infection. During HIV-1 primary infection, we know that the virus concentration increases, reaches a peak, and then decreases until it reaches a set point. We studied longitudinal data from 18 subjects identified as HIV positive during plasma donation screening and applied several models to analyze the dynamics of the systems and determine the most effective model for characterizing the infection. We prove existence, uniqueness, positivity, and boundedness, investigate the qualitative behavior of the models, and find the conditions that guarantee the asymptotic stability of the equilibria. In addition, we conduct numerical simulations and sensitivity analyses to illustrate and extend the theoretical results. Furthermore, we develop and study a new Tumor-Immunodeficiency model which integrates the effects of an immunodeficiency on cancerous tumor cell development.

15. SUBJECT TERMS
Mathematical Modeling, Human Immunodeficiency Virus, Cancer, Stability, Numerical Simulations, Time Delay, Optimal Control

16. SECURITY CLASSIFICATION OF:			**17. LIMITATION OF ABSTRACT**	**18. NUMBER OF PAGES**	**19a. NAME OF RESPONSIBLE PERSON**
a. REPORT	**b. ABSTRACT**	**c. THIS PAGE**		134	**19b. TELEPHONE NUMBER** *(include area code)*

Abstract

The Human Immunodeficiency Virus (HIV) targets CD4 T-cells which are crucial in regulating the immune system's response to foreign pathogens and cancerous cell development. Furthermore, several studies link HIV infection with the proliferation of specific forms of cancer such as Kaposi Sarcoma and Non-Hodgkin's Lymphoma; HIV infected individuals can be several thousand times more likely to be diagnosed with cancer. While our understanding of both HIV and cancer has increased in the past decade, much remains unknown about the dynamic interaction between cancer development and immunodeficiency. In this project, we seek to apply systems of nonlinear ordinary differential equations to analyze how the dynamics of primary infection affect the proliferation of cancer. We first begin by characterizing the dynamics of HIV infection. During HIV-1 primary infection, we know that the virus concentration increases, reaches a peak, and then decreases until it reaches a set point. We studied longitudinal data from 18 subjects identified as HIV positive during plasma donation screening and applied several models to analyze the dynamics of the systems and determine the most effective model for characterizing the infection. We prove existence, uniqueness, positivity, and boundedness, investigate the qualitative behavior of the models, and find the conditions that guarantee the asymptotic stability of the equilibria. In addition, we conduct numerical simulations and sensitivity analyses to illustrate and extend the theoretical results. Furthermore, we develop and study a new Tumor-Immunodeficiency model which integrates the effects of an immunodeficiency on cancerous tumor cell development. The obtained results are consistent with the known biological behavior and yield a better understanding of the interaction between cancer and immunodeficiency.

Keywords: Mathematical Modeling, Human Immunodeficiency Virus, Cancer, Stability, Numerical Simulations, Time Delay, Optimal Control

Acknowledgments

This research was sponsored by the United States Naval Academy's Trident Scholar Program and the Department of Mathematics. Tom would like to personally thank his adviser at the Naval Academy, Dr. Sonia Garcia, who has helped Tom learn and grow tremendously throughout this process. He is forever grateful for all of the hard work and time she spent working with him, not only on the Trident work, but over the course of his time at the Academy. The authors would also like to thank the members of the Theoretical Biology and Biophysics Division at Los Alamos National Laboratory, specifically Dr. Ruy Ribeiro and Dr. Alan Perelson, for linking them with the data for this study and for hosting Tom as an intern this past summer. Furthermore, Tom would like to thank Ruy for all of his effort and energy in helping him during the initial stages of the project. In addition, Tom would like to thank Dr. Aaron Lim for hosting him at the University of Oxford and providing great mentorship and sound reason. Perhaps most importantly, Tom would like to thank his family and friends especially his parents, Sue and Joe; sister, Laura; and fiancé, Meredith for all of their continued support and encouragement.

For the patient I interacted with at Aurora Medical Center and his family. You are always in my thoughts and prayers.

Contents

List of Figures

List of Tables

1 Introduction

A mathematical model is a platform for understanding the behavior of any dynamical system. The goal of this project is to use mathematical modeling as a tool to examine and analyze immune system dynamics in the presence of cancer and immunodeficiency. In this project, we will begin by describing the biological background necessary to understand the basics of the immune system, the Human Immunodeficiency Virus (HIV), and cancer. In addition, we will provide the biological basis for understanding the models we develop and interpreting our results.

Next, we will discuss the four mathematical models we used to characterize the infection and analyze the dynamics of the system. In the development of the models, we will utilize current understanding of biological dynamics, apply a few biologically reasonable assumptions, and then develop systems of nonlinear ordinary differential equations to describe the interactions between populations within the immune system. We will then prove existence, uniqueness, positivity, and boundedness for each of the models and carry out several forms of analyses in order to gain a greater understanding of the interaction of HIV and the immune system as well as the qualitative behavior of the system including the conditions which guarantee asymptotic stability. We will then apply longitudinal patient data from 18 subjects identified as HIV positive during plasma virus donation screening in order to estimate the parameters for our models and determine which of the models most accurately characterizes the infection. Furthermore, we will use this data to conduct numerical simulations and sensitivity analyses in order to extend the theoretical results.

We will then use our results, in conjunction with a small study of several tumor-immune dynamic models, in order to develop and study a new Tumor-Immunodeficiency Model which will integrate the effects of an immunodeficiency on cancerous tumor cell development. Our results will yield new insights into the behavior of the cancer during the early stages of HIV infection. Next, we will discuss treatment protocol options for HIV infected individuals, and develop and examine the dynamics of a model which integrates treatment protocols for HIV infection. Ultimately, we will use the proposed treatment model to understand and predict how treatment can possibly modify the dynamics of the system as well as derive the level of treatment necessary in order to clear HIV infection from the immune system. The obtained results from our study during this project will be consistent with the known biological behavior of the immune system and will reveal a better understanding of the complex interaction and dynamics between cancer and immunodeficiency.

1.1 A Look Forward

Upon conclusion of our study, we will be able to characterize the relationship between cancer and HIV within the immune system. In doing so, we will illustrate that the immune system plays a key role in describing the dynamics of infection and limiting the spread of the virus. In addition, we will show that CD4 T-cells (and thus the immune system) have the ability to control cancerous cell development, however, when infected by HIV, they lose this ability and the cancer proliferates uncontrollably. Furthermore, we will explore a model which incorporates treatment therapies, and use our analysis to determine the treatment levels which are required to eliminate HIV infection

from the system. Lastly, we will discuss some of the other characteristics that are important to note during treatment and describe some areas for future work, both extending from our models as well as work that will be essential for ultimately curing HIV.

1.2 Biological Background

Prior to the discussion of the mathematical model, it is critical to develop a fundamental understanding of immune system dynamics. The role of the immune system is to recognize self from non-self and fight off foreign pathogens. The immune system is composed of two types of immunity, innate and adaptive (acquired) immunity. The innate immune system requires no external stimuli to initiate a response and is our body's first line of defense against a foreign pathogen [22]. In other words, the innate immune system is always present and functioning. One component of the innate immune system is the anatomic barrier that includes our skin and mucus [22]. Our skin has an increased acidity in which most organisms cannot survive, and our mucus traps and dispels unwanted organisms. Both the skin and mucus are constantly functioning in these manners and require no stimuli from cells within the body. On the other hand, the adaptive immune system is highly specific. In contrast to the innate immune system, the adaptive immune system responds to the first exposure to a pathogen to fight off potential infections. Furthermore, the adaptive immune system possesses the ability to create a memory of previous attacks leading to a more robust response upon repeat exposure to a pathogen [14]. The focus of the models we develop in this project will be the adaptive immune system and its interactions with both immunodeficiency and cancer. Thus, we will begin by describing how the immune system responds to these threats.

1.2.1 HIV

The Human Immunodeficiency Virus (HIV) is special type of virus known as a retrovirus. Retroviruses are RNA viruses, meaning they contain two copies of a single-stranded, positive sense ribonucleic acid (RNA) genome. Additionally, a single HIV virion (virus particle) encodes the enzymes integrase and reverse transcriptase as well as nucleocapsid and gp120 proteins [4]. The process of viral infection begins when the virus and its contents are transported to the host cell where gp120, a protein located on the surface of the virus, recognizes the $CD4^+$ receptor located on the membrane of the target (host) cell [4]. In the case of HIV, this target cell is a CD4 T-cell, so called due to the receptor located on the surface of the cell. In addition to binding to a $CD4^+$ receptor, the virus must also attach to a co-receptor on the host cell's surface; this co-receptor is either the chemokine co-receptor CCR5 or CXCR4 [4]. Once attached, the interaction between the gp120 protein and the co-receptor results in the virus piercing into the host cell and the fusion of the virus and host cell membranes. In addition, when fused the release of the viral particles in the form of the reverse transcription complex (pre integration complex), comprised of the viral enzymes and viral RNA continues the infectious cycle [4].

Once the reverse transcription complex is released, replication begins. Retroviruses are special in the sense that during replication they copy their genomes, contained in a reverse transcription complex, into single-stranded deoxyribose nucleic acid (DNA) through a process known as reverse

transcription. Subsequently, the single-stranded DNA is further transcribed into double-stranded DNA. Both steps of reverse transcription are performed by the enzyme reverse transcriptase, which is co-packaged in the reverse transcription complex [21]. The enzyme integrase carries the double stranded DNA through a nuclear pore into the nucleus of the host cell. The double-stranded DNA is then either randomly integrated into the host-cell genome by means of DNA splicing performed by integrase, or forms stable DNA circles [4]. If integrated into the host cell, the integrated form of HIV is known as the provirus which then undergoes replication as a part of the host genome. After replication, RNA transcripts are produced which may either be spliced in preparation for translation of viral proteins which will facilitate viral replication, or be exported from the nucleus in an unspliced form for packaging into newly produced viral particles [21]. The enzyme protease cuts the unspliced viral protein chains into individual proteins. When these proteins are paired with the genetic material of the virus, a new virus particle is produced. The newly produced viral particles will then seek new hosts for infection.

Upon the initiation of infection, kinetics are characterized by the number of virions in plasma which increases rapidly, reaches a peak, and then decays to a steady state (also commonly referred to as a viral steady state or viral set point level). Correspondingly, there is a decline in the number of CD4 T-cells from the initial equilibrium value to a minimum which then increases to a new steady state which is less than the pre-infection equilibrium. The subsequent chronic long term stage is asymptomatic, generally for a period of several years, until the onset of Acquired Immunodeficiency Syndrome (AIDS) [4]. Furthermore, plasma viral load and immune activation at the viral steady state have been shown to be predictors of disease evolution and progression to AIDS. Thus, an improved knowledge of the initial kinetics during HIV primary infection will be beneficial to develop a greater understanding of the complex virus-host interaction and its effects on the establishment of chronic infection.

This initial time period during which these dynamics occur lasts approximately 100 days and is known as primary infection. Phillips suggested that the behavior of the virus during primary infection could be the result of target cell limitation in which the virus runs out of new CD4 T-cells to infect [14]. Biologically this is feasible since we know that HIV is able to lyse HIV-infected CD4 T-cells in vitro. He demonstrated that simulations of a simple model produced a peak in the concentration of virus which mimicked the behavior seen in patients. Stafford et al. also explored the possibility of a target-cell-limited model in modeling the course of primary infection [34]. Yet, experiment studies have correlated the control of HIV during primary infection with the development of a productive anti-viral immune response; for example in Wilson et al. a CD8 cytotoxic T-cell response was correlated with control of viral replication at early stages in humans [39]. Here we seek to apply several models, both with and without accounting for an immune response, in order to characterize the events in primary HIV infection in order to better understand the biological underpinnings of the infection.

1.2.2 Immune System

To understand how the body interacts with HIV, we must first understand how the immune

system responds to pathogens. A primary component of the immune system is the T-cell which is a lymphocyte that matures in the thymus. T-cell activation is the central event in the initiation of the adaptive immune response [25]. These cells exist in two distinct populations within the immune system, Helper T-cells and Cytotoxic T-lymphocytes (also known as Cytolytic T-cells, Cytotoxic T-cells, or Killer T-cells). During this project we will refer to these types of cells as Cytotoxic T-lymphocytes (CTLs) or in some cases as a significant subset of Immune Effector cells. The two types of T-cells are distinguished by a specific protein located on their surface; the Helper T-cell is distinguished by the $CD4^+$ protein located on the surface whereas the Cytotoxic T-lymphocyte exhibits a $CD8^+$ protein [22].

The interaction between a naïve T-cell and an antigen presenting cell (APC), such as a dendritic cell or macrophage, initiates the immune response. Upon recognition of a pathogen, APCs process and present peptides from the pathogen on their surface using either Major Histocompatibility Complex (MHC) Class I or Class II molecules. Both Helper T-cells and CTLs contain specialized antibody-like receptors that recognize these molecules; the $CD4^+$ protein of the Helper T-cell recognizes the MHC class II peptide that is expressed by APCs while the $CD8^+$ protein of the CTL cell recognizes the MHC Class I molecule. Upon recognition, these cells become activated [25].

Activated Helper T-cells serve as the alarm system of the immune system [29]. Their activation causes them to secrete cytokines and proliferate (by division). Cytokines are a chemical mediator that serve as the communication network for the immune system [14]. In addition, cytokines secreted by Helper T-cells play a large role in the activation and proliferation of CTLs. When a T-cell with the $CD8^+$ protein is exposed to the cytokines released by the activated Helper T-cell the CTL itself becomes activated [22]. When activated, T-cells exhibiting the $CD8^+$ protein are referred to as Cytotoxic T-Lymphocytes. Once activated, CTLs maintain the ability to kill specific cells. This occurs when the CTL binds to the target cell and releases a potent chemical called perforin. Perforin perforates the cell membrane of the infected cells and causes the cells to lyse (burst) and die [22]. The CTLs kill the infected cell that the Helper T-cells discriminate as harmful.

However, as stated previously, HIV strains will recognize and target the $CD4^+$ protein located on the surface of the Helper T-cells. The HIV virion bonds with the $CD4^+$ protein of the Helper T-cell and releases the reverse transcription complex, thereby infecting the cell. Once infected, the Helper T-cell can no longer function properly and rather is used as a platform for producing additional copies of the virus [4].

1.2.3 Cancer

Cells that are produced in an uncontrolled manner will produce a tumor or neoplasm. There are two basic types of tumors, benign and malignant. A tumor that is not capable of indefinite growth and does not invade the surrounding healthy tissue is known as a benign tumor. On the other hand, a tumor that continues to grow and becomes progressively more invasive is called a malignant tumor.

Cancer cells can be thought of as altered self cells that either possess or acquire mutations in

proto-oncogenes or tumor suppressor genes [25]. Proto-oncogenes encode proteins that are involved in normal cellular growth. Specific cells have the ability to convert proto-oncogenes by mutation or genetic rearrangements, into oncogenes which are genes that have the potential to cause cancer. This conversion is a key step in the initiation of most human cancers [25]. For instance, mutations in the proto-oncogene Ras are known to be the cause of many forms of cancer. However, cells which acquire mutations in tumor suppressor genes can also result in the development of cancer. Tumor suppressor genes are normal cellular genes which are crucial for dampening cell growth and proliferation. Mutations in tumor suppressor genes, such as the TP53 gene, result in an increase in cell division which, if uncontrolled, will lead to the transformation of a normal cell into a cancerous cell [29].

There are three proposed mechanisms by which the immune system is thought to control cancer: destroying viruses that transform cells, eliminating pathogens and reducing pro-tumor inflammation, and actively identifying and eliminating cancerous cells [25]. The latter mechanism is known as immunosurveillance. Immunosurveillance suggests that the immune system continuously monitors for and destroys neoplastic cells. Cytokines secreted by cancerous cells or immune cells that infiltrate tumors can encourage the development of an immunosuppressive response. For instance, the immunosuppressive cytokine IL-10 plays a role in cancer immunity [25]. This cytokine, secreted by Helper T-cells, can encourage innate anti-cancer immune responses including the proliferation of CTLs.

Cancerous cells can be eliminated by two primary cell-types, CTLs and Natural Killer Cells. CTLs are cytotoxic to cancerous cells provided previous sensitization (activation) has occurred. In addition, Natural Killer Cells target cancerous cells via a process called antibody-dependent cell-mediated cytotoxicity [22]. It is important to note that Natural Killer Cells do not need activation in order to attack a foreign cell and maintain the ability to attack many types of cells. Thus, both CTLs and Natural Killer Cells contribute to the decrease in the population of cancerous cells.

1.3 Motivation

The protection of individuals from biological threats will be a major challenge for the coming century. Over 35 million people are currently living with HIV and in 2012 alone, HIV claimed an estimated 1.6 million lives making it one of the world's leading infectious killers [29]. Yet, there is still no vaccine to prevent or cure HIV. Furthermore, development of novel drugs and vaccines takes well over a decade, has a failure rate of 95%, and costs more than $1 billion per success [20]. Current approaches to developing new drugs and treatment protocols rely primarily on biological techniques. Traditionally, biology is an experimental science which relies on qualitative observations; however, in the past decade the need for quantitative analysis has become much more evident. Furthermore, recent advances in our understanding of viral and immune system dynamics as well as medical breakthroughs for combating infections and cancer have created an environment yearning for advanced mathematical analysis [33].

The application of mathematical analysis allows for the implementation of treatment protocols and generates the ability to predict and possibly modify system behavior. As recently as twenty

years ago, this understanding could only be gained through experimentation and repetition [33]. As a result of the development of high-speed computing and a new field of study combining biological understanding and mathematical concepts, biological dynamics can now be analyzed using mathematical models. Analysis of these models expands understanding of biological processes, and when paired with research in treatment protocols, can lead to the development of innovative approaches to both address and solve perplexing biological problems.

Recent developments in biological understanding, as it relates to HIV and cancer, have created a platform for mathematical analysis. A report in 2011 denoted that individuals infected with HIV have a substantially higher risk of certain types of cancers compared with uninfected people of the same age [22]. For example, individuals infected with HIV are believed to be several thousand times more likely than uninfected individuals to be diagnosed with Kaposi's Sarcoma, and at least 70 times more likely to be diagnosed with Non-Hodgkin's Lymphoma [22]. This is thought to be a function of the weakened immune system due to infection by the HIV virus. Since the virus infects the Helper T-cells critical to regulating an immune response, the immune system's ability to fight infections and prevent abnormal growth which may lead to cancer is significantly lowered. Experimental evidence has shown that an uninfected immune system can, and often does, prevent tumors from developing and thus plays a strong protective role against cancer [22]. However, when an immune system is exposed to infection by HIV, it is significantly less effective at suppressing cancerous cell development. This project will use mathematical modeling as a tool to examine and analyze the interaction between HIV and cancer within the immune system to develop a greater understanding of this dynamic.

In current bio-mathematical literature there are many papers focused on either tumor growth modeling or HIV virus dynamics [31]. Many mathematical models have been developed which analyze the immune system – cancer dynamic as well as the immune system – HIV dynamic; however, few papers link the two areas of research. Due to the relationship between cancer and HIV within the immune system during infection, it is important to combine the ongoing research to accurately describe the interaction. A more advanced understanding of the dynamic within the immune system during infection can, when coupled with research in combination drug therapies, lead to the development of optimum treatment protocols or parameter goals to control both the spread of HIV and the possible onset of cancer.

Numerous biological operators are included in the adaptive immune system and can be used to model the interaction between HIV and cancer. In our project, we will use differential equations to represent changes in cellular populations. While many of these cells are present in large populations within the body, the models we will consider deal with a subset of the entire cellular population.

We will begin our project by analyzing several models to examine and quantify the behavior of HIV. We know that during infection, the virus concentration increases, reaches a peak, and then decreases to a set point. There are two schools of thought as to why the virus reaches a peak level; first is that the virus runs out of target cells, and second is that the immune responses begins to impact the level of the virus. We will explore both of these hypotheses. In doing so, we will examine four separate models which do not incorporate treatment in order to determine how to best characterize the dynamics of the virus. We will then examine some basic models for cancer-

ous cell development and determine which one is best for characterizing the dynamics of HIV and cancer. Then we will develop and analyze more advanced models for HIV which incorporate the means of combating infection via treatment protocols and time delays present in the natural viral infectious cycle. Lastly, we will develop and conduct some preliminary analysis on a novel model which examines the behavior of cancer and immunodeficiency.

We examine the longitudinal viral load data from 18 plasma virus donors who were identified as HIV positive during the course of their plasma virus donations. In modeling the data, we seek to capture the dynamics of the viral load behavior during infection and estimate parameters for the various models and determine the best fit. In addition, we extend our analysis to include a characterization and estimation of the expansion as well as decay of the virus. Furthermore, we also intend to define the basic reproductive ratio, R_0 for each of the patients, which is a measure of whether or not a virus can establish infection. Essentially, R_0 represents the number of infected cells produced by a productively HIV-infected cell; thus, If the value of R_0 is greater than 1, we will see the establishment of infection, whereas if R_0 is less than one, the infection will not persist. Our analysis will be able to work towards a better understanding of the complex dynamics of HIV primary infection as well as the interaction between HIV and Cancer.

2 Data

The set of longitudinal data gathered from 18 plasma donor samples obtained from 18-23 year-old HIV-negative women at very high risk of HIV-1 clade C infection in Durban, South Africa [23]. Patients attended twice weekly HIV prevention sessions which included counseling. At each session, samples were taken to monitor for plasma HIV RNA. The samples consisted of blood and female reproductive tract samples. Upon positive detection of viremia by NucliSens EasyQ v2.0 assay, patients were contacted and additional samples were collected and health counseling was provided. Thus, for each donor, both pre as well as a serial of post infection samples were obtained. All of the patients provided written informed consent for and the Biomedical Research Ethics Committee (BREC) of the University of Kwa-Zulu-Natal and the institutional review board of Massachusetts General Hospital approved the study [23].

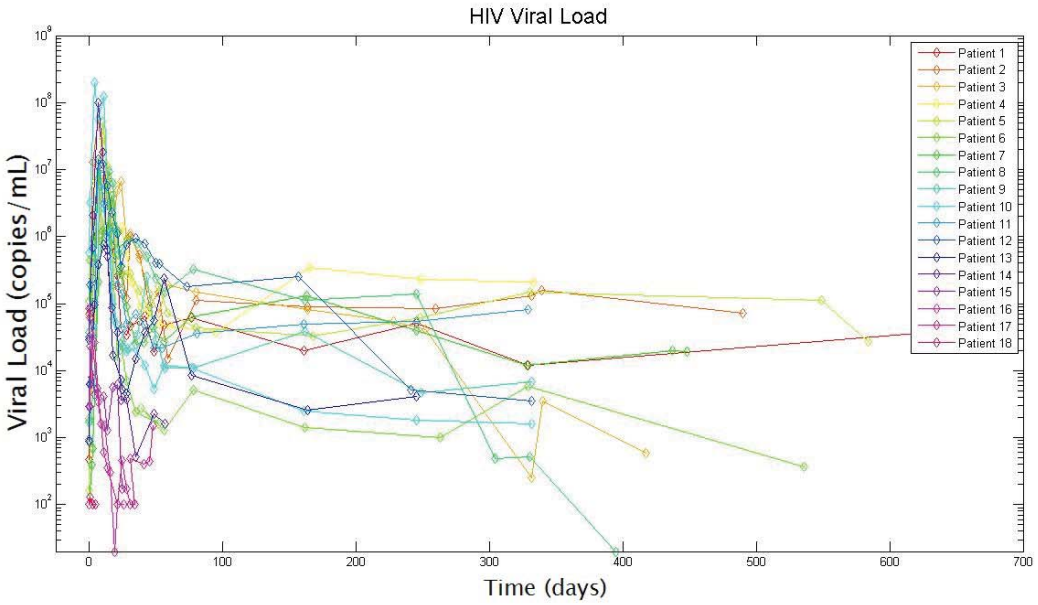

Figure 1: Viral Load measurements from all 18 patients identified as HIV-1 positive during plasma testing. Day 0 indicates the date of the first positive test.

The fitting of the data was performed after three preprocessing steps. First, we removed the subjects that received Highly Active Anti-retrovial Therapy (HAART) treatment in the very early stages of infection. For patients 15, 16, 17, and 18 early treatment was initiated on the first day (day 1) that they were measured to have any viral load present in the plasma. For patient 15, the initial viral load was 23,500 $\frac{virions}{mL}$; for patient 16, the initial viral load was 2,900$\frac{virions}{mL}$; for patient 17, the initial viral load was 62,000$\frac{virions}{mL}$; and for patient 18, the initial viral load was 100$\frac{virions}{mL}$. For patients 15, 16, and 17, the initiation of the HAART treatment resulted in a dramatic decrease in viral loads making their data not as useful for establishing a "baseline" for the un-treated parameter values. For instance, in all three patients that received treatment, viral load levels were on the order of $10^2 - 10^3$ $\frac{virions}{mL}$. In the case of patient 18, the initiation of early treatment resulted in a sustained viral load levels which was very low (around 100$\frac{virions}{mL}$). Thus, in

all four of the patients, early treatment resulted in viral load levels that were significantly smaller than the remaining 14 patients, which were approximately $10^4 - 10^6 \frac{virions}{mL}$ as illustrated by Figure 1.

We can see that the purple and pink lines in Figure 2, which represent the viral load levels for these four patients, are noticeably lower than those for the other patients. Since we are primarily examining acute infection without treatment (untreated infection which occurs within the first $\approx$ 95 days of infection), all four patients were removed from our analysis. It is important to note, that patients 3, 4, and 8 also received HAART treatment: patient 3's HAART treatment began on day 310, patient 4's HAART treatment began on day 297, and patient 8's HAART treatment began on day 297.

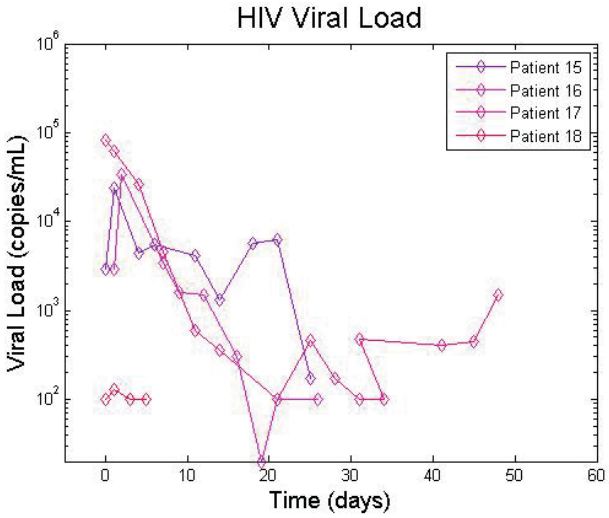

Figure 2: The viral load measurements of the four patients that received early treatment.

Examining Figure 3 we can clearly see the effects of the HAART treatment in patient 8. By day 304, just seven days after the initiation of treatment, the viral load fell from approximately 125,000 $\frac{virions}{mL}$ to 480 $\frac{virions}{mL}$. Additionally, we can see that the viral load level appears to continue to decrease and ultimately achieve a new lower steady state value after initiation of treatment.

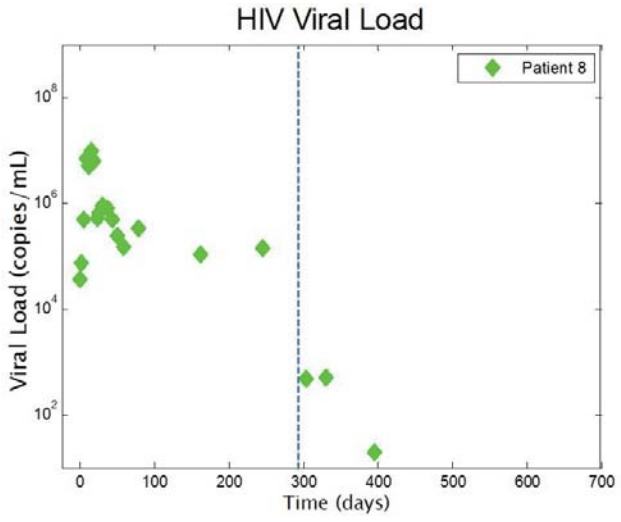

Figure 3: The viral load measurements of patient 8 which received HAART treatment at day 297. The blue dashed line denotes the day that HAART treatment was administered.

The significant decrease in viral load and persistence of a lower steady state value suggests that the treatment is not only effective at very quickly reducing the viral load, but also that the treatment is effective at limiting and containing the infection. This is because, as the viral population decreases, we expect that the infected cell population will decrease as well. A lower infected cell population is commonly associated with a decrease in the negative physiological effects seen by the patient, meaning that the patient will be much less susceptible to outside infection. Thus, by significantly decreasing the population of the virus, the HAART is therefore extremely effective at limiting and controlling the infection. Yet, for patient 8, these data points fall outside the time frame that we are considering (we are considering data points up

to day $\approx$ 95) and thus we did not remove this patient from our analysis since doing so would be unnecessary. Finally, we eliminated any data points before time zero or prior to the onset of infection (when the viral load was zero) and removed all data points after day 95 since our goal was to examine the dynamics of primary infection.

We can see from Figure 4 that once we perform the three preprocessing steps and examine the time in which primary infection occurs, the patients show approximately the same functional form. This type of behavior is exactly what we expect given what we know about the behavior of HIV infection. HIV infection is typically characterized by four primary phases of infection: viral growth phase, peak viral load, viral decay phase, and the steady state phase. Each patient has an exponential increase in viral load during the first stage of infection, the viral growth phase. Then, the viral load reaches it's maximum value at approximately one to two weeks after the onset of the infection; this peak value is commonly known as the peak viral load. After reaching a peak value, we see an exponential decrease in the viral load during the third stage of infection commonly referred to as the viral decay phase. Yet, the viral load does not decay to zero; it achieves a steady state and remains approximately consistent as the virus becomes latent within the body known as the viral steady state.

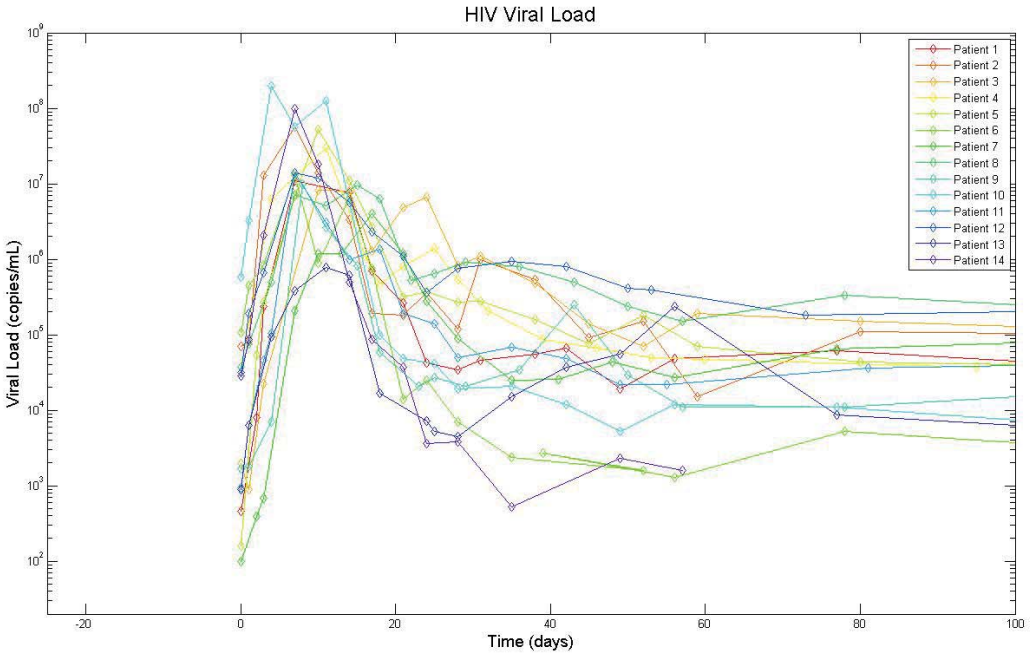

Figure 4: The patient data from the 14 patients that we modeled.

The data that was collected in this study is unique and provides a great opportunity for advanced analysis and interpretation due to the robustness it provides during the course of primary infection. Typically, patient data that is collected from HIV infected individuals does not include the four phases of primary infection. This is primarily due to the means that is used to collect

patient data, plasma virus donations. Plasma virus donations are typically carried out by private companies looking to make profits. They test each sample for HIV and test whether or not HIV is present within the sample. However, if they find that a sample is HIV positive, that specific donor becomes no longer pertinent for the company since they are not able to use their donations any longer to make a profit. Thus, if they even track the virus at all, typical HIV data sets sometimes consist of the initial viral growth phase, and perhaps the peak viral load, but rarely contain data on the viral decay and steady state.

The study that we obtained the data from was unique due to the nature (and organizations) that collected the data. The U.S. Army was not concerned with the profits that can be made from plasma virus donations, rather was much more interested in characterizing the dynamics of the infection. Thus, when they discovered that a patient was HIV positive, they had them return almost daily during the first three phases of the infection (viral production, peak viral load, and viral decay) in order to obtain a robust set of data during this time period. This proves to be extremely useful for our analysis and gives us an unprecedented glimpse into the dynamics of the primary infection of HIV.

3 Fitting

While the patients illustrate the same functional form, there is still variability among the individual patients. Thus, we use a nonlinear mixed effects model in order to capture both the fixed and random effects within the data.

3.1 Nonlinear Mixed Effects Model

The data we gathered was longitudinal patient data from 14 patients meaning that the data was generated by observing a number of individuals at multiple time points under different experimental conditions. In this case, we assume that the patients constitute a random sample from a larger population of interest. Thus, we fit the data with a nonlinear mixed effects model which borrows information across subjects while estimating both the population average and subject-specific parameters.

Table 1: Parameters for the Nonlinear Mixed Effects Model

Parameter	Description
y_{ij}	j^{th} response on the i^{th} individual
x_{ij}	predictor vector for the j^{th} response on the i^{th} individual
f	nonlinear function of the predictor vector (x_{ij}) and ϕ_i
e_{ij}	normally distributed noise term
A_i	design matrix of size $r \times p$ for the fixed effects
β	p vector of fixed population parameters"
B_i	design matrix of size $r \times q$ for the random effects
b_i	q vector of random effects
$\sigma^2 D$	covariance matrix

By using a mixed effects model we account for both fixed and random effects within the data. Essentially this means that we assume that all of the patients responses follow a similar functional form with parameters that vary among individuals. Here we present a general form of a nonlinear mixed effects model, that is a generalization of both the linear mixed effects model and the standard fixed effects nonlinear model, taken from Bates and Lindstrom [16]. In the case of our study, we define a general nonlinear mixed effects model for the j^{th} observation on the i^{th} individual as:

(1a) $y_{ij} = f(\phi_i, x_{ij}) + \epsilon_{ij}$
(1b) $\phi_i = A_i\beta + B_i b_i$
(1c) $b_i \sim N(0, \sigma^2 D)$

where the parameters and their descriptions are listed in Table 1.

3.2 Fitting with Monolix

Using Monolix, we applied the Stochastic Approximation Expectation Maximization Algorithm in order to estimate various parameters for the model. Monolix uses this algorathim as an optimization method in order to produce population fits which provide estimates for population as well as individual fit parameters. In using this method, Monolix assumes that the data points

constitute a random sample from a normally distributed larger population. Thus, Monolix abides by the assumption we made in applying the nonlinear mixed effects model. As a result, we receive outputs the estimates for the fixed effects as well as estimates for the random effects (reported as standard deviations) and the standard errors which are determined using a linearization method.

In addition to the data fitting and providing estimates for a number of parameters, Monolix also calculates the log-likelihood as well as the Akaike and Bayesian Information Criteria. We used Monolix's output for the log-likelihood, Akaike Information Criteria, and the Bayesian Information Criteria in addition to a calculated corrected Akaike Information Criteria and Bayesian Information Criteria using residuals in order to measure the "goodness of fit" for the models and to ultimately compare each of the model's fit of the data.

4 Target-Cell-Limited Model

A basic model of HIV infection which was developed and has been widely studied in an effort to describe the viral dynamics of primary infection. The Target-cell-limited Model suggests that the spread of HIV infection is limited by the availability of target cells. This results from the high infectivity of the virus, which causes it to eliminate a large population of target cells upon the initiation of infection. Thus, the target cells act in a manner which limits the growth of the virus, and the model is hence known as the Target-Cell-Limited Model. The model highlights three distinct populations which are denoted:

$T(t)$: concentration of target cells at time t,
$I(t)$: concentration of infected cells at time t,
$V(t)$: concentration of free virus at time t.

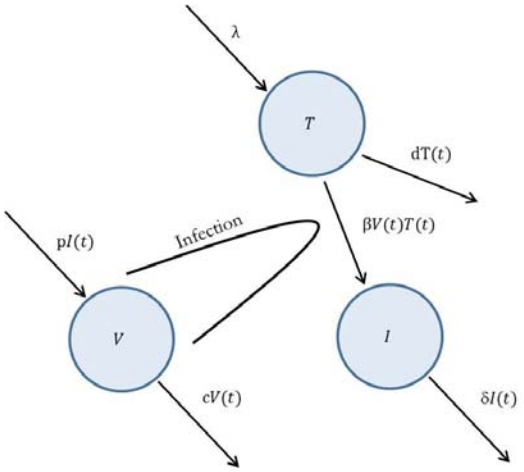

Figure 5: A visual representation of the dynamics that governs the interactions in the model.

Thus, we consider the mathematical model of HIV-1 infection given by the nonlinear system of ordinary differential equations:

$$\text{(2a)}\quad \frac{dT}{dt} = \lambda - dT(t) - \beta V(t)T(t)$$
$$\text{(2b)}\quad \frac{dI}{dt} = \beta V(t)T(t) - \delta I(t)$$
$$\text{(2c)}\quad \frac{dV}{dt} = pI(t) - cV(t)$$

With initial conditions $T(0) = T_0$, $I(0) = I_0$, $V(0) = V_0$.

4.1 Model Development

Equation 2a models the dynamics of the uninfected cellular population. The equation can be represented by production rate, infection rate, and death rate. The equation is determined to be:

Rate of change of target cell population = (Production rate) - (Infection rate) - (Death rate)

Production rate: We assume that target cells are produced at a constant rate, the target cell production rate, λ [11, 14, 25].

Infection rate: Target cells can be eliminated by becoming infected by the virus. The interaction between the virus and the target cells is widely known as the mass action principle [14]. This principle describes, from a mathematical perspective the rate at which the virus infects target cells. The mass action principle, derived from our current understanding of enzyme kinetics, results in a term which suggests that the rate of interaction between the virus and target cells, β, is directly

proportional to the product of the participating populations [11, 14].

Death rate: The target cell death rate term is determined by the elimination of target cells not due to infection as a result of the virus. The death rate, d, can be assumed to be proportional to the target cell population [11].

Equation 2b represents the dynamics of infected cells. The equation for the rate of change of the infected cell population is dictated by both the rate of infection and death rate. The equation can be represented as:

Rate of change of infected cell population = (Infection rate) - (Death rate)

Infection rate: This term is the same as the infection rate term in the target cell differential equation with a reversal in sign. This is a result of the fact that the only way that infected cells can be created is by infecting previously uninfected target cells [14]. The human immune system does not naturally produce infected cells; thus, the term remains the same as previously determined.

Death rate: Similar to target cell death, infected cells are cleared by the immune system at a rate, δ, proportional to the infected cell population [14].

Equation 2c mathematically describes the dynamics of the virus cell population. This equation consists of the virus production rate and viral clearance rate and is:

Rate of change of virus population = (Growth rate) - (Clearance rate)

Production rate: While the virus production rate varies from cell to cell and individual to individual, when considering the aggregate population this model assumes the rate of proliferation is constant and that new viruses are produced at a rate, p, proportional to the infected cell population [14].

Clearance rate: There are two manners in which the virus-infected cells are eliminated, viral cytopathic effects and immune-mediated cellular destruction [8]. Viral cytopathic effects occur as a result of the virus infecting healthy uninfected cells. When a viral particle infects a previously uninfected cell, the viral particle is removed from the population of virus that maintains the ability to infect additional uninfected cells. However, viral cytopathic effects are insignificant when assessing the overall elimination of viral particles and thus, are not illustrated in the model [4]. Immune-mediated cellular destruction is the immune system's ability to clear, or eliminate, the virus from the body. This method typically eliminates a majority of the virus population [6]. The model assumes that the virus is then killed off at a clearance rate, c, proportional to the virus population [14].

It is important to note that all of the model parameters are presumed to be positive. In addition, there are two biologically reasonable assumptions we are able to make with regard to the values of parameters in relation to one another. Notably, it is biologically reasonable to assume that infected cells have a higher death rate than target cells, namely $\delta \geq d$. Furthermore, in early HIV infection, before the peak in viral load, we assume that the total number of target cells remains approximately constant (ie. at equilibrium). Thus, the equilibrium number of target cells is given by:

$\frac{dT}{dt} = 0 \implies 0 = \lambda - \beta TV - dT$, where V=0, $\implies \lambda = dT_0$. Thus, $\lambda = dT_0$.

Furthermore, estimates of c made during HIV chronic infection indicate that $c \approx 23 day^{-1}$ [27]. While this value is estimated from chronic infection, clinical studies have determined that viral clearance may have the same magnitude during early infection. Furthermore, we know that T_0, the initial number of target cells is fixed.

Table 2: Parameters for the Target-Cell-Limited Model

Parameter	Biological Interpretation	Units	Known Value
λ	Target cell production rate	$(Cells)mL^{-1}days^{-1}$	dT_0
β	Rate of infection	$(mL)Cells^{-1}days^{-1}$	Estimated*
d	Target cell death rate	$days^{-1}$	Estimated*
δ	Infected cell death rate	$days^{-1}$	Estimated*
p	Viral production rate	$days^{-1}$	Estimated*
c	Viral clearance rate	$days^{-1}$	23

Table 3: Initial Conditions for the Target-Cell-Limited Model

Initial Conditions	Value	Units
T_0	5.9×10^5	$(Cells)mL^{-1}$
I_0	$\frac{c}{p}V_0$	$(Cells)mL^{-1}$
V_0	Estimated*	$(Cells)mL^{-1}$

The asterisk in Tables 2 and 3 denotes estimations that we carried our for the Target-cell-limited model using the data from the patients from Section 2.

4.2 Existence and Uniqueness of Solutions

Prior to conducting an in–depth analysis of the model, it is crucial to show that the solutions to the initial-value problem exist, and are positive, bounded, and unique.

4.2.1 Positivity and Boundedness

In order to retain the biological validity of the model, we must prove that solutions to the system of differential equations are positive and bounded for all values of time. For example, concluding that a population is negative is not biologically feasible. Furthermore, the populations must remain finite since the human body can only be composed of a finite number of cells. In addition, boundedness and positivity illustrate that once infected, it is possible that the population of the virus will continue to exist beneath the detectable threshold without doing significant damage [25]. The next step in analyzing our model will be to prove positivity and boundedness for the system of differential equations. We will do so by proving the following theorems.

Lemma (*Positivity*)**.** *Let $t_0 > 0$. In the model, if the initial conditions satisfy $T(0) > 0$, $I(0) > 0$, $V(0) > 0$, then for all $t \in [0, t_0]$, $T(t)$, $I(t)$, $V(t)$ will remain positive in $\mathbb{R}^3_+$.*

Proof: Positivity. We must prove that for all $t \in [0, t_0]$, $T(t)$, $I(t)$, $V(t)$ will be positive in $\mathbb{R}^3_+$. We know that all of the parameters used in the system are positive. Thus, we can place lower bounds on each of the equations given in the model. Thus,

$$\frac{dT}{dt} = \lambda - dT(t) - \beta V(t)T(t) \geq -dT(t) - \beta V(t)T(t)$$
$$\frac{dI}{dt} = \beta V(t)T(t) - \delta I(t) \geq -\delta I(t)$$
$$\frac{dV}{dt} = pT(t) - cV(t) \geq -cV(t)$$

Through basic differential equations methods we can resolve the inequalities and produce:

$$T(t) \geq e^{-\mu t - \beta \int V(t)dt} \geq 0$$
$$I(t) \geq e^{-\delta t} \geq 0$$
$$V(t) \geq e^{-ct} \geq 0$$

Thus, for all $t \in [0, t_0]$, $T(t)$, $I(t)$, $V(t)$ will be positive and remain in $\mathbb{R}^3_+$. □

Lemma (Boundedness)**.** *There exists an* $T_M, I_M, V_M > 0$ *such that for* $T(t)$, $I(t)$, $I(t)$ $\limsup_{t\to\infty}\Big(T(t)\Big) \leq T_M$, $\limsup_{t\to\infty}\Big(I(t)\Big) \leq I_M$, $\limsup_{t\to\infty}\Big(V(t)\Big) \leq V_M$ *for all* $t \in [0, t_0]$.

Proof: Boundedness. We must prove that for all $t \in [0, t_0]$, $T(t)$, $I(t)$, $V(t)$ will be bounded. We know that all of the constants used in the system are positive.

$$\frac{dT}{dt} + \frac{dI}{dt} = \lambda - dT(t) - \delta I(t)$$

Since all of the constants are positive,

$$\frac{d(T+I)}{dt} \leq \lambda - \min\{d, \delta\}(T+I)(t)$$

which implies,

$$(T+I)(t) \leq \frac{\lambda}{\min\{d,\delta\}} + c_0 e^{-\min\{d,\delta\}t}$$

taking the limsup of both sides,

$$\limsup_{t\to\infty}(T+I)(t) \leq \limsup_{t\to\infty}\Big(\frac{\lambda}{\min\{d,\delta\}} + c_0 e^{-\min\{d,\delta\}t}\Big) = \frac{\lambda}{\min\{d,\delta\}}$$

So, choose

$$T_M = I_M = \frac{\lambda}{\min\{d,\delta\}}$$

Thus, $(T+I)(t)$ is bounded, so $T(t)$ and $I(t)$ are all bounded since

$$T(t), I(t) \leq (T+I)(t).$$

So,

$$T(t) \leq T_M, \text{ and } I(t) \leq I_M \text{ for all } t \in [0, t_0]$$

Furthermore, since all of the constants are positive, we can place an upper bound on $\frac{dV}{dt}$ so,

$$\frac{dV}{dt} = pI(t) - cV(t) \leq pI(t)$$

Therefore, we can choose

$$V_M = pI_M$$

Thus,

$$V(t) \leq pI_M = V_M.$$

Hence, since $I(t)$ is bounded for all $t \in [0, t_0]$, we know that $V(t)$ is bounded for all $t \in [0, t_0]$. □

Theorem 1 (Existence)**.** *Let $t_0 > 0$. In the model, if the initial conditions satisfy $T(0) > 0$, $I(0) > 0$, $V(0) > 0$ then $\forall t \in \mathbb{R}$ $T(t)$, $I(t)$, $V(t)$ will exist in $\mathbb{R}^3_+$.*

Proof: Existence and Uniqueness. In the case of our model we have:

$$\mathbf{x} = \begin{bmatrix} T(t) \\ I(t) \\ V(t) \end{bmatrix} \text{ and } \mathbf{f}(\mathbf{x}) = \begin{bmatrix} \lambda - dT(t) - \beta V(t)T(t) \\ \beta V(t)T(t) - \delta I(t) \\ pI(t) - cV(t) \end{bmatrix}$$

Note that f has a continuous derivative on $\mathbb{R}^3$ and thus, f is locally Lipschitz in $\mathbb{R}^3$. Hence, by the Fundamental Existence and Uniqueness Theorem located in the appendix as well as the lemmas proved on positivity and boundedness of solutions, we know that there exists a unique, positive, and bounded solution to the ordinary differential equations given in $2(a) - 2(c)$. □

4.3 Local Stability Analysis

Since the virus reaches a steady state, the first major type of analysis that we will conduct will be a local stability analysis. This analysis allows us to determine the stability of the system of differential equations around several points, known as critical points (also known as equilibria or equilibrium points). This form of analysis provides insights into the behavior of the system and can provide the basis for more advanced forms of analysis such as bifurcation analysis or global stability analysis.

4.3.1 Critical Points

Theorem (*Critical Points*)**.** *Given the differential equation $\frac{dx}{dt} = f(x(t))$ a point is considered a critical point if $\frac{dx}{dt} = f(x(t)) = 0$ for all $t \in \mathbb{R}$.*

For the model we consider the critical points for the values corresponding to the various populations (T, I, V). A critical point represents a point in the system where, if the system will remain at that point, the populations will no longer change. Thus, the rate of change for each population is zero. We obtain the critical points by setting each differential equation equal to zero.

Thus,

$$\frac{dT}{dt} = 0, \frac{dI}{dt} = 0, \frac{dV}{dt} = 0$$

So,

$$y = \begin{bmatrix} T(t) \\ I(t) \\ V(t) \end{bmatrix} \text{ and } f(y) = \begin{bmatrix} \lambda - dT(t) - \beta V(t)T(t) \\ \beta V(t)T(t) - \delta I(t) \\ pI(t) - cV(t) \end{bmatrix} = \begin{bmatrix} 0 \\ 0 \\ 0 \end{bmatrix}$$

From a biological perspective we will be able to classify the critical points as persistence or elimination points. If the values for any population at the critical point is zero $(T = 0, I = 0, V = 0)$, those cells are defined as extinct. Thus, if $V = I = 0$, the virus is extinct from the body. A critical point with these characteristics is known as a viral clearance or viral extinction point. However, if the value for any population at the critical point is not zero $(T \neq 0, I \neq 0, V \neq 0)$ those cells are

defined as persistent. If $V \neq 0$ and $I \neq 0$ then the infection persists within the system and the critical point is known as a viral persistence point.

If the system takes on the value of a critical point at any time, it will remain at the point for all remaining time. However, unless the initial conditions are exactly one of the critical points, the system need not necessarily obtain these values. The system may approach the critical point, move away from the critical point, or cycle between specific values. In order to accurately determine the behavior and thus how the system will interact with the equilibrium we must undergo a stability analysis for the system.

4.3.2 Linearization and the Jacobian

In modeling systems it becomes apparent that nearly all systems are non-linear, including the simple model we are examining. However, most of the theory that has been developed by mathematicians governing the behavior of systems of differential equations, especially stability, is centered upon linear systems. Thus, in order to further understand the behavior of a non-linear system it is first crucial to linearize the system. Essentially, this process approximates a non-linear system in a linear manner. The linear approximation occurs at the critical points which will be denoted P_n, where $n = 1, 2, 3....$ Near the critical points we can make a linear approximation and so determine the local character of the paths. This technique allows the stability of the critical points to be determined and provides a starting point for global investigations of solutions. The goal of this stability analysis is to perturb the system from a critical point and examine if the system returns to the original critical point.

In order to linearize the system, we must compute the Jacobian matrix of the system. The Jacobian is the matrix of the partial derivatives of each function with respect to each variable. Essentially, the Jacobian provides a linear approximation of a system at any given point. In addition, the Jacobian can be generalized to a system of autonomous differential equations:

$$\begin{bmatrix} \frac{dy_1}{dt} \\ \vdots \\ \frac{dy_n}{dt} \end{bmatrix} = \begin{bmatrix} F_1(x_1, ..., x_m) \\ \vdots \\ F_n(x_1, ..., x_m) \end{bmatrix}$$

as

$$J = \begin{bmatrix} \frac{dF_1}{dx_1} & \cdots & \frac{dF_1}{dx_m} \\ \vdots & \ddots & \vdots \\ \frac{dF_n}{dx_1} & \cdots & \frac{dF_n}{dx_m} \end{bmatrix}$$

Where J is the Jacobian matrix.

4.3.3 Derivation of the Viral Reproduction Number

The notion of a viral reproduction number was initially developed for the field of epidemiology in order to mathematically characterize the volatility of an infectious disease [5]. In an epidemi-

ological setting, R_0 represents the number of people that an infected individual will infect during their lifetime. However, this notion can be applied to the study of viral dynamics in vivo. In fact, the viral reproduction number is an extremely important quantity in our analysis of our models. Biologically, in an in vivo model, R_0 represents the average number of infected cells produced by an initially infected cell over its lifetime [24]. The value of R_0 is a well established norm when discussing viral infections [24] and is commonly discussed when approaching modeling problems. We will also see later that the value of R_0 has large impacts on the stability properties of the system as well as the persistence or elimination of infection.

The literature which focuses on HIV typically characterized the R_0 value for HIV to be between 3 and 6. This means that for every cell that is infected with HIV, 3 to 4 more infected cells will be produced. This suggests that the infection will tend to persist within the immune system. We will conduct analysis to determine the course of infection and mathematically characterize this behavior, but first we must derive the expression for R_0 for the Target-Cell-Limited model.

We know from epidemiological studies that

$$R_0 = \Big(\frac{infection}{contact}\Big)\Big(\frac{contact}{time}\Big)\Big(\frac{time}{infection}\Big)$$

This expression reveals that R_0 is also a unit-less quantity. When examining the viral reproduction number in vivo, we can modify the above expression in order to help us understand the expression for R_0.

R_0 = (transmissibility)(avg. rate of contact between susceptible and infected)(duration of infectiousness)

In deriving the expression for R_0 for a compartmental model, we use a method called the next generation operator method. In using this method, we consider the next generation matrix, denoted G. This matrix is comprised of two parts: F and V^{-1} where

$$F = \left[\frac{\partial F_i(x_0)}{\partial x_j}\right]$$

and

$$V = \left[\frac{\partial V_i(x_0)}{\partial x_j}\right]$$

In this case, F_i are the new infections, V_i represents the transfers of infections from one compartment to another, and x_0 is the disease free equilibrium state.

R_0 can then be defined as the spectral radius (dominant eigenvalue) of the next generation operator, G.

4.3.4 Analysis

Analysis of the eigenvalues of the Jacobian matrix evaluated at the critical points gives insights into the stability properties at that critical point. There are three possible values for an eigenvalue: positive, negative, and imaginary. In more complex systems, combinations of all three types of

values are possible and lead to different interpretations of the stability at the point.

For analysis of a non-linear system, it is necessary to use:

Theorem (Poincare-Perron)**.** *Let A be a constant matrix in the system $\frac{dx}{dt} = Ax$ with eigenvalues $\lambda_i, i = 1, 2, ..., n$*

i. If the system is stable, then $Re\{\lambda_i\} \leq 0$. $i = 1, 2, ..., n$

ii. If either $Re\{\lambda_i\} < 0$, $i = 1, 2, ..., n$; or if $Re\{\lambda_i\} \leq 0$ $i = 1, 2, ..., n$ and there is no zero repeated eigenvalue; then the system is uniformly stable.

iii. The system is asymptotically stable if and only if $Re\{\lambda_i\} < 0$, $i = 1, 2, ..., n$; note that it is also uniformly stable by ii.

iv. If $Re\{\lambda_i\} > 0$, for any $i = 1, 2, ..., n$ the solution is unstable

Note: This theorem was adopted from [12].
Remark: If any of the eigenvalues have a positive real part, we define the critical point to be a source, and thus, unstable. If all of the real parts of the eigenvalues are negative real numbers, we define the critical point to be a sink, and thus, stable.

One way to find the sign of the eigenvalue is to solve for the eigenvalue explicitly. However, for more complex systems the eigenvalues can be incredibly complex and difficult to work with. Thus, in order to determine the sign of the eigenvalue we can use the Routh-Hurwitz Criteria.

Theorem (Routh-Hurwitz Criteria)**.** *Given the polynomial*

$$P(x) = x^n + a_1 x^{n-1} + ... + a_{n-1} x + a_n,$$

where the coefficients a_i are real constants, $i = 1, ..., n$, define the $n \times n$ Hurwitz matrix using the coefficients a_i of the characteristic polynomial:

$$H_n = \begin{bmatrix} a_1 & 1 & 0 & 0 & \cdots & 0 \\ a_3 & a_2 & a_1 & 1 & \cdots & 0 \\ a_5 & a_4 & a_3 & a_2 & \cdots & 0 \\ \vdots & \vdots & \vdots & \vdots & \cdots & \vdots \\ 0 & 0 & 0 & 0 & \cdots & a_n \end{bmatrix}$$

where $a_i = 0$ if $j > n$. All of the roots of the polynomial $P(x)$ are negative or have negative real parts iff the determinants of all Hurwitz matrices are positive:

$$det(H_j) > 0, j = 1, 2, ..., n$$

Considering n=4 and n=5, the theorem simplifies and we are able to apply the theorem to the analysis of our system.

For n=3, the following conditions must be met:

(1) $a_1, a_2, a_3 > 0$

(2) $a_1 a_2 > a_3$

For n=4, the following conditions must be met:

(1) $a_1, a_2, a_3, a_4 > 0$

(2) $a_1 a_2 > a_3$

(3) $a_1 a_2 a_3 > a_3^2 + a_1^2 a_4$

For n=5, the following conditions must be met:

(1) $a_1, a_2, a_3, a_4, a_5 > 0$

(2) $a_1 a_2 > a_3$

(3) $a_1 a_2 a_3 > a_3^2 + a_1^2 a_4$

(4) $(a_1 a_4 - a_5)(a_1 a_2 a_3 - a_3^2 - a_1^2 a_4) > a_5(a_1 a_2 - a_3)^2 + a_1 a_5^2$

Note: The proof of the Routh Hurwitz Criteria is well known and can be found in [38].

The signs of the roots of the polynomials will tend to depend on several parameters known as threshold parameters. The values of these parameters, sometimes called, the reproductive constants influence and determine the stability of the system. An important part of our analysis will be deducing and applying these quantities effectively.

The Hartman-Grobman theorem is essential for showing how our analysis of the linearized system relates to the non-linear system. The Hartman-Grobman Theorem shows that near a critical point for a nonlinear system

(1) $\frac{dx}{dt} = f(x)$

the nonlinear system (1) exhibits the same qualitative structure as the linear system.

(2) $\frac{dx}{dt} = Jx$

Definition. *Two autonomous systems of differential equations are said to be topologically equivalent in a neighborhood of the origin or to have the same qualitative structure near the origin if there is a homeomorphism H mapping an open set U containing the origin onto an open set V containing the origin which maps trajectories of* (1) *in U onto trajectories of* (2) *in V and preserves their orientation by time in the sense that if a trajectory is directed from x_1 to x_2 in U, then its image is directed from $H(x_1)$ to $H(x_2)$ in V. If the homeomorphism H preserves the parameterization by time, then the systems* (1) *and* (2) *are said to be topologically conjugate in a neighborhood of the origin [28].*

Theorem (The Hartman-Grobman Theorem)**.** *Let E be an open subset of $\mathbb{R}^n$ containing the origin, let $f \in C^2(E)$ and letϕ_t be the flow of the nonlinear system (1). Suppose that $f(0) = 0$ and that the matrix $J(0)$ has no eigenvalue with zero real part. Then there exists a homeomorphism H of an open set U containing the origin onto an open set V containing the origin such that for each $x_0 \in U$ there is an open interval $I_0 \subset \mathbb{R}$ containing zero such that for all $x_0 \in U$ and $t \in I_0$*

$$H \circ \phi_t(x_0) = e^{At} H(x_0)$$

Note: Additional details and the proof for the Hartman Grobman Theorem are well known and can be found in [28].

This theorem essentially states that H maps the trajectories of the nonlinear system near the critical points onto the trajectories of the linear system near the critical points and preserves the parameterization of time [28]. In other words, if the Jacobian matrix has no zero or purely imaginary eigenvalues, then the stability properties of the system of nonlinear equations is the same as those for the system of linear equations at the critical points.

4.4 Application to the Model

The model has two biologically relevant equilibria denoted $P_n = (T, I, V)$ for $n = 1, 2$:

$$P_1 = \left(\frac{\lambda}{d}, 0, 0\right)$$
$$P_2 = \left(\frac{c\delta}{p\beta}, \frac{p\beta\lambda - \delta dc}{c\delta\beta}, \frac{p\beta\lambda - \delta dc}{c\delta\beta}\right)$$

We characterize P_1 as a viral free or viral clearance equilibrium; this means that as $t \to \infty$, the virus will be eliminated from the body. In addition, P_1 represents an infection clearance equilibrium which is highlighted by the fact that $V = 0$ and $I = 0$. P_2 describes the persistence of the virus, and thus can be characterized as a viral persistence equilibrium. At these values, the virus will remain in the system as $t \to \infty$. In addition, it is important to denote that both of the equilibria have a persistence of uninfected cells.

4.4.1 Jacobian

The Jacobian for the linearized system is:

$$J = \begin{bmatrix} -d - V\beta & 0 & -T\beta \\ V\beta & -\delta & T\beta \\ 0 & p & -c \end{bmatrix}$$

The characteristic polynomial is defined as the polynomial side of the characteristic equation, $det(A - xI) = 0$ where A is a square matrix, I is the identity matrix, and x is an eigenvalue. The roots of the characteristic polynomial of the Jacobian will tend to depend on several parameters known as threshold parameters. The values of these parameters, sometimes called the reproductive constants, influence and determine the stability of the system.

From Section 4.3.3 we can define:

$$R_0 = \frac{p\beta\lambda}{\delta dc}$$

to be the reproductive constant of the system.

Two theorems will be presented to highlight the relationship between the two reproductive constants and the local asymptotic stability of the equilibria. Thus, we are able to examine the value of R_0 to determine whether viral persistence or viral extinction occurs as $t \to \infty$. As a result, we may be able to predict the persistence of the HIV upon initial infection simply by determining the values of these expressions.

4.4.2 Stability Analysis for P_1

The Jacobian evaluated at $P_1 = \left(\frac{\lambda}{d}, 0, 0\right)$ becomes:

$$J_1 = \begin{bmatrix} -d & 0 & -\frac{\beta\lambda}{d} \\ 0 & -\delta & \frac{\beta\lambda}{d} \\ 0 & p & -c \end{bmatrix}$$

Furthermore, the characteristic equation for P_1 is

$$-\frac{1}{d}(x+d)(cd\delta + cdx + dx^2 + d\delta x - \beta\lambda p) = 0$$

From the characteristic equation we can define:

$$\begin{aligned} a_1 &= c + d + \delta \\ a_2 &= cd + c\delta + \delta d - \frac{\beta\lambda p}{d} \\ a_3 &= cd\delta - p\beta\lambda \end{aligned}$$

such that

$$-\frac{1}{d}(x+d)(cd\delta + cdx + dx^2 + d\delta x - \beta\lambda p) = x^3 + a_1x^2 + a_2x + a_3$$

.

4.4.3 Analysis

Theorem 2 (Local Asymptotic Stability of P_1)**.** *For the viral clearance equilibrium (P_1) given by*

$$(T, I, V) = \left(\tfrac{\lambda}{d}, 0, 0\right)$$

if $R_0 < 1$, then P_1 is stable; however if $R_0 > 1$, then P_1 is unstable.

Proof. We will use the Routh-Hurwitz Criteria and the values of $a_1, a_2,$ and a_3 to derive the stability of P_1.

We know that all of the parameters are positive. Therefore, $a_1 = c + d + \delta$ is clearly > 0.

Furthermore, we can express a_2 as

$$a_2 = cd + c\delta + \delta d - \frac{\beta\lambda p}{d} = cd + c\delta + \delta d - c\delta R_0$$

Simplifying the above expression,

$$a_2 = d\delta + dc + c\delta(1 - R_0).$$

Therefore, if $R_0 < 1$, then $a_2 > 0$.

In addition, we can express

$$a_3 = cd\delta - p\beta\lambda$$

as

$$a_3 = cd\delta(1 - R_0)$$

Thus, if $R_0 < 1$, then $a_3 > 0$. However, $R_0 > 1$, then $a_3 < 0$

Also, we can express

$$a_2a_1 - a_3 = cd\delta + (c + d + \delta)(c(d + \delta) + d\delta - \tfrac{\beta\lambda p}{d}) + \beta\lambda p$$

Solving in terms of R_0 we notice that

$$a_2a_1 - a_3 = cd\delta + (c + d + \delta)(c(d + \delta) + d\delta - c\delta R_0) + \beta\lambda p.$$

Thus,

$$a_2a_1 - a_3 = cd\delta + (c + d + \delta)(cd + c\delta(1 - R_0) + d\delta) + \beta\lambda p.$$

Therefore, if $R_0 < 1$ we know that $a_2a_1 - a_3 > 0$ and thus, $a_2a_1 > a_3$.

As a result, if $R_0 < 1$ then P_1 will clearly be stable. However, if $R_0 > 1$ then $a_3 < 0$ and as a result P_1 will be unstable. □

4.4.4 Stability Analysis for P_2

The Jacobian evaluated at $P_2 = \left(\frac{c\delta}{\beta p}, \frac{\beta\lambda p - cd\delta}{\beta\delta p}, \frac{\beta\lambda p - cd\delta}{\beta\delta p}\right)$ is:

$$J_2 = \begin{bmatrix} -d - \frac{p\beta\lambda - cd\delta}{c\delta} & 0 & -\frac{c\delta}{p} \\ \frac{p\beta\lambda - cd\delta}{c\delta} & -\delta & \frac{c\delta}{p} \\ 0 & p & -c \end{bmatrix}$$

Furthermore, the characteristic equation for P_2 is

$$\frac{c\delta p^2(-c - x)(\delta + x)(c\delta x + \beta\lambda p) - p(-c^3d\delta^3p - c^3\delta^3px)}{c^2\delta^2p^2} = 0$$

From the characteristic equation we can define:

$$a_1 = \frac{\beta\lambda p}{c\delta} + c + \delta$$
$$a_2 = \frac{\beta\lambda p}{c} + \frac{\beta\lambda p}{\delta}$$
$$a_3 = \beta\lambda p - cd\delta$$

such that

$$\frac{c\delta p^2(-c-x)(\delta+x)(c\delta x+\beta\lambda p) - p(-c^3 d\delta^3 p - c^3\delta^3 p x)}{c^2\delta^2 p^2} = x^3 + a_1 x^2 + a_2 x + a_3$$

4.4.5 Analysis

Theorem 3 (Local Asymptotic Stability of P_2)**.** *For the viral persistence equilibrium (P_2) given by*

$$(T, I, V) = \left(\tfrac{c\delta}{\beta p}, \tfrac{\beta\lambda p - cd\delta}{\beta\delta p}, \tfrac{\beta\lambda p - cd\delta}{\beta\delta p}\right)$$

will always be stable.

Proof. P_2 will only exist if $R_0 > 1$.

From our proof of positivity and boundedness, we know that V and I will always be positive and thus,

$$\beta\lambda p - cd\delta > 0$$

which implies that

$$\frac{1}{cd\delta}(R_0 - 1) > 0$$

and thus that $R_0 > 1$.

Furthermore, we know that all of the parameters are positive. Thus, clearly

$$a_1 = \frac{\beta\lambda p}{c\delta} + c + \delta$$

and

$$a_2 = \frac{\beta\lambda p}{c} + \frac{\beta\lambda p}{\delta}$$

are both > 0.

Additionally, we can express

$$a_3 = \beta\lambda p - cd\delta$$

as

$$a_3 = \frac{1}{cd\delta}(R_0 - 1)$$

Thus, since $R_0 > 1$, we know that $a_3 > 0$.

Also,

$$a_1a_2 - a_3 = cd\delta + \left(\frac{\beta\lambda p}{c} + \frac{\beta\lambda p}{\delta}\right)\left(\frac{\beta\lambda p}{c\delta} + c + \delta\right) - \beta\lambda p$$

which can be expanded to

$$a_1a_2 - a_3 = \frac{\beta^2\lambda^2p^2}{c^2\delta} + cd\delta + \frac{\beta^2\lambda^2p^2}{c\delta^2} + \frac{\beta\delta\lambda p}{c} + \frac{\beta c\lambda p}{\delta} + \beta\lambda p$$

.

Thus, since all of the parameters are positive $a_1a_2 - a_3 > 0$ and thus $a_1a_2 > a_3$.

Therefore, whenever $R_0 > 0$, P_2 will exist and be stable. □

4.5 Parameter Estimates

Initial estimation of the parameters was extremely difficult and inaccurate since several of the parameters, specifically the rate of infection, β, were extremely sensitive to initial conditions inputs and had a large residual standard error and thus very difficult to estimate. This is likely due to its small magnitude (typically $O(10^{-8}) - O(10^{-6})$). Thus, we recognized a need to apply an alternative approach to the estimation of this difficult to estimate parameter. We did so by estimating r, the viral expansion rate, which is simple to estimate and then solving for β in terms of r. A visual representation of the rate of viral production, r, can be seen in Figure 6.

In calculating the value for r, we utilized the data for the entire viral production phase prior to the peak viral load which consisted of data from approximately the first 7 to 10 days of infection. Furthermore, in the case where the peak in the data appeared to be lower than the expected peak viral load, we eliminated the peak from our estimation. In addition, we estimated the viral expansion rate via two means. First, we calculated the value of r by using a linear regression population fit for the exponential production phase in Monolix. We call the r obtained from this method r_{pop}. Next, we calculated value of r by fitting a linear regression to the data in MATLAB on a logarithmic scale, this r value is named

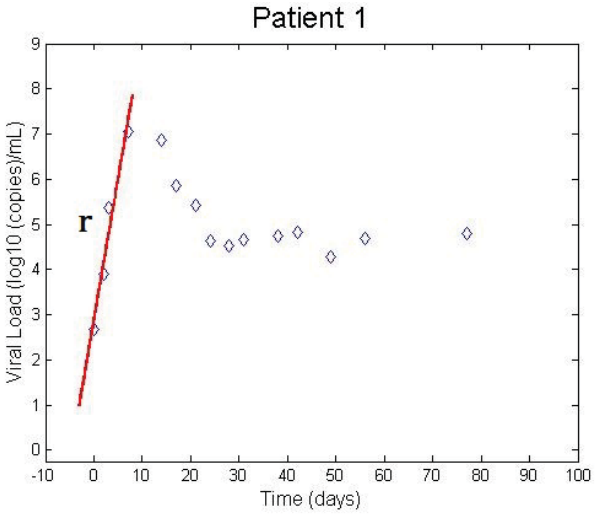

Figure 6: A schematic of the calculation of the viral expansion rate, r.

r_{ind}.

Next, we know that the population of the virus increases exponentially during the viral production phase and thus, $\frac{dV}{dt} = rV$ during this time period. This allows us to solve for β in terms of r since,

$$\frac{dV}{dt} = \big(\beta\tfrac{p}{c}T - \delta\big)V = rV \implies r = \beta\tfrac{p}{c}T_0 - \delta \implies \beta = (r+\delta)\tfrac{c}{pT_0}.$$

Thus, our new system of equations becomes

$$\text{(2d)}\quad \frac{dT}{dt} = \lambda - dT(t) - (r+\delta)\frac{c}{pT_0}V(t)T(t)$$

$$\text{(2e)}\quad \frac{dI}{dt} = (r+\delta)\frac{c}{pT_0}V(t)T(t) - \delta I(t)$$

$$\text{(2f)}\quad \frac{dV}{dt} = pI(t) - cV(t)$$

Table 4: Parameters for the Target-Cell-Limited Model with Estimating the Rate of Viral Production

Parameter	**Biological Interpretation**	**Units**	**Known Value**
λ	Target cell production rate	$(Cells)mL^{-1}days^{-1}$	dT_0
β	Rate of infection	$(mL)Cells^{-1}days^{-1}$	$(r+\delta)\frac{c}{pT_0}$
d	Target cell death rate	$days^{-1}$	Estimated*
δ	Infected cell death rate	$days^{-1}$	Estimated*
p	Viral production rate	$days^{-1}$	Estimated*
c	Viral clearance rate	$days^{-1}$	23

Table 4 shows the parameters for the equations 2d - 2f where we estimated the rate of viral production in order to better estimate the value of β which was extremely difficult to estimate. The asterisk in Table 4 denotes the parameters which we carried our for estimates the Target-Cell-Limited model using the data from the patients from Section 2. Table 5 includes the values of r_{ind} and r_{pop} obtained from our estimates.

Table 5: Parameter Estimates for the Target-Cell-Limited Model

Parameter	**Value**	$s.e._{lin}$	$r.s.e._{lin}$
p_{pop}	374.75589	121.46572	32.41
d_{pop}	0.00728	0.00098	13.39
δ_{pop}	0.24168	0.033	13.66
$V_{0_{pop}}$	3.84428	0.2951	7.68

As illustrated in Table 5, we obtained an average value for r_{pop} of 0.966 $days^{-1}$ and an average of 1.256 $days^{-1}$ for r_{ind}. Furthermore we see that r_{pop} ranges from 0.818 $days^{-1}$ to 1.104 $days^{-1}$ and r_{ind} ranges from 0.640 $days^{-1}$ to 1.456 $days^{-1}$; thus, the variance of r_{pop} is less than r_{ind} which is what we expect given the individual variability. In addition the values of both r_{ind} and r_{pop} are approximately 1.1 $days^{-1}$ which is what we expect and is consistent with the results from the literature [30]. While we used these r values in order to estimate β within the models, the value for r is also crucial for our estimation and ultimately derivation of the viral reproduction numbers for each of the patients.

Table 6: Estimations for r_{pop} and r_{ind}

Patient	r_{pop}	r_{ind}
1	1.104	1.440
2	0.999	1.854
3	0.911	1.613
4	0.819	1.284
5	1.057	1.416
6	0.886	0.640
7	0.818	1.308
8	0.904	0.741
9	0.986	1.086
10	1.046	1.436
11	1.070	1.253
12	0.930	0.954
13	0.952	1.107
14	1.037	1.456
Average	0.966	1.256

In addition, Table 5 provides the standard errors (se) and residual standard errors (rse) for both the population fixed and random parameters. The standard error measure indicates the extent to which an estimate deviates from the true population. The rse is the standard error expressed as a percentage of the estimate. In general, rse of 25% or higher should be used with caution. As we can see, the rse values for the population parameters are less than 25 with the exception of p_{pop} which is 32.41. Furthermore, upon examination of the parameter estimates in Table 5, we notice that the value for the rate of viral decay, δ, is much greater than d, however is approximately 0.242 $days^{-1}$. While this estimation is much greater than that for d, it is much smaller than we expected given previous studies and the regular behavior of the virus. For instance, in numerous other studies, the value for δ has been approximately 0.8 $days^{-1}$ [27]. A rate of viral decay of approximately 0.8 $days^{-1}$ is a much more realistic than 0.24 $days^{-1}$ given the known behavior of the virus. This is because, an infected target cell dies much faster than a standard non-infected target cell. In order to further investigate this discrepancy, as well as the overall behavior of the model, we plotted the solution to the differential equation along with the data, the phase portrait, and conducted a sensitivity analysis.

As previously stated, we first implemented ode45 in MATLAB with the individual fit parameters gained from Monolix in order to simulate the individual fits which are displayed below for patients 7-9. We can see from the graphs that the Target-Cell-Limited model appears to do a reasonably good job of capturing the viral growth phase, yet, as mentioned previously, the model seems to consistently underestimate the rate of viral decay phase post peak. This is illustrated by the fact that the model overestimates the values for the viral load during the decay phase (which is the phase immediately following the peak viral load until the steady state and occurs between days 15 and 25). This is also highlighted in the figure since the green dotted line lies above the blue data points. during this time period.

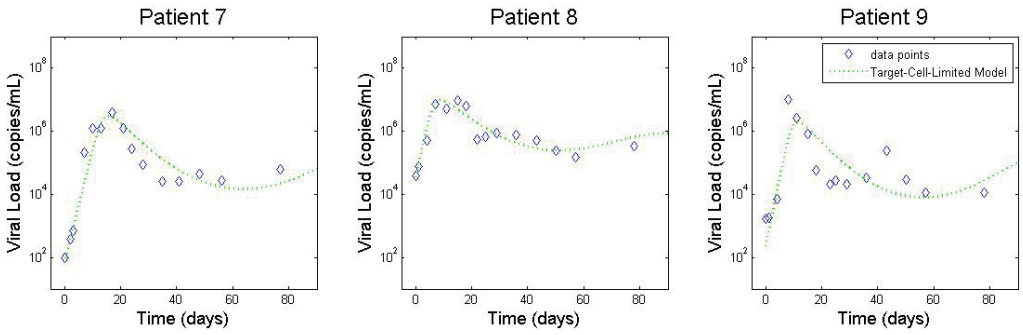

Figure 7: The Target-Cell-Limited Model Applied to Patients 7 - 9.

Table 7: Individual Patient R_0 Values

Patient	R_0
1	5.326
2	5.872
3	5.914
4	5.310
5	6.043
6	3.574
7	4.532
8	6.213
9	4.994
10	3.965
11	5.766
12	6.442
13	3.940
14	2.559
Mean	5.032
Median	5.318
Standard Deviation	1.157

We know from our derivation in section 4.3.3 that the viral reproduction number can be expressed as:

$$R_0 = \frac{\beta p \lambda}{cd\delta}$$

Where $\beta = (r+\delta)\frac{c}{pT_0}$ and $\lambda = dT_0$

Thus,

$$R_0 = \frac{(r+\delta)}{\delta}$$

For the target-cell-limited model we calculated the value of the viral reproduction number, R_0, for each of the patients using their individual estimated parameters. We can see from Table 7 that the mean value for R_0 is 5.032, which is lower than those found in previous studies. For instance in Stafford et. al [34] they analyzed 10 patients and calculated R_0 using the same expression we implemented. They found a median R_0 of 5.7 with a range between 2.8 and 11, which is greater than the values found in our study: Patient 12 has the highest value for R_0 at 6.442 and patient 14 has the lowest at 2.559. Comparing our parameter estimates to those in Stafford, we find that our estimate for the viral growth rate is much smaller (approximately 350 $days^{-1}$ compared to 850 $days^{-1}$).

Furthermore, Ribeiro et. al [30] provided estimates of R_0 based on data gathered from 47 patients. They obtained a mean value for R_0 of 8.63 with an interquartile range of 4.88 - 10.62. Yet, our results seem to be more consistent from patient to patient, suggesting that some of the effects may be due to usage of a population fitting vs. individual fitting. For instance, the standard deviation of our values for R_0 is 1.157 compared with 5.30 [30] and 2.6 [34].

A histogram of the distribution of R_0 values is shown in Figure 8 which illustrates that most of the values for R_0 are between 5 and 6. Additionally, while there is some deviation among the individual patients, most of the values for R_0 are within the range that we expect of approximately 3 to 6.

4.6 Effects of the Value of R_0

We know that the value of R_0 has significant effects on the behavior of the model; specifically with regard to the stability as illustrated in section 4.4. However, there are also correlations between the value of the viral reproduction number and several of the other quantities that are important in terms of defining the infection, specifically in this section we will examine the effects of R_0 on the peak and steady state viral loads. These relationship are crucial because they may be able to yield insights into the long term behavior of the infection, as well as inform us more of the progression of AIDS.

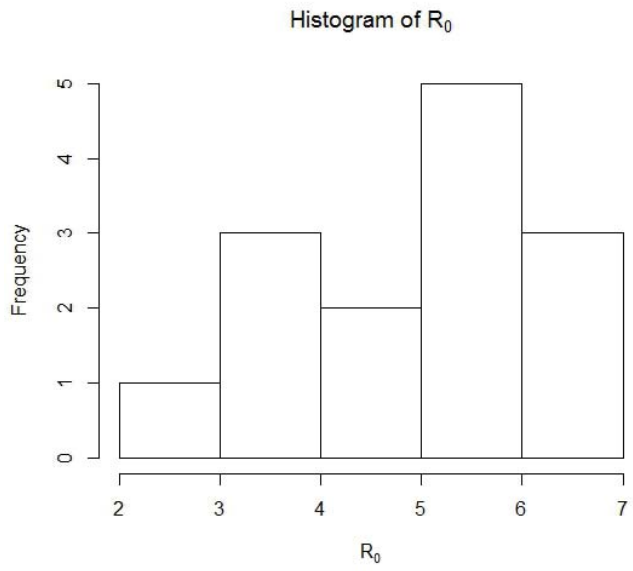

Figure 8: A histogram of the Distribution of R_0 for all 14 patients

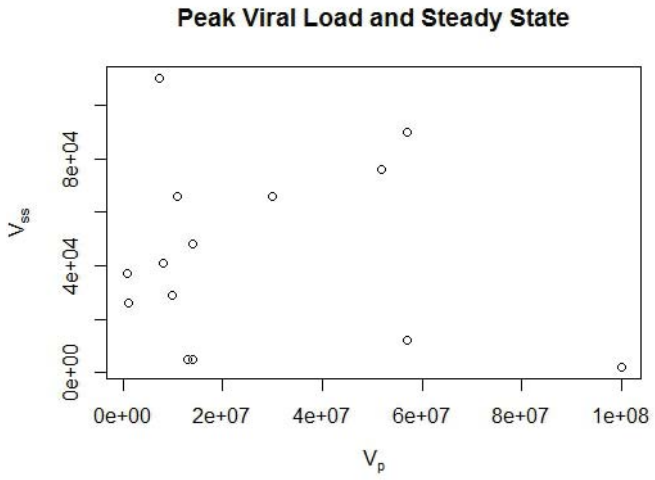

Figure 9: Relationship between peak and steady state viral loads

One quantity that we wish to examine is the viral steady state load. This is because the viral steady state load can yield many insights about the infection and its behavior. For instance, a larger steady state population of the virus is associated with an increased impact of the virus on the immune system in the long term. A larger viral steady state population is commonly associated with a smaller Target cell steady state population. Since the Target cell is the primary active component of the immune system, this results in a greater propensity for long term chronic health conditions associated with HIV, a faster progression to AIDS, as well as a greater risk of cancer cell development. In addition, a greater peak viral load is commonly associated with a more infectious virus, and thus the ability of the virus to be transmitted from one person to another is likely greater. As a result, it is crucial to determine and understand the relationship between the viral reproduction number and the behavior of some of the quantitative metrics of the system.

First, we examined the relationship between the value of the peak viral load and the steady state value. We can see that, in some cases, as the peak viral load increases, the value of the steady state increases as well, suggesting a positive correlation. However, this is not true for all of the patients and when we conduct a linear regression fit, we receive a p value of 0.6971. Thus, we cannot say that there is a strong positive correlation between peak viral load and the value of the steady state. Next we examined the relationship between the viral reproduction number and the peak viral load. Again, in the figure we can see that there seems to be little relationship between the two quantities and the p value of 0.1656 further highlights this claim. Additionally, the graph shows that there is generally a weak negative relationship between the two quantities. However, if we remove one of the outlying data points, specifically, patient number 12, we see that there is generally a positive relationship within the data which is what we expect. However, even thought it is existent, the relationship is still very weak.

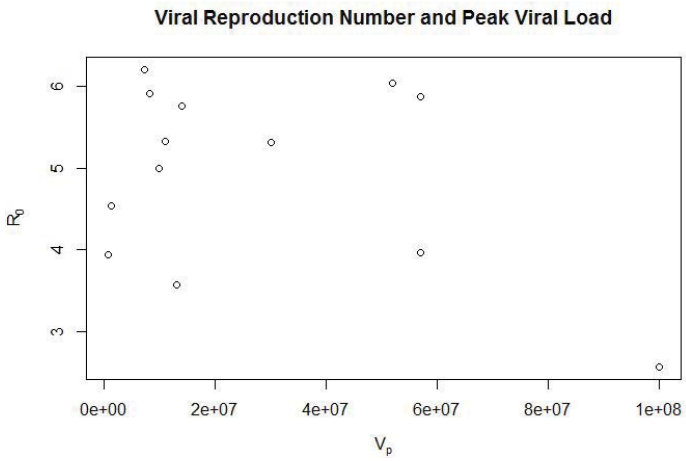

Figure 10: Relationship between R_0 and peak viral load

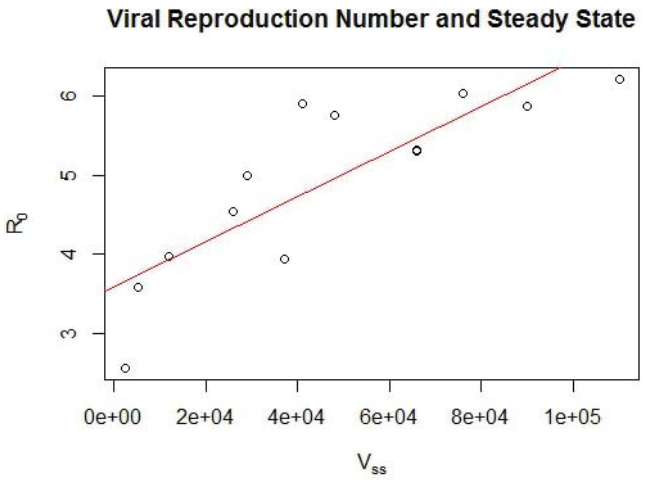

Figure 11: Relationship between R_0 and steady state viral load

Lastly, we examined the relationship between the viral reproduction number and the viral load of the steady state. As we can see in Figure 11, there appears to be a strong positive correlation between the two quantities. Upon further analysis, we determine the p value for a linear correlation to be 0.003529. This suggests, as we expected, that there is a strong positive relationship between the viral reproduction number and the steady state. Biologically, this means that the more infectious the virus is, and thus the larger the value of R_0 is, the larger the population of the virus will be when the system reaches the steady state. This notion has massive implications on predicting the effects of the infection. For instance, we can safely say that patients with a higher R_0 value will have a higher steady state population, and will thus be subject to significantly more long term chronic health issues. Additionally, their propensity for developing cancer will be higher since the immune system will be much weaker during this time period. Ultimately, this means that in the long term, the will be more likely to see

cancerous tumor cell development vice if they had lower levels of virus. It also means that we can focus on reducing the value of the viral reproduction number in an effort to reduce the negative implications of the higher viral load.

4.7 Numerical Simulations

In order to further examine the behavior of the model, we conducted several numerical simulations using the estimates obtained in Table 5. In our simulations, we investigated the overall system dynamics as well as the stability properties of the model in order to characterize the behavior.

Figure 12 illustrates the System Dynamic interaction between the Target Cells and the Virus. We can see that both the virus as well as the target cells behave exactly as expected. Upon initiation of infection, the population of the virus increases significantly until it reaches the peak viral load. After achieving the peak viral load, the virus decays until it reaches a steady state. However, Figure 12 also illustrates the behavior of the target-cells during infection, which is extremely important since the target cells are the primary actors in the immune system, as well as the cells that have the ability to interact with foreign pathogens, such as cancer.

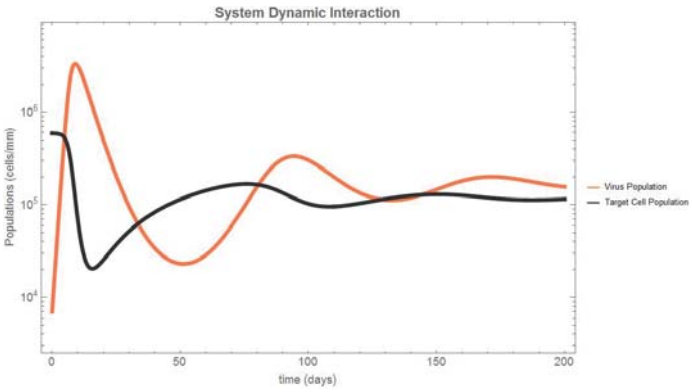

Figure 12: The Target-Cell-Limited Model simulation using the population parameters.

We see from Figure 12 that as the virus population increases, the population of target cells decreases (from $5.9 \times 10^5 \frac{cells}{mL}$ to $1.5 \times 10^4 \frac{cells}{mL}$) leaving the individual increasingly prone to further infection and ultimately cancerous cell development. It is important to note that the target cell population reaches its minimum after the peak viral load point. This suggests that increases in susceptibility to infection and foreign pathogens increases even after the virus reaches its maximum population.

However, after reaching the minimum, the target cell population begins to increases until it ultimately reaches a steady state. In this case, the steady state ($\approx 1 \times 10^5 \frac{cells}{mL}$) is approximately 17% of the original population of T-cells which is what we see in clinical trials and other studies [21]. This may be associated with a loss of functionality of the cells the virus infects, and may prove to be deleterious for an infected individual.

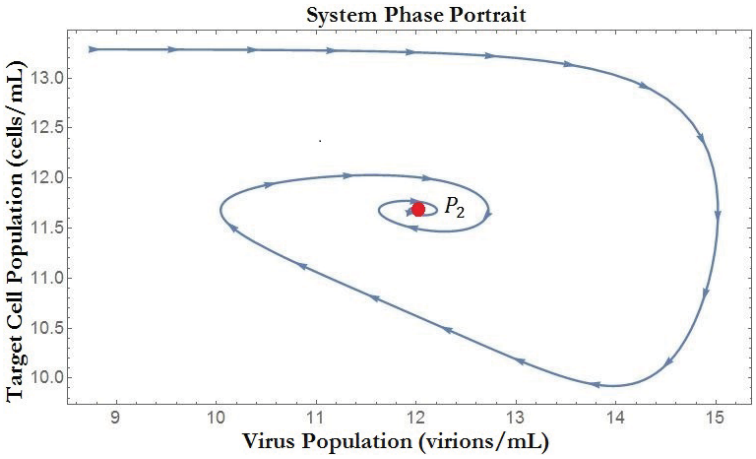

Figure 13: Target-Cell-Limited Model 2D Phase Portrait illustrating the relative changes in the viral and target cell populations.

Figure 13 is a phase portrait for the system. Essentially, this figure illustrates a single trajectory to show how the populations of the target cells and virus change relative to one another over time. We can see that there is an initial spike in the population of the virus, until it peaks at approximately $10^{15} \frac{virions}{mL}$. During this time, the Target cell population remains relatively constant until just before the virus reaches its peak, at which time the population of the target cells begins to decrease. We then see a resurgence of the target cells and a decrease in the population of the virus. Eventually, the target cell concentration begins to decrease significantly and then we see an oscillatory relationship between the population of target cells and that of the virus. This is illustrated by the spiral like nature of the graphs and suggests a "predator-prey" type relationship between the target cells and virus.

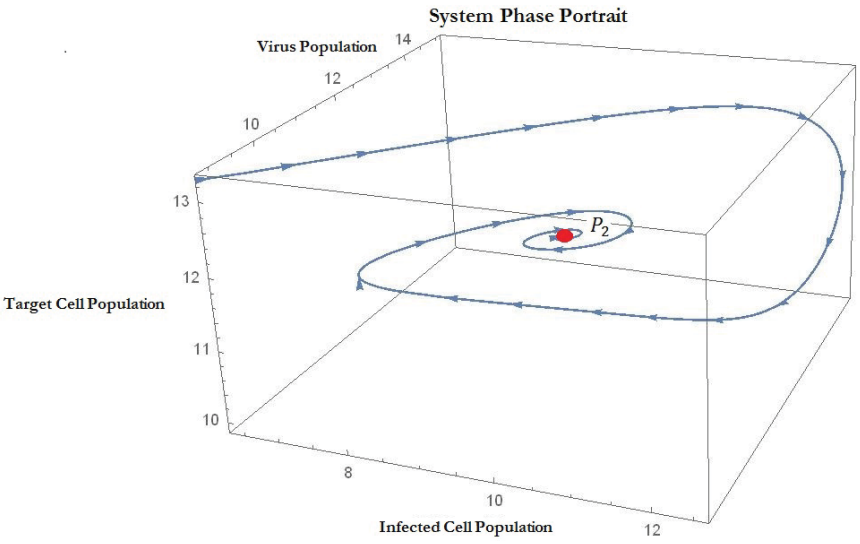

Figure 14: Target-Cell-Limited Model 3D Phase Portrait comparing the Viral, Infected, and Target Cell populations.

However, in addition to showing how the populations change relative to one another, the phase portrait in Figure 13 also illustrates the stability characteristics of the system. For instance, we can see that the trajectory approaches a single point. In this case, this point is a viral persistence point. This suggests that in the long term the population of the virus as well as target cells (infected and

uninfected) will remain positive. Based on our previous analysis, we know that the viral reproduction number for this system is approximately 5, and thus we know that it is clearly greater than one. Thus, we should expect that the system is asymptotically stable at P_2 (the viral persistence equilibrium), which is exactly what we see in the figure. Figure 13 therefore serves to show that the trajectory approaches the long term steady state P_2 and remains there as $t \to \infty$.

Figure 14 again shows the stability, however, Figure 14 highlights how all three of the populations, the target cells, infected target cells, and virus interact with one another. Importantly, Figure 14 suggests that the population of the virus and infected cells are proportional to one another. This means that if we are able to eliminate the viral population, we will also be eliminating the infected cell population. Thus, in order for infection clearance to occur, both $V = 0$ and $I = 0$.

4.8 Sensitivity Analysis

In this section we study the sensitivity of the Target-Cell-Limited Model, specifically the plasma virus concentration to small changes in the model parameters. Essentially, this means that we will see how the model reacts to changes in the values of individual parameters. The more robust the model is, the less it will be impacted by changes in a parameter value; the more sensitive a model is, the more that those changes will impact the behavior, even dramatically.

In conducting this analysis, we will take the partial derivatives of the system with respect to the individual parameter. This will help us to illustrate the changes in the system that result from changes in that specific parameter. In a sensitivity analysis, it is very common for models to display sensitivity to changes of value in specific parameters, yet, display robustness to variance in others. This type of analysis is useful in refining parameter estimation as well as yielding insights which are able to reduce the complexity of the model. In our analysis we will use the direct approach to find the sensitivity functions for the model and simulate the variance of several parameters of the Target-Cell-Limited Model.

4.8.1 Sensitivity Functions

We denote the sensitivity functions of T, I, and V with respect to an arbitrary parameter q, as $S_{T_q(t)}, S_{I_q(t)}, S_{V_q(t)}$ where:

$$S_{T_q(t)} = \frac{\partial}{\partial q} T(t); S_{I_q(t)} = \frac{\partial}{\partial q} I(t); S_{V_q(t)} = \frac{\partial}{\partial q} V(t)$$

Previous work has shown that the dynamics of viral infection are primarily controlled by a few of the parameters of the model. Specifically, the model is dependent on the values of β, δ, and p. The corresponding sensitivity systems with respect to β, δ, and p are shown below.

For β:

$$\text{(2g)}\quad S'_{T_\beta(t)} = -\big(V(t)S_{T_\beta(t)} + S_{V_\beta(t)}T(t)\big) - dS_{T_\beta(t)}$$

$$\text{(2h)}\quad S'_{I_\beta(t)} = \big(V(t)S_{T_\beta(t)} + S_{V_\beta(t)}T(t)\big) - \delta S_{I_\beta(t)}$$

$$\text{(2j)}\quad S'_{V_\beta(t)} = pS_{I_\beta(t)} - cS_{V_\beta(t)}$$

For δ:

$$\text{(2k)}\quad S'_{T_\delta(t)} = -\beta\big(V(t)S_{T_\delta(t)} + S_{V_\delta(t)}T(t)\big) - dS_{T_\delta(t)}$$

$$\text{(2l)}\quad S'_{I_\delta(t)} = \beta\big(V(t)S_{T_\delta(t)} + S_{V_\delta(t)}T(t)\big) - S_{I_\delta(t)}$$

$$\text{(2m)}\quad S'_{V_\delta(t)} = pS_{I_\delta(t)} - cS_{V_\delta(t)}$$

For p:

$$\text{(2n)}\quad S'_{T_p(t)} = -\beta\big(V(t)S_{T_p(t)} + S_{V_p(t)}T(t)\big) - dS_{T_p(t)}$$

$$\text{(2o)}\quad S'_{I_p(t)} = \beta\big(V(t)S_{T_p(t)} + S_{V_p(t)}T(t)\big) - \delta S_{I_p(t)}$$

$$\text{(2p)}\quad S'_{V_p(t)} = S_{I_p(t)} - cS_{V_p(t)}$$

We then plot the sensitivity functions, illustrating changes in increments of 5% the parameter by $\pm 25\%$. The Following Figure shows how these changes in the parameter impact the overall behavior of the system. Importantly, they also show which parameters are the most sensitive to changes in their value. We define most sensitive parameters to be the ones where small changes greatly impact the overall behavior of the system. For instance, examining Figure 15 in the three patients shown, the rate of viral production, p, appears to be the least sensitive. This is because the changes in the value of p seem to have very little impact on the overall behavior of the system in all three cases. However, this cannot be said of the rate of infection, β, or the death rate of infected cells, δ. With regard to both of these parameters, the changes impact the behavior of the system much more dramatically.

Variation of the parameter β seems to have a small, but somewhat negligible impact on the behavior of the system during the viral growth, peak, and viral decay stages. However, immediately following the viral decay stage, β seems to have a large impact on the system. Specifically, β seems to be impacting the size of the oscillations as the system approaches the steady state. Notably, the larger the value of β, the larger the oscillations. However, within the context of our model, this type of impact is not extremely significant to the overall behavior of the model. However, the same cannot be said for δ.

Changes in the parameter δ seem to have very little impact during the viral growth phase, which makes sense in the context of our previous discussion as there would likely not be a lot of infected cells and the response may be delayed. In our simulations, we determined that the target

cell population remains relatively constant during the very initial stages of the infection. Thus, we would expect that a parameter which primarily impacts the population of target cells would not have a large impact during this time frame. Additionally, the value of δ does not seem to impact the peak viral load. However, variation in δ significantly changes the rate of viral decay, and thus the behavior of the model during the viral decay phase. Figure 15 illustrates that the larger the value of δ, the steeper the rate of decay. Since our model underestimates the rate of viral decay, as discussed previously, this suggests that our value for δ is lower than it should be, given the data. Thus, we need to examine this behavior more closely. This will lead us to developing constraints for the model, which we do in Section 5.

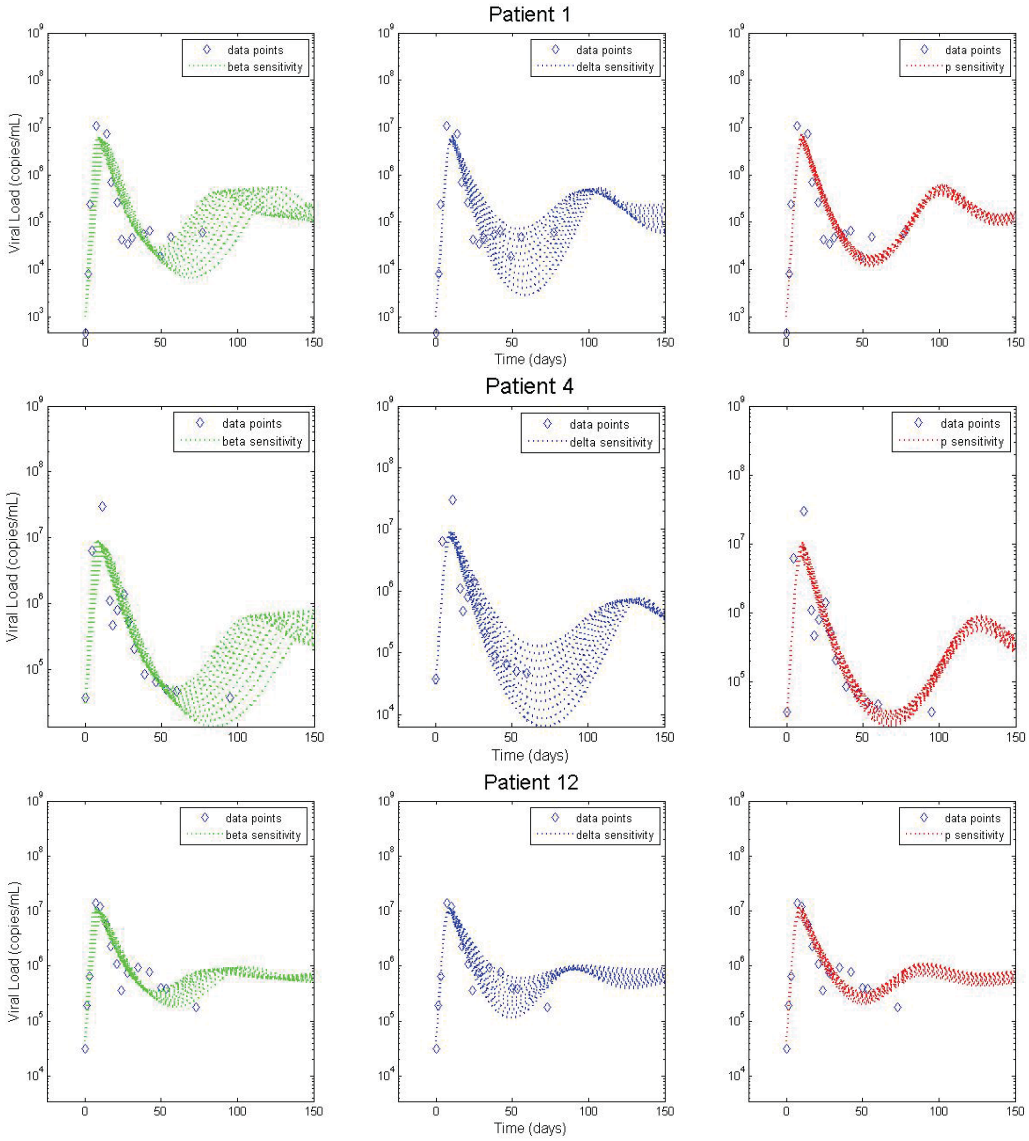

Figure 15: The effect of varying the parameters β, δ, and p on the Virus Dynamics of the Target-cell-limited Model.

4.9 Introduction of a Time Delay

In this section, we introduce a time delay into the target-cell-limited model in order to represent a biologically relevant delay during a stage of the viral life cycle known as the viral eclipse phase. While such a delay is usually extremely small (and sometimes even negligent) it is important to consider and may have an impact when we explore treatment options, as treatment often results in an effective delay on the system. The viral eclipse phase is the portion of time during the virus life cycle where the virus becomes uncoated upon entering the host cell and prior to the production of new virions. The delay, denoted τ, represents the time, in days, between infection of a target cell by a virus and production of new virus particles within the host.

4.9.1 Delayed Target-Cell-Limited Model

Thus, in order to represent the delay, our systems of ordinary differential equations becomes a system of three nonlinear delay differential equations denoted:

$$\text{(3a)}\quad \frac{dT}{dt} = s - dT(t-\tau) - \beta V(t)T(t-\tau)$$
$$\text{(3b)}\quad \frac{dI}{dt} = \beta V(t-\tau)T(t-\tau) - \delta I(t)$$
$$\text{(3c)}\quad \frac{dV}{dt} = pI(t) - cV(t)$$

With initial conditions $T(\theta) = T_0$, $I(\theta) = I_0$, $V(\theta) = V_0$ where $\theta \in [-\tau, 0]$.

These initial conditions are different from those of the standard target-cell-limited model. This is because $\frac{dT}{dt}$ and $\frac{dI}{dt}$ depend on solutions other than the present, and thus more information is required beyond the value of the populations at $t = 0$. For a delay differential equation information of the interval $[t_0 - \tau, t_0]$ is required. Thus in our case, initial conditions must be defined on the interval $[0 - \tau, 0]$ where τ is the value of the delay since we are starting at time $t_0 = 0$. All parameters remain the same as in the standard target-cell-limited model, except for the positive constant τ, which we have introduced. It is important to note that we also defined the rate of target cell production from the parameter λ to the parameter s for simplicity when explaining the eigenvalues. Furthermore, we can view the target-cell-limited model as a special case of the delayed model when $\tau = 0$.

4.9.2 Equilibrium Points

The Equilibrium points for the delayed target-cell-limited model remain the same as they were for the standard target-cell-limited model. Thus, the delayed target-cell-limited model has two biologically relevant equilibria denoted $P_n = (T, I, V)$ for $n = 1, 2$ where:

$$P_1 = \left(\frac{s}{d}, 0, 0\right)$$
$$P_2 = \left(\frac{c\delta}{p\beta}, \frac{p\beta s - \delta dc}{c\delta\beta}, \frac{p\beta s - \delta dc}{c\delta\beta}\right)$$

Similar to the standard system, we can again characterize P_1 as a viral free (viral clearance) equilibrium and P_2 as a viral persistence equilibrium.

In order to determine the stability of these equilibrium, it is necessary to examine the Jacobian for each equilibrium. However, the notion of a Jacobian and stability for a delayed system is distinct from that for a non-delayed system.

4.9.3 Jacobian

For $\tau > 0$, we can express the linearized form of the delay differential equation model in matrix form as follows:

$$\frac{d}{dt}\begin{bmatrix} T(t) \\ I(t) \\ V(t) \end{bmatrix} = J_0 \begin{bmatrix} T(t) \\ I(t) \\ V(t) \end{bmatrix} + J_\tau \begin{bmatrix} T(t-\tau) \\ I(t-\tau) \\ V(t-\tau) \end{bmatrix}$$

We can then define the characteristic equation to be of the form:

$$|J_0 + e^{-\lambda\tau} J_\tau - \lambda I| = 0$$

where $J = J_0 + e^{-\lambda\tau} J_\tau$ is the Jacobian of the system.

4.9.4 Stability and Bifurcation Analysis at P_1

We will now examine the stability of $P_1 = (\frac{s}{d}, 0, 0)$. For P_1

$$J_0 = \begin{bmatrix} -d & 0 & 0 \\ 0 & -\delta & 0 \\ 0 & p & -c \end{bmatrix} \text{ and } J_\tau = \begin{bmatrix} 0 & 0 & -\frac{s\beta}{d} \\ 0 & 0 & \frac{s\beta}{d} \\ 0 & 0 & 0 \end{bmatrix}$$

Thus, the Jacobian for the linearized time-delayed system at P_1 is:

$$J = \begin{bmatrix} -d & 0 & -\frac{e^{-\lambda\tau} s\beta}{d} \\ 0 & -\delta & \frac{e^{-\lambda\tau} s\beta}{d} \\ 0 & p & -c \end{bmatrix}$$

The characteristic equation of the Jacobian can be expressed in the form of the following exponential polynomial:

$$P(\lambda, e^{-\lambda\tau}) = \lambda^n + a_1^{(0)}\lambda^{n-1} + a_2^{(0)}\lambda^{n-2} + ... + a_n^{(0)} + e^{-\lambda\tau}(\lambda^n + a_1^{(1)}\lambda^{n-1} + a_2^{(1)}\lambda^{n-2} + ... + a_n^{(1)})$$

Similar to a non-delayed system, it is known that a critical point is asymptotically stable if all roots of the characteristic equation have negative real parts [7]. However, compared with the characteristic equation for the ordinary differential equation model, the characteristic equation for the delayed system is much more difficult to deal with. This primarily because the characteristic equation is transcendental in nature. Thus, there are infinitely many roots to the equation and it is extremely difficult to find the roots and oftentimes impossible to do so. In addition, we are no longer able to apply the Routh-Hurwitz criteria to help us characterize the sign of the real part of

the roots. Yet, it is often possible to determine analytically whether a given point is stable or not. In doing so, we will utilize Rouche's Theorem, along with the continuity of τ, which imply that the transcendental equation has roots with positive real parts if and only if it has purely imaginary roots. Thus, we shall determine if the characteristic equation has purely imaginary roots. We will then be able to determine conditions which yield negative parts for all of the eigenvalues and thus determine the stability properties of the equilibria.

From the Jacobian we obtain that the characteristic equation for P_1 is:

$$e^{-\lambda\tau}(d+\lambda)\big(-ps\beta - de^{-\lambda\tau}(-c-\lambda)(d+\lambda)\big) = 0$$

which can be expanded such that:

$$\lambda^3 + (c+d+\delta)\lambda^2 + (cd+c\delta+d\delta)\lambda - ps\beta e^{-\lambda\tau} - \frac{ps\beta}{d}e^{-\lambda\tau}\lambda + cd\delta = 0$$

This equation can be expressed as an exponential polynomial of the form:

$$\lambda^3 + a_1\lambda^2 + a_2\lambda + a_3e^{-\lambda\tau} + a_4e^{-\lambda\tau}\lambda + a_5 = 0$$

where

$a_1 = c+d+\delta$
$a_2 = cd+c\delta+d\delta$
$a_3 = -ps\beta$
$a_4 = \frac{-ps\beta}{d}$
$a_5 = cd\delta$

In order to determine the signs of the roots for the characteristic polynomial, we can assume that $\lambda = i\omega$ where $\omega > 0$. Substituting this expression into our characteristic equation, we obtain:

$$(i\omega)^3 + a_1(i\omega)^2 + a_2(i\omega) + a_3e^{-i\omega\tau} + a_4e^{-(i\omega)\tau}(i\omega) + a_5 = 0$$

which is equivalent to

$$-i\omega^3 - a_1\omega^2 + a_2i\omega + a_3(\cos(\omega\tau) - i\sin(\omega\tau)) + a_4(\cos(\omega\tau) - i\sin(\omega\tau))i\omega + a_5 = 0$$

Separating the real and imaginary parts, we get

Real: $-a_1\omega^2 + a_3\cos(\omega\tau) + a_4\sin(\omega\tau)\omega + a_5 = 0$
Imaginary: $-\omega^3 + a_2\omega - a_3\sin(\omega\tau) + a_4\omega\cos(\omega\tau) = 0$

We can rewrite these expressions as a system of equations where

$a_1\omega^2 - a_5 = a_3\cos(\omega\tau) + a_4\sin(\omega\tau)\omega$
$\omega^3 - a_2\omega = a_4\omega\cos(\omega\tau) - a_3\sin(\omega\tau)$

Squaring both sides, we receive

$$a_1^2\omega^4 - 2\omega^2 a_1 a_5 + a_5^2 = a_3^2\cos^2(\omega\tau) + 2\omega\cos(\omega\tau)\sin(\omega\tau)a_3a_4 + a_4^2\sin^2(\omega\tau)\omega^2$$
$$\omega^6 - 2\omega^4 a_2 + a_2^2\omega^2 = a_4\omega\cos(\omega\tau) - a_3\sin(\omega\tau)$$

Adding both equations together we receive

$$\omega^6 + (a_1^2 - 2a_3)\omega^4 + (a_2^2 - 2a_1a_5)\omega^2 + a_5^2 = a_3 + \omega^2 a_4^2$$

so we can definite the transcendental equation as

$$\omega^6 + (a_1^2 - 2a_3)\omega^4 + (a_2^2 - 2a_1a_5 - a_4^2)\omega^2 + (a_5^2 - a_3^2) = 0$$

For our analysis we let $z = \omega^2$.

such that

$$h(z) = z^3 + b_1z^2 + b_2z + b_3 = 0$$

where

$$b_1 = a_1^2 - 2a_2$$
$$b_2 = a_2^2 - 2a_1a_5 - a_4^2$$
$$b_3 = a_5^2 - a_3^2$$

Lemma. *if $b_2 > 0$ and $b_3 > 0$, then $h(z)$ has no positive real roots.*

Proof. We know that since $h(z) = z^3 + b_1z^2 + b_2z + b_3 = 0$,

$$\frac{dh(z)}{dz} = 3z^2 + 2b_1z + b_2$$

Setting equal to zero we can determine that the roots of $\frac{dh(z)}{dz}$ are

$$z_{1,2} = \frac{-b_1 \pm \sqrt{b_1^2 - 3b_2}}{3}$$

if $b_2 > 0$ then $b_1^2 - 3b_2 < b_1^2$ and thus $\sqrt{b_1^2 - 3b_2} < \sqrt{b_1^2} \implies \sqrt{b_1^2 - 3b_2} < b_1$.

As a result, neither z_1 nor z_2 is positive. Thus, $\frac{dh(z)}{dz}$ has no positive real roots. Since $h(0) = b_3 > 0$ by assumption, we know that $h(z)$ has no positive roots as well. □

Remark: This lemma implies that there is no ω such that $i\omega$ is an eigenvalue of the characteristic equation. Thus, the characteristic equation does not have a pair of purely imaginary roots. As a result, the real parts of all the eigenvalues of the characteristic equation are negative for all $\tau \geq 0$.

Theorem 4 (Local Asymptotic Stability of P_1)**.** *For the delayed target-cell-limited model, the viral extinction equilibrium for (P_1) given by*

$$(T, I, V) = \left(\tfrac{s}{d}, 0, 0\right)$$

if $R_0 < 1$, then the real parts of all the eigenvalues of the characteristic equation are negative and P_1 is stable when $0 \leq \tau < \tau_0$ and unstable when $\tau_0 < \tau$ where

$$\tau_0 = \frac{1}{\omega_0}\Big(\cos^{-1}\Big(\frac{a_3a_1\omega_0^2 - a_3a_5 - a_4a_2\omega_0^2 + \omega_0^4a_4}{a_4^2\omega_0^2 + a_3^2}\Big)\Big) + \frac{2\pi}{\omega_0}j \text{ for } j = 0, 1, 2, 3, ...$$

and

$$\begin{aligned} a_1 &= c + d + \delta \\ a_2 &= cd + c\delta + d\delta \\ a_3 &= -ps\beta \\ a_4 &= \tfrac{-ps\beta}{d} \\ a_5 &= cd\delta \end{aligned}$$

Proof. We know that

$$b_3 = a_5^2 - a_3^2$$

Thus,

$$b_3 = (cd\delta)^2 - (ps\beta)^2$$

We know that $R_0 = \frac{ps\beta}{cd\delta}$. Thus, $ps\beta = R_0(cd\delta)$ and

$$b_3 = cd\delta(1 - R_0)$$

Thus, if $R_0 < 1$, then $b_3 > 0$.

Furthermore, we know that

$$b_2 = a_2^2 - 2a_1a_5 - a_4^2$$

Thus,

$$b_2 = (cd + c\delta + d\delta)^2 - s(c + d + \delta)(cd\delta) - \frac{ps\beta^2}{d} = -(\frac{ps\beta}{d})^2 + (d\delta)^2 + c^2(d^2 + \delta^2)$$

.

We know that $\frac{ps\beta}{d} = R_0c\delta$ and thus

$$b_2 = -(R_0c\delta)^2 + (d\delta)^2 + c^2 + \delta^2 + c^2d^2 = c^2\delta^2(1 - R_0^2) + (d\delta)^2 + c^2d^2$$

Thus, if $R_0 < 1$ we know that $b_2 > 0$.

Additionally, by the previous lemma and remark, we know that since $b_3, b_2 > 0$ then $h(z)$ has no positive real roots and therefore the real parts of all the eigenvalues of the characteristic equation are negative for all $\tau \geq 0$. □

However, if $R_0 > 1$ then $b_3 < 0$ and thus, $h(0) < 0$ and as a result, $\lim_{z\to\infty} = \infty$ and thus $h(z)$ has at least one positive root which we will call z_0. As a result, the characteristic equation has a pair of purely imaginary roots $\pm i\omega_0$. Furthermore, if $R_0 > 1$, then there is potential that $b_2 < 0$. If $b_2 < 0$ then $\sqrt{b_1^2 - 3b_2} > b_1$, thus $z_1 = \frac{-b_1^2 + \sqrt{b_1^2 - 3b_2}}{3} > 0$ so $h(z)$ has a positive root and thus the

characteristic equation has a pair of purely imaginary roots $\pm i\omega_0$.

Let $\lambda(\tau) = i\omega(\tau)$ such that $\omega(\tau_0) = \omega_0$.

Then, we know from the system of real and imaginary parts of the characteristic equation that

$$a_1\omega_0^2 - a_5 = a_3\cos\omega_0\tau_0 + a_4\sin\omega_0\tau_0\omega_0$$

and

$$\omega_0^3 - a_2\omega_0 = a_4\omega_0\cos\omega_0\tau_0 - a_3\sin\omega_0\tau_0$$

Thus, we know that

$$a_3\sin\omega_0\tau_0 = a_2\omega_0 + a_4\omega_0\cos\omega_0\tau_0 - \omega_0^3$$

and that

$$\sin\omega_0\tau_0 = \frac{a_2\omega_0 + a_4\omega_0\cos\omega_0\tau_0 - \omega_0^3}{a_3}$$

Substituting this into the first equation, we receive

$$a_1\omega_0^2 - a_5 = a_3\cos\omega_0\tau_0 + a_4(\frac{a_2\omega_0 + a_4\omega_0\cos\omega_0\tau_0 - \omega_0^3}{a_3})\omega_0$$

Therefore,

$$a_1\omega_0^2 - a_5 = a_3\cos\omega_0\tau_0 + \frac{a_4a_2\omega_0^2}{a_3} + \frac{a_4^2\omega_0^2}{a_3}\cos\omega_0\tau_0 - \frac{\omega_0^4a_4}{a_3}$$

so

$$a_1\omega_0^2 - a_5 - \frac{a_4a_2\omega_0^2}{a_3} + \frac{\omega_0^4a_4}{a_3} = \cos\omega_0\tau_0(\frac{a_4^2\omega_0^2}{a_3} + a_3)$$

which implies that

$$a_3a_1\omega_0^2 - a_3a_5 - a_4a_2\omega_0^2 + \omega_0^4a_4 = \cos\omega_0\tau_0(a_4^2\omega_0^2 + a_3^2)$$

Thus,

$$\tau_0 = \frac{1}{\omega_0}\Big(\cos^{-1}\Big(\frac{a_3a_1\omega_0^2 - a_3a_5 - a_4a_2\omega_0^2 + \omega_0^4a_4}{a_4^2\omega_0^2 + a_3^2}\Big)\Big) + \frac{2\pi}{\omega_0}j \text{ for } j = 0, 1, 2, 3, ...$$

Therefore, P_1 is stable when $0 \leq \tau < \tau_0$ and unstable when $\tau_0 < \tau$. Thus, there exists a Hopf bifurcation at τ_0.

4.9.5 Stability and Bifurcation Analyses at P_2

We will now examine the stability of $P_2 = (\frac{c\delta}{p\beta}, \frac{ps\beta - cd\delta}{p\beta\delta}, \frac{ps\beta - cd\delta}{c\beta\delta})$. For P_2

$$J_0 = \begin{bmatrix} -d - \frac{ps\beta - cd\delta}{c\delta} & 0 & 0 \\ \frac{ps\beta - cd\delta}{c\delta} & -\delta & 0 \\ 0 & p & -c \end{bmatrix} \text{ and } J_\tau = \begin{bmatrix} 0 & 0 & -\frac{c\delta}{p} \\ 0 & 0 & \frac{c\delta}{p} \\ 0 & 0 & 0 \end{bmatrix}$$

Thus, the Jacobian for the linearized time-delayed system at P_2 is:

$$J = \begin{bmatrix} -d - \frac{ps\beta - dc\delta}{c\delta} & 0 & -\frac{e^{-\lambda\tau}c\delta}{p} \\ \frac{ps\beta - dc\delta}{c\delta} & -\delta & \frac{e^{-\lambda\tau}c\delta}{p} \\ 0 & p & -c \end{bmatrix}$$

From the Jacobian we obtain that the characteristic equation for P_2 is:

$$\frac{e^{-2\lambda\tau}(\delta p^2 c(\delta+\lambda)(-\lambda-c)e^{2\lambda\tau}(\beta ps + \delta\lambda c) - p(-d\delta^3 pc^3 e^{\lambda\tau} - \delta^3\lambda pc^3 e^{\lambda\tau}))}{\delta^2 p^2 c^2} = 0$$

Which can be expanded such that

$$d\delta^3 p^2 c^3 e^{-\lambda\tau} + \lambda(\delta^3 p^2 c^3 e^{-\lambda\tau} - \beta\delta p^3 c^2 s - \beta\delta^2 p^3 cs - \delta^3 p^2 c^3) - \beta\delta^2 p^3 c^2 s - \delta^2\lambda^3 p^2 c^2 + \lambda^2(-c\beta\delta p^3 s - \delta^2 p^2 c^3 - \delta^3 p^2 c^2) = 0$$

This equation can be expressed as an exponential polynomial of the form:

$$\lambda^3 + a_1\lambda^2 + a_2\lambda + a_3 e^{-\lambda\tau} + a_4 e^{-\lambda\tau}\lambda + a_5 = 0$$

where

$a_1 = c + \frac{p\beta s}{c\delta} + \delta$
$a_2 = \frac{ps\beta}{c} + \frac{ps\beta}{\delta} + c\delta$
$a_3 = -cd\delta$
$a_4 = -c\delta$
$a_5 = ps\beta$

Knowing that $R_0 = \frac{sp\beta}{cd\delta}$ we can rewrite $a_1, a_2, ..., a_5$ as:

$a_1 = c + dR_0 + \delta$
$a_2 = d\delta R_0 + cdR_0 + c\delta$
$a_3 = -ps\beta R_0$
$a_4 = -\frac{ps\beta}{dR_0}$
$a_5 = cd\delta R_0$

Similar to P_1 we can say that $h(z) = z^3 + b_1 z^2 + b_2 z + b_3 = 0$ where

$b_1 = a_1^2 - 2a_2$
$b_2 = a_2^2 - 2a_1 a_5 - a_4^2$
$b_3 = a_5^2 - a_3^2$

Thus, for P_2, we know that:

$$b_2 = d^2 R_0^2(c^2 + \delta^2) \text{ and } b_3 = R_0^2(cd\delta)^2(1 - R_0^2).$$

Furthermore, we know that $R_0 > 1$ for P_2 to exist. Thus, we know that $b_3 < 0$ and $b_2 > 0$.

Since $b_3 < 0$, we know that $h(0) < 0$ and thus that $\lim_{z\to\infty} h(z) = \infty$. Thus, $h(z)$ has a positive root, z_0, and thus the transcendental equation has at least one positive root, ω_0. This implies that the characteristic equation has a pair of purely imaginary toots $\pm i\omega_0$.

For P_1 we derived the expression for a Hopf bifurcation as

$$\tau_0 = \frac{1}{\omega_0}\Big(\cos^{-1}\Big(\frac{a_3a_1\omega_0^2 - a_3a_5 - a_4a_2\omega_0^2 + \omega_0^4a_4}{a_4^2\omega_0^2 + a_3^2}\Big)\Big) + \frac{2\pi}{\omega_0}j \text{ for } j = 0, 1, 2, 3, ...$$

We can again use this expression from P_1 and substitute the values for $a_1, a_2, ...a_5$ for P_2 and can state the following theorem for P_2:

Theorem 5 (Local Asymptotic Stability of P_2)**.** *For the delayed target-cell-limited model, the viral extinction equilibrium for (P_2) given by*

$$(T, I, V) = \Big(\tfrac{c\delta}{p\beta}, \tfrac{ps\beta - cd\delta}{p\beta\delta}, \tfrac{ps\beta - cd\delta}{c\beta\delta}\Big)$$

P_2 is stable when $0 \le \tau < \tau_0$ and unstable when $\tau_0 < \tau$ where $\tau_0 = \frac{1}{\omega_0}\Big(\cos^{-1}\Big(\frac{a_3a_1\omega_0^2 - a_3a_5 - a_4a_2\omega_0^2 + \omega_0^4a_4}{a_4^2\omega_0^2 + a_3^2}\Big)\Big)$. where:

$$a_1 = c + dR_0 + \delta$$
$$a_2 = d\delta R_0 + cdR_0 + c\delta$$
$$a_3 = -ps\beta R_0$$
$$a_4 = -\tfrac{ps\beta}{dR_0}$$
$$a_5 = cd\delta R_0$$

Proof. The proof for Theorem 5 is exactly the same as that for Theorem 4 with the only difference being the values for $a_1, a_2, ...a_5$. □

4.9.6 Parameter Estimation and Numerical Simulations

Table 8 highlights the estimates for the parameters for the delayed target-cell-limited model. From the table, we can see that the estimates for the parameters remain relatively close to those of the standard target-cell-limited model, and that the value of the delay is essentially zero (O^{-9}). Thus, the delay is negligible, and does not play a huge role in governing the overall dynamic of the system. This notion is further illustrated when we conduct some numerical simulations.

From the figures, we can see that for a delay where $\tau = 0, 0.25, 0.5, 0.75, 1$ the behavior of the system looks relatively similar. The only noticeable difference due to the delay is the minimum population of target cells achieved immediately following the peak viral load. As the delay increases, the minimum number of target cells decreases. Yet, importantly, the value for the steady state does not change due to the length of the delay. However, our bifurcation and stability analysis from Section 4.8.4 and 4.8.5 suggest that there is a value of τ that can have a significant impact on the behavior and stability of the system.

Table 8: Parameter Estimates for the Delay Target-Cell-Limited Model

parameter	**value**	$s.e._{lin}$	$r.s.e_{lin}$
p_{pop}	427.95098	141.53865	33.07
d_{pop}	0.00818	0.00105	12.79
δ_{pop}	0.27428	0.04259	15.53
$V_{i_{pop}}$	3.95698	0.27713	7
τ_{pop}	2.18×10^{-9}	7.2×10^{-6}	3.3×10^{5}

In Figure 16, we vary the length of the delay and illustrate the impact that changes in τ have on the behavior of the system. The top image represents the non-delayed system, or where $\tau = 0$. In descending order we increase the value of τ by 0.25, until $\tau = 1$. Given the value of R_0, which we know is greater than one, and according to Theorem 5, we would expect that the system will achieve a stable viral persistence equilibrium when $0 \leq \tau < \tau_0$, however that the equilibrium will become unstable when $\tau_0 < \tau$ where

$$\tau_0 = \frac{1}{\omega_0}\Big(\cos^{-1}\Big(\frac{a_3a_1\omega_0^2 - a_3a_5 - a_4a_2\omega_0^2 + \omega_0^4a_4}{a_4^2\omega_0^2 + a_3^2}\Big)\Big)$$

The figure highlights that as the length of the delay increases from 0 to 1, the population of the virus remains largely unaffected and the viral persistence equilibrium is stable since both the virus and Target cells achieve the same steady state as the non-delayed system. While the virus population over time and equilibria remain the same, the population of the Target cells exhibits increased dynamical behavior during the growth and peak phases of the viral cycle. More specifically, the target cell population changes drastically as it approaches the minimum value which is achieved post peak viral load.

This change would correspond to a much weaker and much more susceptible immune system during this time period where the patient would be prone to infections, and in our case, possibly immense cancerous cell growth. However, as shown above if we keep increasing the value of the delay, a bifurcation will occur within the system.

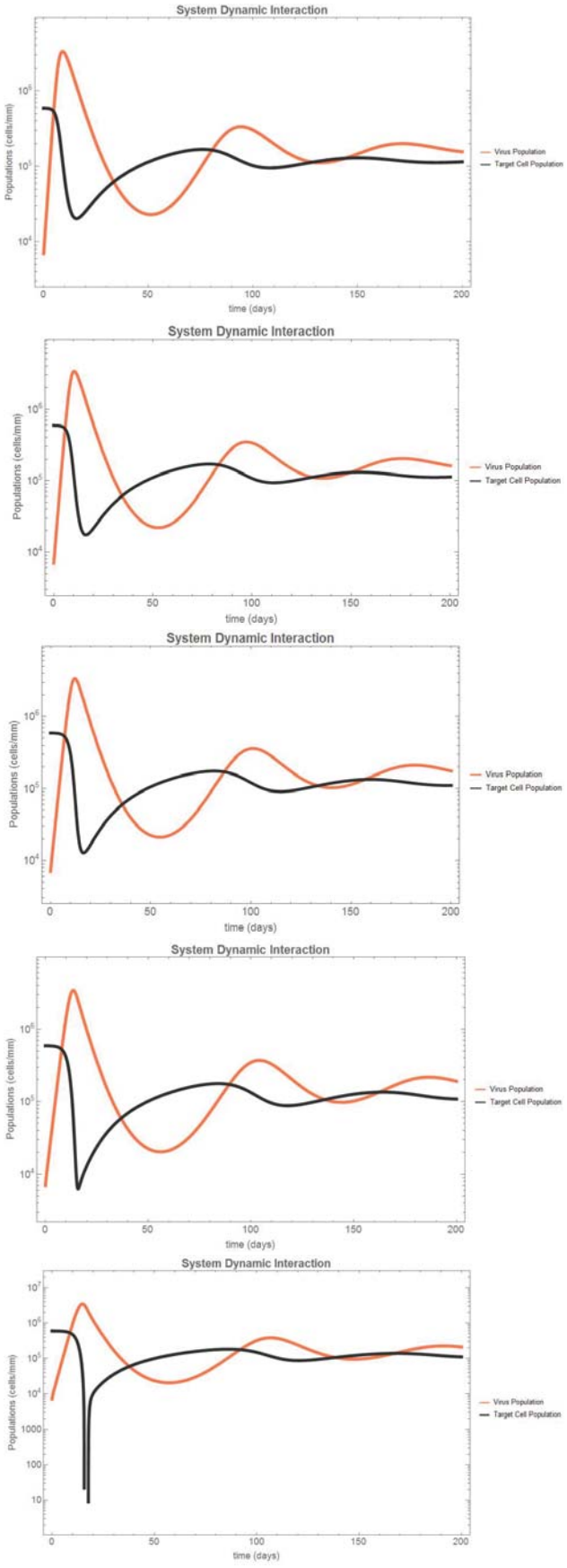

Figure 16: The effect of varying the delay, τ.

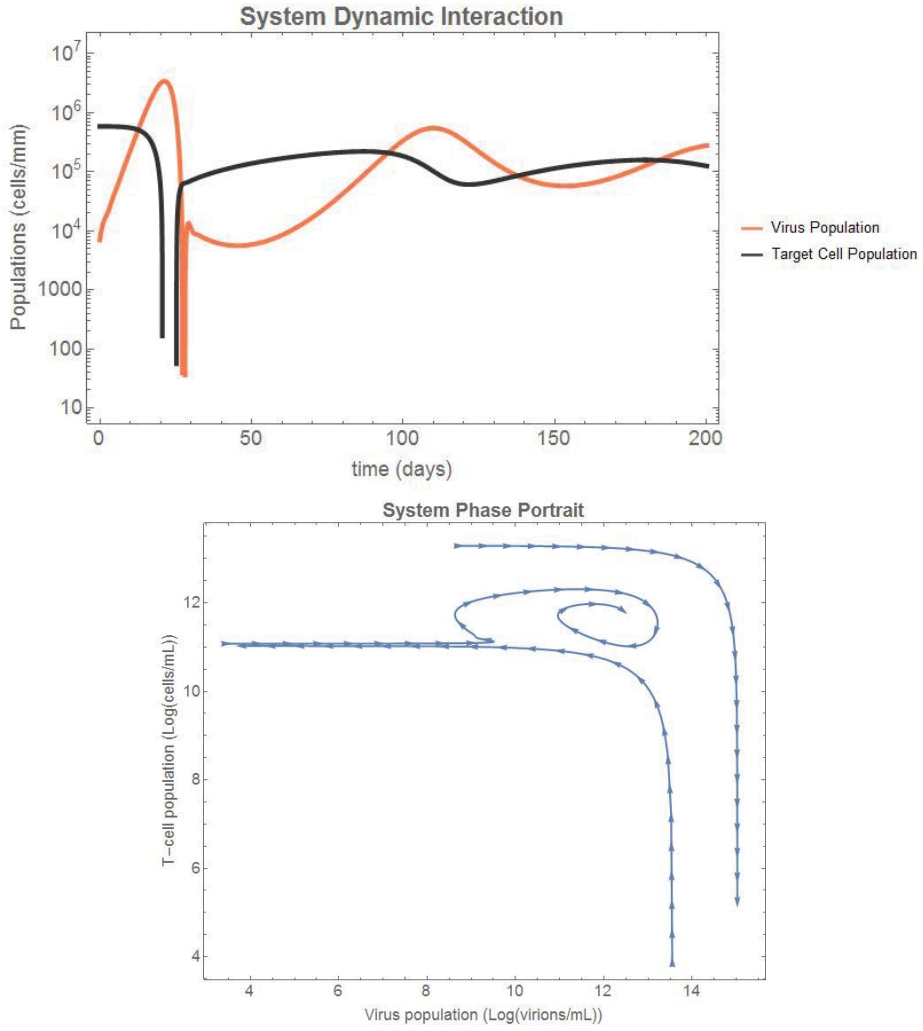

Figure 17: The bifurcation that results from the change in the value of the delay, τ.

Figure 17 illustrates the virus and target cell populations in the system dynamic interaction plot as well as the stability characteristics in the system phase portrait where $\tau = 2.3$. Similar to the plots in Figure 16, the cases where $0 \leq \tau \leq 1$, the viral clearance equilibrium remains stable. However, unlike in Figure 16, we can see in Figure 17 that the delay's effect on both the target cells as well as the virus is much more pronounced and the dynamics are becoming increasingly complicated. This notion is underscored by the increasing complexity of the system phase portrait, especially post peak viral load. Especially notable is the drastic decrease seen in the viral load during this time period. Furthermore, after the decrease in the peak viral load, the virus resurges, returning to a value which is approximately 10% of the steady state value. This dynamic is even more interesting when we consider that during this time period, the population of target cells remains almost unchanged. Yet, despite the fact that the dynamics between the populations seem to be becoming more complicated, the long term equilibria remains unaffected when $\tau = 2.3$.

Next, we explored what occurs with the system when we make small deviations to the delay, and we notice that a bifurcation occurs, just as we predicted. Figure 18 illustrates the notion of a bifurcation occurring with respect to the value of the delay.

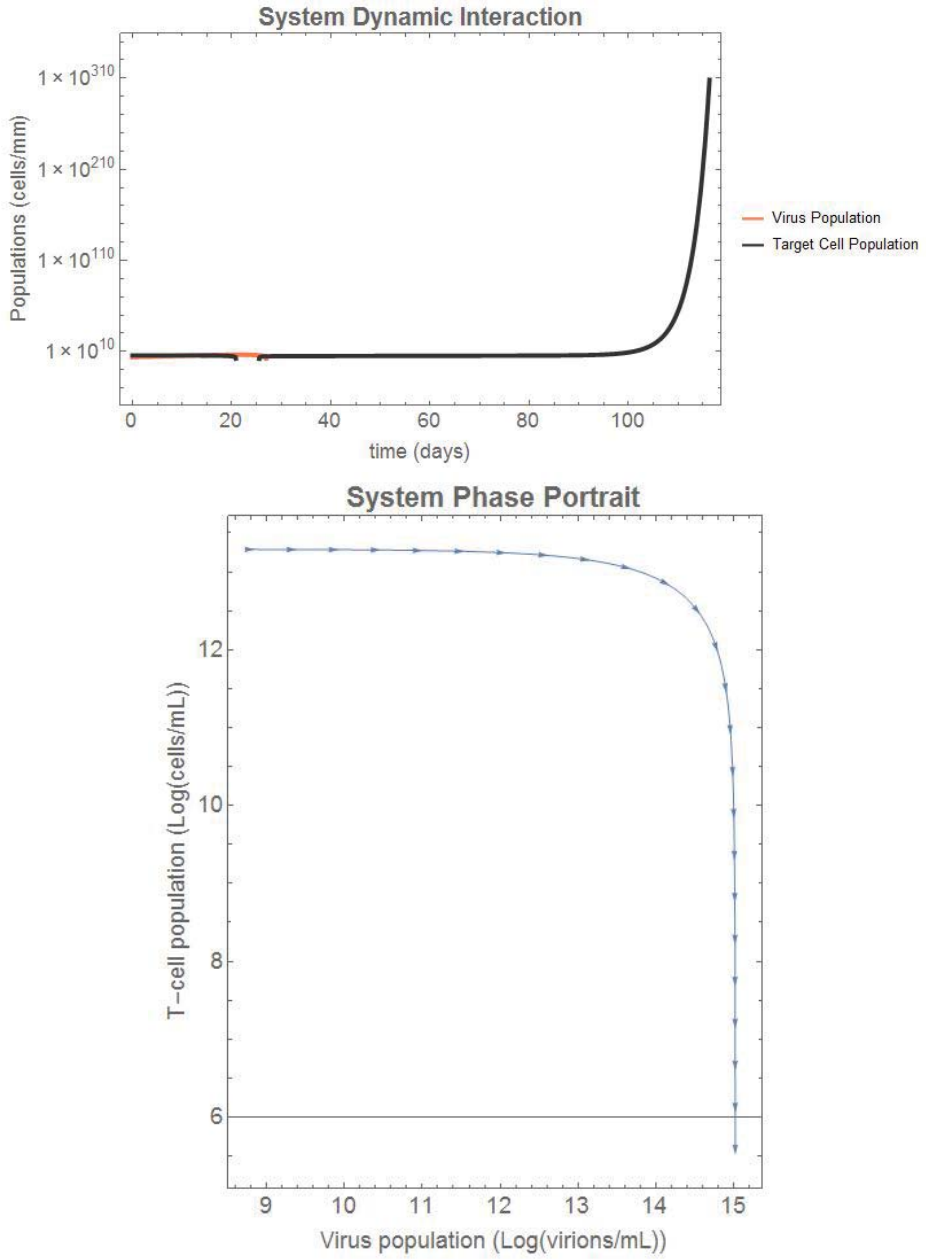

Figure 18: The bifurcation that results from the change in the value of the delay, τ.

When we set $\tau = 2.35$, we see a drastic change in the behavior of the system, specifically the long term equilibria. As highlighted in Figure 18, the population of the Target cells no longer

achieves a steady state, resulting in an unstable equilibria where the virus population remains at a positive population and the target cell population increases indefinitely. This bifurcation represents the case where $\tau > \frac{1}{\omega_0}\Big(\cos^{-1}\left(\frac{a_3a_1\omega_0^2 - a_3a_5 - a_4a_2\omega_0^2 + \omega_0^4a_4}{a_4^2\omega_0^2 + a_3^2}\right)\Big)$. While this is biologically infeasible, the population of the target cells by day 115 is $O(10^{110})$ $\frac{cells}{mL}$, it is an illustration the bifurcation we derived in the previous section does indeed exist within the system.

While this seems like a purely mathematical exercise, especially given that the delay in the system is so small, the bifurcation has extremely important implications for treatment therapies and effective treatment of patients. We will develop and discuss this notion in the section which deals with the Treatment Model.

5 Constrained Target-Cell-Limited Model

5.1 Model Development

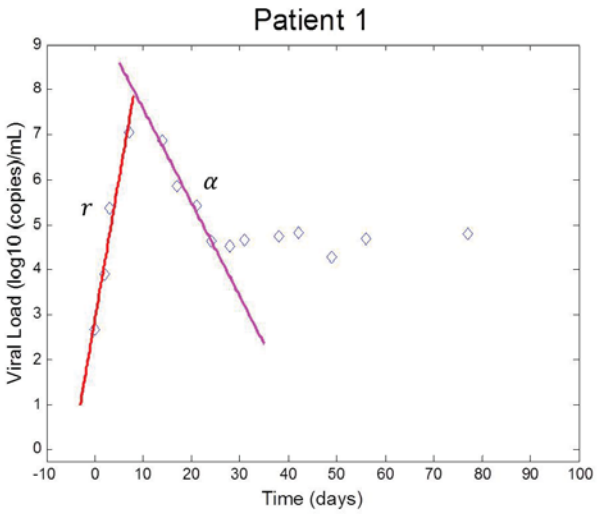

Figure 19: A schematic of the calculation of the rate of viral decay, α.

In examining our fits for patients 1 through 14 given by the target-cell-limited model, we noticed that the model seemed to consistently underestimate the magnitude of the viral decay phase, we received approximately 0.242 $days^{-1}$ vice an expected ≈ 0.8 $days^{-1}$. Furthermore, we can also see that the model does not seem to fit the data very well during the decay phase; the model tends to overestimate the value of the viral load. Thus, using both the qualitative and quantitative analyses, we determined that the model overestimated the viral load during the time from the peak viral load until the steady state. In the target-cell-limited model where $c \gg \delta$ the concentration of infected cells and virus become equilibrated; thus, their values are approximately proportional to one another [30].

Therefore, after the peak viral load and before the establishment of a steady state, the infected cells should decay at approximately the same rate as the virus and thus we use the easy to estimate rate of viral decay from the peak, α, in order to estimate the net loss of infected cells. We know that the rate of viral decay will underestimate the true infected cell death rate, and thus α will be slightly less than δ during the decay phase. However, the approximation should result in a much more accurate value of δ. Thus, the constrained target-cell-limited model uses the individual estimates of α in order to estimate the value of δ during the exponential decay phase of the virus after the peak viral load. This usage of α serves a constraint added to the standard target-cell-limited model and thus we refer to this second model as the constrained target-cell-limited model.

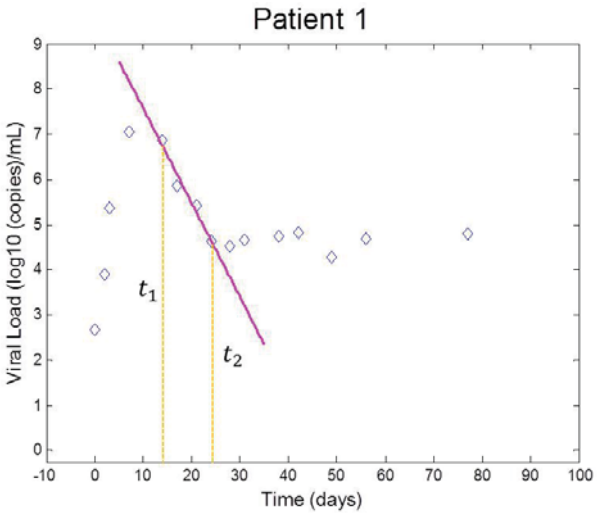

Figure 20: A visual representation of the constraints imposed by the target-cell-limited model.

In deriving the model we know that,

$V \approx \frac{p}{c}I \implies I \approx \frac{c}{p}V \implies \frac{c}{p}\frac{dV}{dt} = \beta VT - \delta\frac{c}{p}V \implies \frac{dV}{dt} = \left(\beta\frac{p}{c}T - \delta\right)V = -\alpha V \implies -\alpha = \beta\frac{p}{c}T - \delta \implies \delta = \beta\frac{p}{c}T + \alpha$

Thus, we can define a piece wise function which describes the three phases of the model the occur during the period of infection (the viral production, viral decay, and steady state phases). The model considers the same populations as the Target-Cell-Limited Model. Thus, we have a system of three nonlinear ordinary differential equations to describe the dynamics of the populations:

$$\text{(4a)}\quad \frac{dT}{dt} = \lambda - dT(t) - (r+\delta)\frac{c}{pT_0}V(t)T(t)$$

$$\text{(4b)}\quad \frac{dI}{dt} = (r+\delta)\frac{c}{pT_0}V(t)T(t) - f(t)I(t)$$

$$\text{(4c)}\quad \frac{dV}{dt} = pI(t) - cV(t)$$

$$\text{where } \begin{cases} f(t) = \delta & 0 \le t \le t_1 \\ f(t) = \beta\frac{p}{c}T(t) + \alpha & t_1 \le t \le t_2 \\ f(t) = \delta & t_2 \le t_{max} \end{cases}$$

Table 9: Parameters for the Constrained Target-Cell-Limited Model

Parameter	**Biological Interpretation**	**Units**	**Known Value**
λ	Target cell production rate	$(Cells)mL^{-1}days^{-1}$	dT_0
β	Rate of infection	$(mL)Cells^{-1}days^{-1}$	$(r+d)\frac{c}{pT_0}$
d	Target cell death rate	$days^{-1}$	Estimated*
δ	Infected cell death rate	$days^{-1}$	Estimated*
p	Viral production rate	$days^{-1}$	Estimated*
c	Viral clearance rate	$days^{-1}$	23
α	Rate of Viral Decay	$days^{-1}$	Estimated* (using α)
t_1	Initial time of viral decay	$days$	From Data*
t_2	final time of viral decay	$days$	From Data*

Table 10: Initial Conditions for the Constrained Target-Cell-Limited Model

Initial Conditions	**Value**	**Units**
T_0	5.9×10^5	$(Cells)mL^{-1}$
I_0	$\frac{c}{p}V_0$	$(Cells)mL^{-1}$
V_0	Estimated*	$(Cells)mL^{-1}$

The asterisk in Tables 9 and 10 denotes estimations that we carried our for the Constrained Target-cell-limited model using the data from the patients from Section 2. In our estimations for the model the value of δ does not apply for all time as is illustrated by the piece wise definition of the death rate of infected cells. During the viral production and steady state stages, the value of δ

will remain the same as previously determined, however, as mentioned previously, during the viral decay we will use the estimation of the rate of viral decay α in order to solve for the death rate of the infected cells.

5.2 Parameter Estimates

Table 11: Estimates for the Rate of Viral Decay

Patient	a_{ind}	a_{pop}
1	0.481	0.478
2	0.542	0.530
3	0.606	0.495
4	0.661	0.523
5	0.507	0.467
6	0.884	0.637
7	0.367	0.394
8	0.423	0.441
9	0.529	0.505
10	1.019	0.675
11	0.377	0.510
12	0.223	0.347
13	0.899	0.639
14	0.896	0.697
Average	0.601	0.524

This hypothesis is supported since the estimate for the rate of viral decay, as indicated by the value of δ displayed within Table 9, underestimates what we expect. As shown in Ribeiro et al. [3], we expect the value of δ to be approximately $0.4 - 0.83$ $days^{-1}$. Our δ value of 0.242 $days^{-1}$ underestimates the true rate of viral decay during the time between the peak viral load and the steady state.

In an effort to achieve a better fit for the data, specifically during the phase between the peak viral load and the steady state, we constrained the standard target-cell-limited model as described in section 5.1. In order to employ the new model, we first estimated α, the rate of viral decay, for each one of the patients. In estimating α, we employed the same process we used to estimate r first using Monolix in order to estimate the individual fits based off the population, which we denote as α_{pop} as well as the individual fits achieved through a linear regression in MATLAB which we call α_{ind}. Similar to our estimates of r, and using both Monolix and MATLAB, we are able to easily determine the value for α both for the population as well as individual fits. The resulting values for α are displayed in the table below.

As mentioned previously, we determined $\delta = \beta \frac{p}{c} T + \alpha$ and fit the virus concentration data using the constrained target-cell-limited model. The constrained target-cell-limited model seems to capture the behavior of the virus during the viral decay phase much more effectively than the standard target-cell-limited model as illustrated by the plots for patients 7 - 9 in Figure 10. We can see from this figure that the constrained target-cell-limited model does a much better at predicting the peak viral load in all three of the patients. Furthermore, the model seems to better predict the viral population during the steady state; as we can see from the figure, the standard target-cell-limited model suggests that the viral population varies significantly during this time period, however, the data does not exhibit the same variance during this stage. Thus, while they both exhibit similar dynamics during the viral growth stage, the constrained model is much better at characterizing the peak viral load and decay phase as well as the long term behavior of the infection.

While the constrained target-cell-limited model appeared to better fit the data, the value for δ achieved by the constrained target-cell-limited model is even smaller than that of the standard target-cell-limited model at 0.154 $days^{-1}$ vs 0.242 $days^{-1}$, and thus still much smaller than the value that we expected.

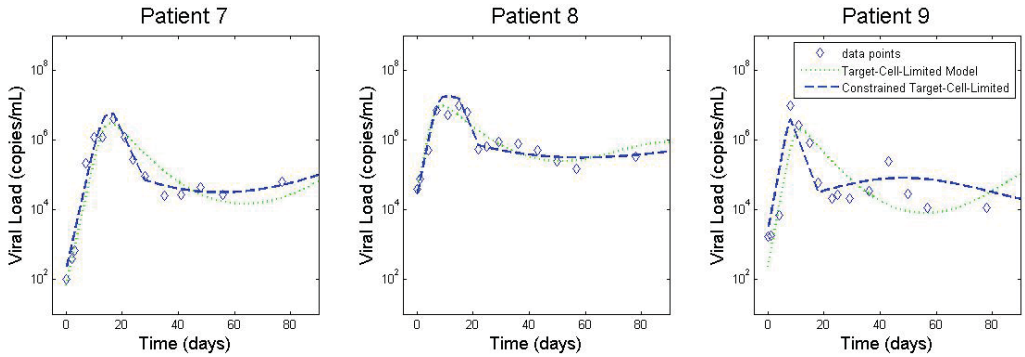

Figure 21: The Target-Cell-Limited Model and Constrained Target-Cell-Limited Model Applied to Patients 7 - 9.

Table 12: Parameter Estimates for the Constrained Target-cell-limited model

Parameters	**Values**	$s.e._{lin}$	$r.s.e._{lin}$
p_{pop}	843.2079	312.499	37.06
d_{pop}	0.00207	0.00076	36.81
δ_{pop}	0.15438	0.05351	34.66
$V_{0_{pop}}$	3.93387	0.30022	7.63

We suspect that there are multiple reasons for this discrepancy. Primarily, the smaller value for the infected cell death rate results from the fact that in the constrained model, δ is only defined during the time periods before the peak viral load and after the steady state as illustrated in Figure 22 by the blue and yellow sections of the graph. A small value for δ during the initial viral expansion stage prior to peak viral load seems reasonable because this initial stage is characterized by a lag in any productive immune response. Immune system responses to HIV infection are extremely complex and thus we anticipate that during the viral growth phase the immune system is not able to mount a robust response. As a result, and thus the death of infected cells is primarily a result of cytopathic effects, which yield a smaller value of δ than we would expect during an

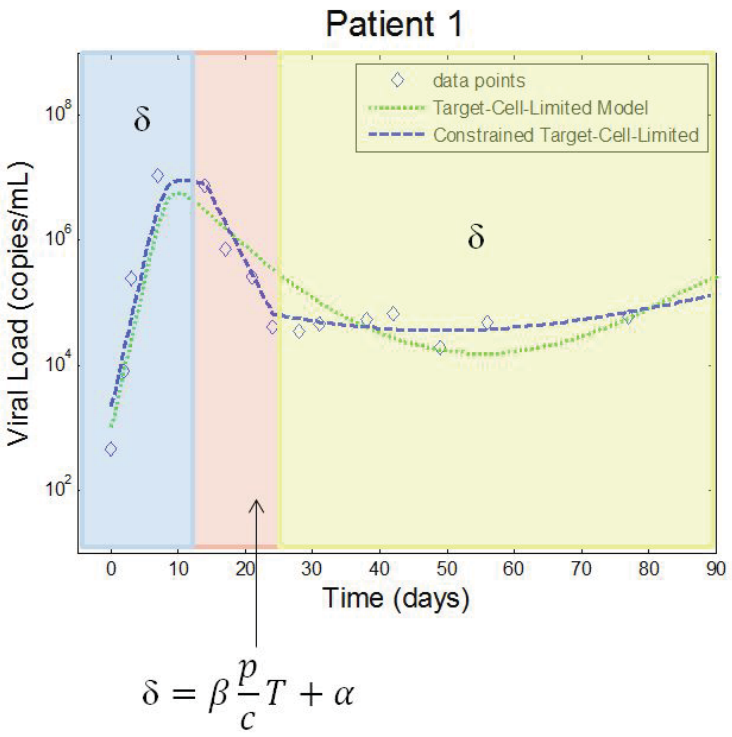

Figure 22: A visual representation of the behavior of delta exhibited by the target-cell-limited model.

immune response. This argument is
strengthened by our knowledge from studies in [34] where they determined that the peak viral load point is often the first time where a significant immune response is seen.

Furthermore, during the period between the peak viral load and the establishment of a steady state, the value for δ is actually defined as $\beta\frac{p}{c}T(t)+\alpha$. Thus, during this stage we know that since all of the parameters are positive that $\delta \geq \alpha$. The value of $\beta\frac{p}{c}T(t)+\alpha$ during that time is ≈ 0.78 $days^{-1}$ meaning that δ will be greater than or equal to 0.78 $days^{-1}$. This estimate is much closer to the behavior that we expect during this phase. This stage where we use α to define δ in our model is highlighted by the red portion of the Figure.

Furthermore, we know that HIV has a high affinity for mutation in order to evade an immune response. Thus, after the virus reaches a steady state, as shown in Figure 22 by the stage highlighted in yellow, the value of δ should be expected to decrease again since the virus would be undergoing significant mutations and thus is able to effectively escape the response. Therefore, similar to the behavior during the viral expansion stage, we expect that the infected cell death is due primarily to cytopahic effects, which would result in a lower natural death rate for the infected cells, causing the numerical value for δ to decrease. Therefore, while the value for δ initially seems much different than the quantity that we expect based on the literature, we can see that the biology supports the case for a smaller δ value.

5.3 Sensitivity Analysis

The corresponding sensitivity systems for β, δ, and p for the constrained target-cell-limited model are:

For β:

(4d) $S'_{T_\beta(t)} = -\big(V(t)S_{T_\beta(t)} + S_{V_\beta(t)}\big) - dS_{T_\beta(t)}$

(4e) $S'_{I_\beta(t)} = \big(V(t)S_{T_\beta(t)} + S_{V_\beta(t)}\big) - g(t)I(t) - f(t)S_{I_\beta(t)}$

(4f) $S'_{V_\beta(t)} = pS_{I_\beta(t)} - cS_{V_\beta(t)}$

where $f(t) = \begin{cases} \delta & 0 \leq t \leq t_1 \\ \beta\frac{p}{c}T(t)+\alpha & t_1 \leq t \leq t_2 \\ \delta & t_2 \leq t_{max} \end{cases}$

and $g(t) = \begin{cases} 0 & 0 \leq t \leq t_1 \\ \frac{p}{c}T(t) + \beta\frac{p}{c}S_{T_\beta} & t_1 \leq t \leq t_2 \\ 0 & t_2 \leq t_{max} \end{cases}$

For δ:

(4g) $S'_{T_\delta(t)} = -\beta\big(V(t)S_{T_\delta(t)} + S_{V_\delta(t)}\big) - dS_{T_\delta(t)}$

(4h) $S'_{I_\delta(t)} = \beta\big(V(t)S_{T_\delta(t)} + S_{V_\delta(t)}\big) - g(t)I(t) - f(t)S_{I_\delta(t)}$

(4i) $S'_{V_\delta(t)} = pS_{I_\delta(t)} - cS_{V_\delta(t)}$

where $f(t) = \begin{cases} \delta & 0 \le t \le t_1 \\ \beta\frac{p}{c}T(t) + \alpha & t_1 \le t \le t_2 \\ \delta & t_2 \le t_{max} \end{cases}$

and $g(t) = \begin{cases} 1 & 0 \le t \le t_1 \\ \beta\frac{p}{c}S_{T_\delta} & t_1 \le t \le t_2 \\ 1 & t_2 \le t_{max} \end{cases}$

For p:

(4j) $S'_{T_p(t)} = -\beta\big(V(t)S_{T_p(t)} + S_{V_p(t)}\big) - dS_{T_p(t)}$

(4k) $S'_{I_p(t)} = \beta\big(V(t)S_{T_p(t)} + S_{V_p(t)}\big) - g(t)I(t) - f(t)S_{I_p(t)}$

(4l) $S'_{V_p(t)} = S_{I_p(t)} - cS_{V_p(t)}$

where $f(t) = \begin{cases} \delta & 0 \le t \le t_1 \\ \beta\frac{p}{c}T(t) + \alpha & t_1 \le t \le t_2 \\ \delta & t_2 \le t_{max} \end{cases}$

and $g(t) = \begin{cases} 0 & 0 \le t \le t_1 \\ \frac{\beta}{c}T(t) + \beta\frac{p}{c}S_{T_p} & t_1 \le t \le t_2 \\ 0 & t_2 \le t_{max} \end{cases}$

Examining the sensitivity of the system resulting from changes in the same three parameters we did for the standard target-cell-limited model (β, the rate of infection, δ, the death rate of infected cells, and p, the production rate of the virus), Figure 23 suggests that changes in the parameters for the constrained target-cell-limited model do not have a large effect on the behavior of the system. This is illustrated by the fact that as the parameters change, the values for the rate of viral production, peak viral load, rate of viral decay, as well as steady state values remain relatively constant.

In addition, the dynamics during the interim between these stages seem to be consistent and they have the same basic functional form without significant deviation or variation. Patient 13 shows the most change in behavior as the parameters are varied, specifically with regard to δ and β, however, this change is certainly not to the same extent as we saw for patient 13 when examining the standard target-cell-limited model. In fact the limited variation that does occur within the models, only impacts the viral population after the steady state is achieved. Prior to achieving the steady state there is little variance within the population as the changes in parameters occur. Thus, the constrained target-cell-limited model appears to be robust and is not extremely sensitive to parameter inputs.

However, upon further examination of the other patients in the study, it becomes clear that the changes in parameters have a massive impact on the behavior of the system with respect to the viral

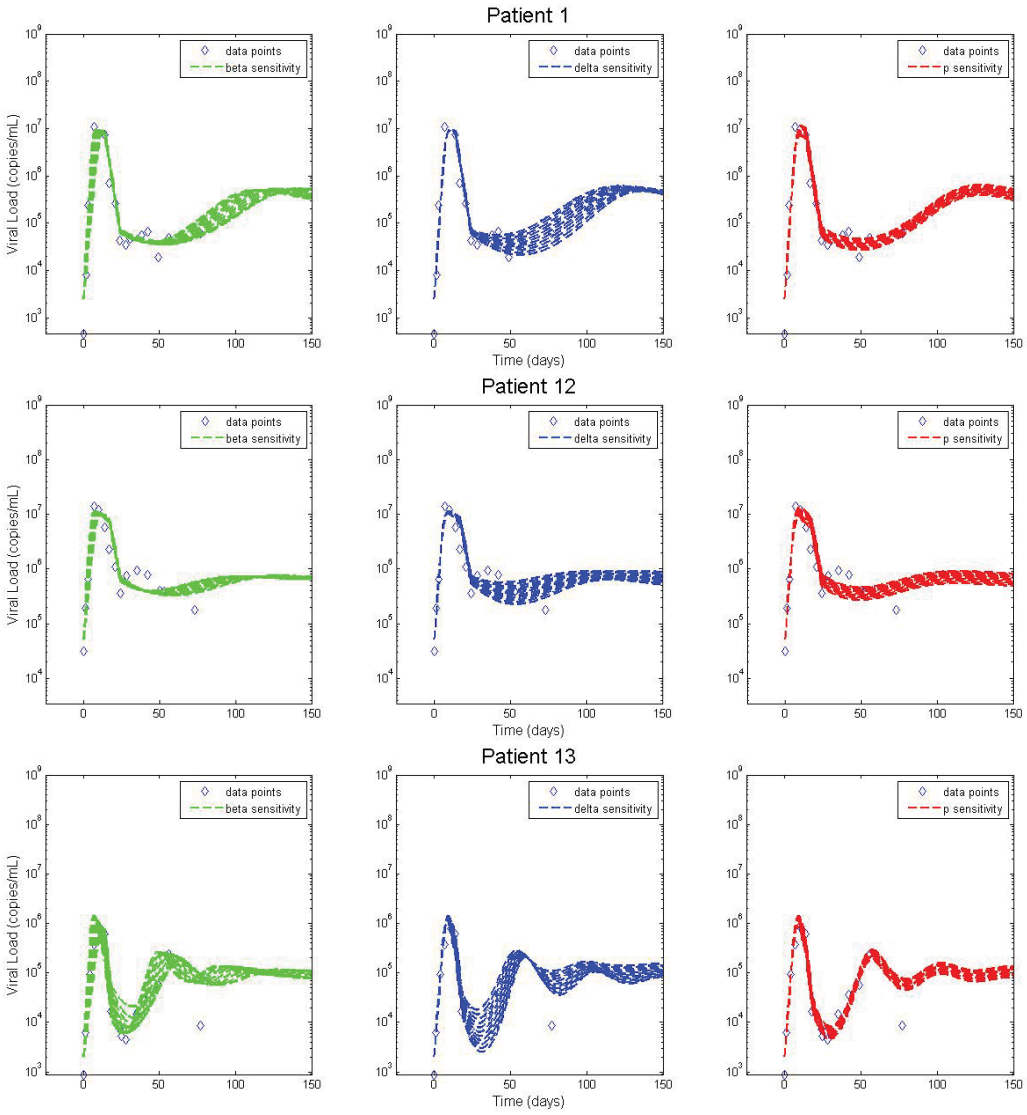

Figure 23: The effect of varying the parameters β, δ, and p in patients 1, 12, and 13.

load. For instance, with regard to patients 4 and 11, the behavior begins to change dramatically as illustrated in figure 24. We can see that specifically, when small changes are made to the value of β, the behavior of the model changes significantly as the parameter is varied.

Furthermore, we see that while the rate of viral production, peak viral load, and rate of viral decay remain relatively the same during the change in parameter values, the behavior during the steady state is dramatically different. This suggests that the model is extremely sensitive to the value of the parameters with respect to these patients.

In addition, the model appears to be sensitive to changes in δ and even p, something that we did not see in the standard model. Yet, similar to the patients we examined with the constrained

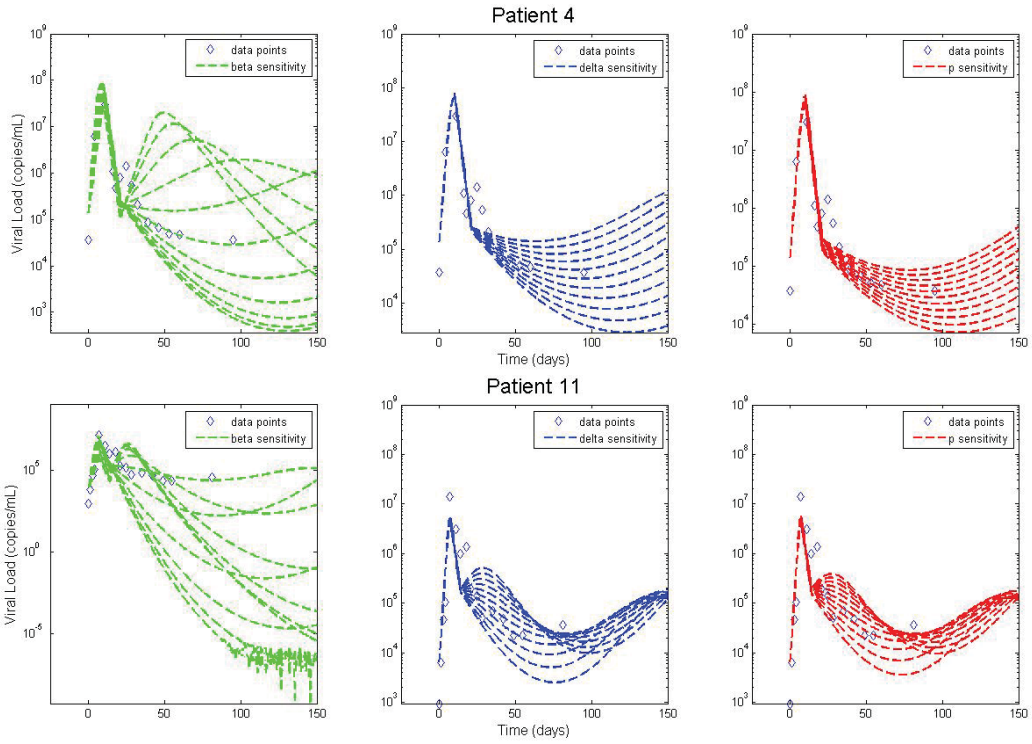

Figure 24: The effect of varying the parameters β, δ, and p.

target-cell-limited model previously, this sensitivity exhibited by the model seems to only be occurring during the steady state. Prior to that time, the model is relatively robust. This is likely a result of careful estimation of the rate of viral production and rate of viral decay which are easily estimated with a large degree of confidence and certainty and implemented in the constrained model.

This difference in stability for the constrained model when compared to the standard model likely results from the manner in which we defined the parameters. Specifically with respect to the infected cell death rate, we define δ during a time where the death rate would likely be extremely difficult to estimate as a result of having to distinguish between the natural death rate and any sort of lagged immune response. This sensitivity also permeates that for the other parameters, which explains why all three (β, δ, and p) exhibit the sensitivity characteristic in this model.

6 Simple Immune Model

The Simple Immune Model was proposed by in order to include the effects of a cell-mediated immune response. The model extends the target-cell-limited model by accounting for the loss of infected cells during the viral transient peak by the proliferation of an immune response, specifically represented by the growth of an immune effector cell population and proliferation of a robust immune response. The response is dependent upon the interaction between infected cells and the immune cells via michaelis-menten dynamics. Furthermore, this response allows for the possible early control of the virus. Since we added an additional compartment of the immune response, the Simple Immune model considers four distinct populations which are denoted:

$T(t)$: concentration of target cells at time t,
$I(t)$: concentration of infected cells at time t,
$V(t)$: concentration of free virus at time t,
$E(t)$: concentration of immune effector cells at time t.

The model is a system of four nonlinear ordinary differential equations denoted:

$$\text{(5a)}\quad \frac{dT}{dt} = \lambda - \beta V(t)T(t) - dT(t)$$
$$\text{(5b)}\quad \frac{dI}{dt} = \beta V(t)T(t) - \delta I(t) - k_E E(t)I(t)$$
$$\text{(5c)}\quad \frac{dV}{dt} = pI(t) - cV(t)$$
$$\text{(5d)}\quad \frac{dE}{dt} = k_E E(t)I(t) - d_E E(t)$$

With initial conditions $T(0) = T_0$, $I(0) = I_0$, $V(0) = V_0$, $E(0) = E_0$. Here effector cells or cytotoxic T-lymphocytes can serve to represent short-lived cells which have cytopathic effects (for example, $CD8^+$ T-cells as we discussed in section 1.1.2). In this model k_E is the constant rate at which immune effector cells are stimulated and d_E is the death rate of the effector cells. The other parameters remain the same as defined previously; however, we conduct simulations .

6.1 Model Development

Equation 5a models the dynamics of the uninfected cellular population. The development of this equation is synonymous with that for the standard target-cell-limited model.

Equation 5b represents the dynamics of infected cells. The equation for the rate of change of the infected cell population is dictated by both the rate of infection and death rate. The equation can be represented as:

Rate of change of infected cell population = (Infection rate) - (Immune Interaction rate) - (Death rate)

Infection rate: This term is the same as the infection rate term in the target cell differential equation with a reversal in sign. This is a result of the fact that the only way that infected cells can be created is by infecting previously uninfected target cells [14]. The human immune system does

not naturally produce infected cells; thus, the term remains the same as previously determined.

Interaction rate: Immune effector cells are activated when contact between a effector cell and an infected cell is made within the infected host. This interaction causes the infected cell to be removed from the infected cell population since it no longer maintains the ability to infect previously uninfected target cells. The interaction rate for the activated effector cells, k_E, can be assumed to be proportional to the product of the CTL and infected cell populations which is consistent with Michaelis-Menten interaction dynamics [27].

Death rate: Similar to target cell death, infected cells are cleared by the immune system at a rate, δ, proportional to the infected cell population [14].

Equation 5c mathematically describes the dynamics of the virus cell population. The development of this equation is synonymous with that for the standard Target-cell-limited model.

Equation 5d highlights the dynamics of immune effector cells. The effector cell population is composed of production rate and death rate. The overall equation is:

Rate of change of Effector cell population = (Production rate) - (Death rate)

Production rate: Effector cells are activated when contact between the effector cell and an infected cell is made within the infected host. Thus, the production rate, k_E, can be assumed to be proportional to the product of the effector cell and infected cell populations and is the same as in equation 5b with a reversal in sign.

Death rate: Similar to target cell death, effector cells are cleared by the immune system at a rate, d_E, proportional to the effector cell population.

It is important to note that all of the model parameters are presumed to be positive. In addition, there are two biologically reasonable assumptions we are able to make with regard to the values of parameters in relation to one another. Notably, it is biologically reasonable to assume that infected cells have a higher death rate than target cells, namely $\alpha \geq \mu$. Furthermore, we are also able to assume that the death rate of infected cells is greater than the natural death rate of CTLs, and thus $\alpha \geq \delta$.

6.2 Existence and Uniqueness of Solutions

Prior to conducting an in–depth analysis of the model, it is crucial to show that the solutions to the initial-value problem exist and are unique.

6.2.1 Positivity and Boundedness

Lemma (*Positivity*)**.** *Let $t_0 > 0$. In the model, if the initial conditions satisfy $T(0) > 0$, $I(0) > 0$, $V(0) > 0$, $E(0) > 0$ then for all $t \in [0, t_0]$, $T(t)$, $I(t)$, $V(t)$, $E(t)$ will remain positive in $\mathbb{R}^4_+$.*

Proof: Positivity. We must prove that for all $t \in [0, t_0]$, $T(t)$, $I(t)$, $V(t)$, $E(t)$ will be positive in $\mathbb{R}^4_+$. We know that all of the parameters used in the system are positive. Thus, we can place lower bounds on each of the equations given in the model. Thus,

$$\frac{dT}{dt} = \lambda - dT(t) - \beta V(t)T(t) \geq -dT(t) - \beta V(t)T(t)$$

$$\frac{dI}{dt} = \beta V(t)T(t) - \delta I(t) - k_E I(t)E(t) \geq -\delta I(t) - k_E I(t)E(t)$$
$$\frac{dV}{dt} = pI(t) - cV(t) \geq -cV(t)$$
$$\frac{dE}{dt} = k_E E(t)I(t) - d_E E(t) \geq -d_E E(t)$$

Through basic differential equations methods we can resolve the inequalities and produce:

$$T(t) \geq e^{-dt-\beta\int V(t)dt} \geq 0$$
$$I(t) \geq e^{-\delta t-k_E\int E(t)dt} \geq 0$$
$$V(t) \geq e^{-ct} \geq 0$$
$$E(t) \geq e^{-d_E t} \geq 0$$

Thus, for all $t \in [0, t_0]$, $T(t)$, $I(t)$, $V(t)$, $E(t)$ will be positive and remain in $\mathbb{R}^4_+$. □

Lemma (Boundedness)**.** *There exists an $T_M, I_M, V_M, E_M > 0$ such that for $T(t)$, $I(t)$, $I(t)$, $E(t)$ $\limsup_{t\to\infty}\Big(T(t)\Big) \leq T_M$, $\limsup_{t\to\infty}\Big(I(t)\Big) \leq I_M$, $\limsup_{t\to\infty}\Big(V(t)\Big) \leq V_M$, $\limsup_{t\to\infty}\Big(E(t)\Big) \leq E_M$ for all $t \in [0, t_0]$.*

Proof: Boundedness. We must prove that for all $t \in [0, t_0]$, $T(t)$, $I(t)$, $V(t)$, $E(t)$ will be bounded. We know that all of the constants used in the system are positive.

$$\frac{dT}{dt} + \frac{dI}{dt} + \frac{dE}{dt} = \lambda - dT(t) - \delta I(t) - d_E E(t)$$

Since all of the constants are positive,

$$\frac{d(T+I+E)}{dt} \leq \lambda - \min\{d, \delta, d_E\}(T+I+E)(t)$$

which implies,

$$(T+I+E)(t) \leq \frac{\lambda}{\min\{d, \delta, d_E\}} + c_0 e^{-\min\{d,\delta,d_E\}t}$$

taking the limsup of both sides,

$$\limsup_{t\to\infty}(T+I+E)(t) \leq \limsup_{t\to\infty}\Big(\frac{\lambda}{\min\{d, \delta, d_E\}} + c_0 e^{-\min\{d,\delta,d_E\}t}\Big) = \frac{\lambda}{\min\{d, \delta, d_E\}}$$

So, choose

$$T_M = I_M = E_M = \frac{\lambda}{\min\{d, \delta, d_E\}}$$

Thus, $(T+I+E)(t)$ is bounded, so $T(t), I(t)$, and $E(t)$ are all bounded since

$$T(t), I(t), E(t) \leq (T+I+E)(t).$$

So,

$$T(t) \leq T_M,\ I(t) \leq I_M,\ \text{and } E(t) \leq E_M \text{ for all } t \in [0, t_0]$$

Furthermore, since all of the constants are positive, we can place an upper bound on $\frac{dV}{dt}$ so,

$$\frac{dV}{dt} = pI(t) - eV(t) \leq pI(t)$$

Therefore, we can choose

$$V_M = pI_M$$

Thus,

$$V(t) \leq pI_M = V_M.$$

Hence, since $I(t)$ is bounded for all $t \in [0, t_0]$, we know that $V(t)$ is bounded for all $t \in [0, t_0]$. □

Theorem 6 (Existence)**.** *Let $t_0 > 0$. In the model, if the initial conditions satisfy $T(0) > 0$, $I(0) > 0$, $V(0) > 0$, $E(0) > 0$ then $\forall t \in \mathbb{R}$ $T(t)$, $I(t)$, $V(t)$, $E(t)$ will exist in $\mathbb{R}^4_+$.*

Proof: Existence and Uniqueness. In the case of our model we have:

$$\mathbf{x} = \begin{bmatrix} T(t) \\ I(t) \\ V(t) \\ E(t) \end{bmatrix} \text{ and } \mathbf{f}(\mathbf{x}) = \begin{bmatrix} \lambda - dT(t) - \beta V(t)T(t) \\ \beta V(t)T(t) - \delta I(t) - k_E I(t)T(t) \\ pI(t) - cV(t) \\ k_E I(t)T(t) - d_E T(t) \end{bmatrix}$$

Note that f has a continuous derivative on $\mathbb{R}^4$ and thus, f is locally Lipschitz in $\mathbb{R}^4$. Hence, by the Fundamental Existence and Uniqueness Theorem located in the appendix as well as the lemmas proved on positivity and boundedness of solutions, we know that there exists a unique, positive, and bounded solution to the ordinary differential equations given in $5(a) - 5(d)$. □

6.3 Local Stability Analysis

6.3.1 Critical Points

The model has three biologically relevant equilibria denoted $P_n = (T, I, V, E)$ for $n = 1, 2, 3$:

$$P_1 = \Big(\frac{\lambda}{d}, 0, 0, 0\Big)$$
$$P_2 = \Big(\frac{\delta c}{p\beta}, \frac{p\beta\lambda - \delta cd}{p\delta\beta}, \frac{p\beta\lambda - \delta cd}{\delta\beta c}, 0\Big)$$
$$P_3 = \Big(\frac{c\lambda k_E}{p\beta d_E + cdk_E}, \frac{d_E}{k_E}, \frac{pd_E}{ck_E}, \frac{-p\delta\beta c + p\beta\lambda k_E - \delta ck_E d}{k_E(p\beta d_E + cdk_E)}\Big)$$

We characterize P_1 as a viral free (or viral clearance) equilibrium; this means that as $t \to \infty$, the virus will be eliminated from the body. In addition, it represents the point where the infection will be cleared since both $V = 0$ and $I = 0$. P_2 and P_3 describe the persistence of the virus, and thus can be characterized as a viral persistence equilibria. At these values, the virus will remain in the system as $t \to \infty$ and the infection will persist with the patient. The equilibria also describe the persistence of an immune response. We denote that at P_2 and P_1 the immune response is either not required, or may even be suppressed as $t \to \infty$ since $E = 0$, while at P_3 the immune system's response remains present for all time, even after the virus population reaches a stable level since $E \neq 0$. Notably, P_3 is the only equilibrium which describes the co-existence of virus and immune effector cells as $t \to \infty$. In addition, it is important to denote that all of the equilibria have a persistence of uninfected cells.

6.3.2 Linearization and the Jacobian

The Jacobian for the linearized system is:

$$J(T, I, V, E) = \begin{bmatrix} V\beta - d & 0 & -T\beta & 0 \\ V\beta & \delta - Ek_E & T\beta & -Ik_E \\ 0 & p & -c & 0 \\ 0 & Ek_E & 0 & -d_E + Ik_E \end{bmatrix}$$

6.3.3 Derivation of R_0 and R_1

The characteristic polynomial is defined as the polynomial side of the characteristic equation, $det(A - \lambda I) = 0$ where A is a square matrix, I is the identity matrix, and λ is an eigenvalue. The roots of the characteristic polynomial of the Jacobian will tend to depend on several parameters known as threshold parameters. The values of these parameters, sometimes called the reproductive constants, influence and determine the stability of the system.

We can define:

$$R_0 = \frac{p\beta\lambda}{\delta cd}$$
$$R_1 = \frac{p\beta\lambda k_E}{\delta(ck_E d + p\beta d_E)}$$

to be the reproductive constants of the system. Biologically, R_0 represents the average number of infected cells produced by an initially infected cell over its lifetime [5]. The value of R_0 is a well established norm when discussing viral infections [5]. As previously determined, the R_0 value associated with HIV is generally accepted to range from 3 to 6 [14]. This value depends upon the parameters of the individual who is infected, but also varies based on the geographical location of the disease. R_1 translates the notion of viral reproductive constants to the immune system response. Thus, R_1 represents the number of infected cells that a single immune cell (CD8 or CTL in the case of our model) is able to address. The interpretation of R_1 will be discussed in greater detail in a later section.

Three theorems will be presented to highlight the relationship between the two reproductive constants and the local asymptotic stability of the equilibria. Thus, we are able to examine the values of R_0, R_1 and a few other simple expressions to determine whether viral persistence or viral extinction occurs as $t \to \infty$. As a result, we may be able to predict the persistence of the HIV upon initial infection simply by determining the values of these expressions. In addition, we will also be able to determine whether or not the immune response is suppressed or continues to persist during the course of the infection.

6.3.4 Stability Analysis for P_1

The Jacobian evaluated at $P_1 = (\frac{\lambda}{d}, 0, 0, 0)$ becomes :

$$J_1 = \begin{bmatrix} -d & 0 & -\frac{\beta\lambda}{d} & 0 \\ 0 & \delta & \frac{\beta\lambda}{d} & 0 \\ 0 & p & -c & 0 \\ 0 & 0 & 0 & -d_E \end{bmatrix}$$

Furthermore, the characteristic equation for P_1 is

$$-\frac{1}{d}(-x - d_E)(x + d)(-p\beta\lambda + x^2 d + x\delta d + xcd + \delta cd) = 0$$

From the characteristic equation we can define:

$$a_1 = \delta + c + d_E + d$$
$$a_2 = \delta(c + d_E + d) - \frac{\beta p \lambda}{d} + c(d_E + d) + d_E d$$
$$a_3 = \frac{d(\delta(c(d_E + d) + d_E d) + c d_E d) - \beta p \lambda (d_E + d)}{d}$$
$$a_4 = \delta c d_E d - \beta p d_E \lambda$$

such that

$$-\frac{1}{d}(-x - d_E)(x + d)(-p\beta\lambda + x^2 d + x\delta d + xcd + \delta cd) = x^4 + a_1 x^3 + a_2 x^2 + a_3 x + a_4$$

Theorem 7 (Local Asymptotic Stability of P_1)**.** *For the viral extinction equilibrium (P_1) given by*

$$(T, I, V, E) = (\frac{\lambda}{d}, 0, 0, 0)$$

if $R_0 < 1$, then P_1 is stable; however if $R_0 > 1$, then P_1 is unstable.

Proof. We will use the Routh-Hurwitz Criteria and the values of a_1, a_2, a_3, and a_4 to derive the stability of P_1.

We know that all of the parameters are positive. Therefore, $a_1 = \delta + c + d_E + d$ is clearly > 0.

We can write a_2 as,

$$a_2 = (1 - R_0)\frac{1}{\delta cd}\Big((\delta + c)d(d_E + d) + d_E d^2\Big)$$

Thus, if $R_0 < 1$, then $a_2 > 0$ since all the parameters are positive. However, if $R_0 > 1$, then clearly $a_2 < 0$.

Furthermore, a_3 can be represented by,

$$a_3 = (1 - R_0)(d_E + d)\frac{1}{\delta d_E d}\Big(d_E d(\delta + c)\Big)$$

Thus, if $R_0 < 1$, then $a_3 > 0$; however, if $R_0 > 1$, then $a_3 < 0$.

In addition,

$$a_4 = (1 - R_0)\frac{d_E}{\delta cd}$$

Thus, if $R_0 < 1$, then $a_4 > 0$; however, if $R_0 > 1$, then $a_4 < 0$.

Finally,

$$a_1 a_2 a_3 - (a_3^2 + a_1^2 a_4) = \frac{1}{d^2}\Big((\delta + c)(d_E + d)(1 - R_0 + \delta d_E d + c d_E d + d_E^2 d)(1 - R_0 + \delta d^2 + cd^2 + d^3)\Big)$$

Thus, if $R_0 < 1$, then $a_1 a_2 a_3 - (a_3^2 + a_1^2 a_4) > 0$. and therefore, $a_1 a_2 a_3 > a_3^2 + a_1^2 a_4$.

As a result, if $R_0 < 1$ all of the conditions necessary for stability are met and P_1 is stable. However, if $R_0 > 1$, then $a_2, a_3, a_4 < 0$ and P_1 is unstable. □

6.3.5 Stability Analysis for P_2

The Jacobian evaluated at $P_2 = \left(\frac{\delta c}{p\beta}, \frac{p\beta\lambda - \delta cd}{p\delta\beta}, \frac{p\beta\lambda - \delta cd}{\delta\beta c}, 0\right)$ is:

$$J_2 = \begin{bmatrix} -d - \frac{p\beta\lambda - \delta cd}{\delta c} & 0 & -\frac{\delta\lambda}{p} & 0 \\ \frac{p\beta\lambda - \delta cd}{\delta c} & \delta & \frac{\delta\lambda}{p} & -\frac{(p\beta\lambda - \delta cd)k_E}{p\delta\beta} \\ 0 & p & -c & 0 \\ 0 & 0 & 0 & -d_E + \frac{(p\beta\lambda - \delta cd)k_E}{p\delta\beta} \end{bmatrix}$$

Furthermore, the characteristic equation for P_2 is

$$-\frac{1}{p^2\delta^2\beta c^2}(p^2\delta(x+\delta)\beta(-x-c)c(x\delta c+p\beta\lambda)-p(-px\delta^3\beta c^3-p\delta^3\beta c^3 d))\left(-x-d_E+\frac{(p\beta\lambda - \delta cd)k_E}{p\delta\beta}\right) = 0$$

Theorem 8 (Local Asymptotic Stability of P_2)**.** *For the viral persistence equilibrium and immune suppressive equilibrium (P_2) given by*

$$(T, I, V, E) = \left(\frac{\delta c}{p\beta}, \frac{p\beta\lambda - \delta cd}{p\delta\beta}, \frac{p\beta\lambda - \delta cd}{\delta\beta c}, 0\right)$$

P_2 is stable iff P_2 exists and $R_1 < 1$.

Proof. In order for P_2 to be defined, $R_0 \geq 1$, since if $R_0 < 1$, $p\beta\lambda - \delta dc < 0$ and P_2 will not be biologically reasonable.

One eigenvalue of J_2 is

$$x_1 = \frac{p\beta\lambda k_E - (p\delta\beta d_E + \delta cdk_E)}{p\delta\beta}$$

Thus, we can simplify the characteristic equation.

As a result the remaining eigenvalues are solutions to the equation,

$$x^3 + x^2\frac{\delta^2 c + \delta c^2 + p\beta\lambda}{\delta c} + x\frac{p\beta(\delta + c)}{\delta c} + p\beta\lambda - \delta cd = 0$$

We will then use the Routh-Hurwitz criteria to prove that all of the roots are negative given $R_0 > 1$ and $R_1 < 1$. From the characteristic equation we obtain,

$$a_1 = \frac{\delta^2 c + \delta c^2 + p\beta\lambda}{\delta c}$$
$$a_2 = \frac{p\beta(\delta + c)}{\delta c}$$
$$a_3 = p\beta\lambda - \delta cd$$

We know $a_1, a_2 > 0$ since all of the parameters are positive.

Furthermore, we can denote:

$$a_3 = p\beta\lambda - \delta cd = (R_0 - 1)\frac{1}{\delta cd}$$

Thus, if $R_0 > 1$ then $a_3 > 0$, however, if $R_0 < 1$ then $a_3 < 0$ and P_2 is unstable.

In addition, we can define:

$$a_1a_2 - a_3 = p\beta\lambda + \frac{p\beta\delta\lambda}{c} + \frac{p\beta c\lambda}{\delta} + \frac{p^2\beta^2\lambda^2}{\delta c^2} + \frac{p^2\beta^2\lambda^2}{\delta^2 c} + \delta cd$$

Also, since all of the parameter are positive $a_1a_2 - a_3 > 0$ which implies that $a_1a_2 > a_3$. □

6.3.6 Stability Analysis for P_3

The Jacobian evaluated at $P_3 = \left(\frac{c\lambda k_E}{p\beta d_E + cdk_E}, \frac{d_E}{k_E}, \frac{pd_E}{ck_E}, \frac{-p\delta\beta c + p\beta\lambda k_E - \delta ck_E d}{k_E(p\beta d_E + cdk_E)}\right)$ is:

$$J_3 = \begin{bmatrix} -d - \frac{p\beta d_E}{k_E c} & 0 & -\frac{\beta c\lambda k_E}{p\beta d_E + ck_E d} & 0 \\ \frac{p\beta d_E}{k_E c} & \delta - \frac{-p\delta\beta d_E + p\beta\lambda k_E - \delta cdk_E}{p\beta d_E + cdk_E} & \frac{\beta c\lambda k_E}{p\beta d_E + cdk_E} & -d_E \\ 0 & p & -c & 0 \\ 0 & \frac{-p\delta\beta d_E + p\beta\lambda k_E - \delta cdk_E}{p\beta d_E + ck_E d} & 0 & 0 \end{bmatrix}$$

Furthermore, the characteristic equation for P_3 is

$$\frac{-x\left(\beta pc^2\lambda k_E^2(d+x) - (\delta+x)(c+x)(\beta pd_E + cdk_E)(\beta pd_E + ck_E(d+x))\right) - k_E(c+x)(\beta pd_E + ck_E(d+x))(\delta cdk_E + \beta p(\delta d_E - \lambda k_E))}{ck_E(\beta pd_E + cdk_E)} = 0$$

Therefore,

$$a_1 = \frac{\beta^2p^2d_E^2 + c^2dk_E^2(c+d) + \beta pck_E(cd_E + 2d_Ed + \lambda k_E)}{ck_E(\beta pd_E + cdk_E)}$$

$$a_2 = \frac{c^2dk_E^2(cd - \delta d_E) + \beta^2p^2d_E(cd_E + \lambda k_E) + \beta pck_E\left(-\delta d_E^2 + 2cd_Ed + \lambda k_E(d_E + d)\right)}{ck_E(\beta pd_E + cdk_E)}$$

$$a_3 = \frac{d_E\left(-\delta c^2dk_E^2(c+d) + \beta^2p^2\left(\lambda k_E(c+d_E) - \delta d_E^2\right) + \beta pck_E(\lambda k_E(c+d) - \delta d_E(c+2d))\right)}{ck_E(\beta pd_E + cdk_E)}$$

$$a_4 = d_E\left(\beta p\left(\lambda - \frac{\delta d_E}{k_E}\right) - \delta cd\right)$$

Theorem 9 (Local Asymptotic Stability of P_3)**.** *For the viral persistence equilibrium and immune response persistence equilibrium (P_3) given by*

$$(T, I, V, E) = \left(\frac{c\lambda k_E}{p\beta d_E + cdk_E}, \frac{d_E}{k_E}, \frac{pd_E}{ck_E}, \frac{-p\delta\beta c + p\beta\lambda k_E - \delta ck_E d}{k_E(p\beta d_E + cdk_E)}\right)$$

If $R_1 > 1$, $R_0 > \frac{d_E}{d}$, $p\beta > \delta k_E$, $\lambda(c + d_E) > \delta d_E^2$ then P_3 is stable.

Proof. We know that since all the parameters are positive, $a_1 > 0$.

Taking the numerator of a_2, we want

$$d_E(-\delta c^2dk_E^2(c+d) + \beta^2p^2(\lambda k_E(c+d_E) - \delta d_E^2) + \beta pck_E(\lambda k_E(c+d) - \delta d_E(c+2d))) > 0$$

Thus, if

$$c^3d^2k_E^2 + \beta^2p^2d_E(cd_E + \lambda k_E) + \beta pck_E(2cd_Ed + \lambda k_E(d_E + d)) > \delta cd_Ek_E(\beta pd_E + cdk_E)$$

then $a_2 > 0$.

Since

$$\frac{p\beta\lambda}{\delta cd_E} = \frac{d}{d_E}R_0$$

if

$$R_0 > \frac{d_E}{d}$$

then

$$p\beta\lambda > \delta cd_E$$

Thus, if $p\beta > \delta k_E$ and $R_0 > \frac{d_E}{d}$ then $p\beta\lambda > \delta cd_E$.

Therefore, if $R_0 > \frac{d_E}{d}$ and $\lambda(c + d_E) > \delta d_E^2$ then $a_2 > 0$.

Considering the numerator of a_3, we want to prove that

$$d_E(-\delta c^2dk_E^2(c + d) + \beta^2p^2(\lambda k_E(c + d_E) - \delta d_E^2) + \beta pck_E(\lambda k_E(c + d) - \delta d_E(c + 2d))) > 0$$

Additionally, if

$$\beta pd_E\lambda k_E(\beta p(c + d_E) + ck_E(c + d)) > \delta d_E\left(\beta^2p^2d_E^2 + c^2dk_E^2(c + d) + \beta pcd_Ek_E(c + 2d)\right)$$

then $a_3 > 0$. Thus, if $R_1 > 1$, and $\lambda k_E(c + d_E) > \delta d_E^2$, then $a_3 > 0$.

Furthermore, a_4 can be written as

$$a_4 = \frac{d_E}{k_E(p\delta\beta d_E + \delta cdk_E)}(R_1 - 1)$$

Thus, if $R_1 > 1$ then $a_4 > 0$; however, if $R_1 < 1$, then $a_4 < 0$ and P_3 is unstable.

The expression for $a_1a_2a_3 - (a_3^2 + a_1^2a_4)$ can be found in the appendix. However, if $p\beta > \delta k_E, p\beta\lambda > \delta d_Ec, R_1 > 1, R_0 > 1$, and $\lambda k_E(c + d_E) > d_E^2\delta$, then $a_1a_2a_3 - (a_3^2 + a_1^2a_4) > 0$ and thus, $a_1a_2a_3 > (a_3^2 + a_1^2a_4)$. □

6.4 Parameter Estimates and Numerical Simulation

In estimating the parameters for the simple immune model, we adopted the same approach as we did for both the Target-cell-limited model and constrained target-cell-limited model where we will use the viral expansion rate, r, to solve for the infection rate, β. Thus, our new system of differential equations becomes:

$$\text{(5a)}\quad \frac{dT}{dt} = \lambda - dT(t) - (r+\delta)\frac{c}{pT_0}V(t)T(t)$$

$$\text{(5b)}\quad \frac{dI}{dt} = (r+\delta)\frac{c}{pT_0}V(t)T(t) - \delta I(t) - k_E E(t)I(t)$$

$$\text{(5c)}\quad \frac{dV}{dt} = pI(t) - cV(t)$$

$$\text{(5d)}\quad \frac{dE}{dt} = k_E E(t)I(t) - d_E E(t)$$

Table 13: Parameter Estimations for the Simple Immune Model

Parameter	Value	s.e._lin	r.s.e._lin
p_{pop}	1671.071	1391.479	83.27
d_{pop}	0.00715	0.00146	20.42
δ_{pop}	0.60062	0.38926	64.81
$V_{0_{pop}}$	3.96462	0.27561	6.95
$k_{E_{pop}}$	0.00069	0.08004	11673.81
$d_{E_{pop}}$	2.6109	85.00994	3255.96
ρ_{pop}	0.0172	2.07614	12072.52

From Table 13 we can see that the estimates given for the death rate of the target cells, d, and the initial virus population V_0 for the simple immune model are similar to those for the target cell, and the constrained target-cell-limited model. For instance, the initial population of virus is approximately $10^{3.9}$ $\frac{virions}{mL}$ and the death rate of target cells is about 0.007 $days^{-1}$. However, the rate of viral production, p, as well as the death rate of infected cells, δ, are quite different in the three models. For instance, the rate of viral production, p is 1671.071 $days^{-1}$ for the simple immune model, whereas it is much smaller 374.76 $days^{-1}$ for the standard Target-Cell-Limited model. This discrepancy is likely due to the increased impact that the immune system has on the growth of the virus which is not only reflected in the immune population, but is also reflected within the growth rate for the virus which is dominated by the parameter p. This is because the immune system directly targets the growth of the virus, and as a result the parameter must be larger to compensate for the same amount of growth in the presence of an immune response as when the immune response is not included within the effects of the model. Thus, it seems very reasonable that we would expect the value of the rate of viral production to be much larger for the simple immune model.

Furthermore, it is interesting to note that the value for δ is approximately 0.60 $days^{-1}$ which is much more consistent with the literature and what we expect from all of the models, which is much different from the results achieved by the both the target-cell-limited as well as the constrained target-cell-limited models. However, despite the fact that the parameter is so close to what we expect, the plot seems to suggest that the model is still underestimating the rate of viral decay. What is further surprising is that we would expect this value to be smaller than what the

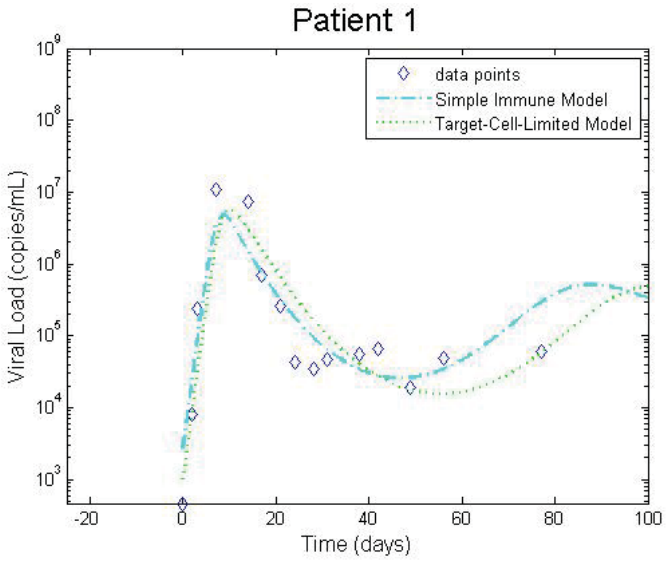

Figure 25: Simulation of the Simple Immune Model.

literature suggests for the standard death rate of infected cells since the immune system would be partaking in the killing of the infected cells, thus making the natural rate appear smaller in nature. Furthermore, Figure 25 suggests that the model exhibits qualitative characteristics that are very similar to the standard target cell model and is overall not a fantastic fit of the data. For instance, the model does not do a good job estimating the peak viral load; in fact, it significantly underestimates the peak load. In addition, the model seems to suggest that there are major oscillations after the patient achieves a steady state viral load. This behavior is very similar to that which is exhibited by the target-cell-limited model and, as mentioned earlier, somewhat inconsistent with what we are seeing from the data.

6.5 Sensitivity Analysis

Similar to the sensitivity analysis we conducted for the target cell and constrained Target-Cell-Limited models, we examined the sensitivity properties of the simple immune model. The corresponding sensitivity systems with respect to β, δ, and p are shown below.

For β:

(5i) $S'_{T_\beta(t)} = -\big(V(t)S_{T_beta(t)} + S_{V_\beta(t)}\big) - d(S_{T_\beta(t)})$

(5j) $S'_{I_\beta(t)} = \big(V(t)S_{T_\beta(t)} + S_{V_\beta(t)}\big) - \delta S_{I_\beta(t)} - k_E\big(E(t)S_{I_\beta(t)} + I(t)S_{E_\beta}\big)$

(5k) $S'_{V_\beta(t)} = pS_{I_\beta(t)} - cS_{V_\beta(t)}$

(5l) $S'_{E_\beta(t)} = k_E\big(E(t)S_{I_\beta(t)} + I(t)S_{E_\beta}\big) - d_E(S_{E_\beta(t)})$

For δ:

(5m) $S'_{T_\delta(t)} = -\beta\big(V(t)S_{T_\delta(t)} + S_{V_\delta(t)}\big) - d(S_{T_\delta(t)})$

(5n) $S'_{I_\delta(t)} = \beta\big(V(t)S_{T_\delta(t)} + S_{V_\delta(t)}\big) - S_{I_\delta(t)} - k_E\big(E(t)S_{I_\delta(t)} + I(t)S_{E_\delta}\big)$

(5o) $S'_{V_\delta(t)} = pS_{I_\delta(t)} - cS_{V_\delta(t)}$

(5p) $S'_{E_\delta(t)} = k_E\big(E(t)S_{I_\delta(t)} + I(t)S_{E_\delta}\big) - d_E(S_{E_\delta(t)})$

For p:

(5q) $S'_{T_p(t)} = -\beta\big(V(t)S_{T_p(t)} + S_{V_p(t)}\big) - d(S_{T_p(t)})$

(5r) $S'_{I_p(t)} = \beta\big(V(t)S_{T_p(t)} + S_{V_p(t)}\big) - \delta S_{I_p(t)} - k_E\big(E(t)S_{I_p(t)} + I(t)S_{E_p}\big)$

(5s) $S'_{V_p(t)} = S_{I_p(t)} - cS_{V_p(t)}$

(5t) $S'_{E_p(t)} = k_E\big(E(t)S_{I_p(t)} + I(t)S_{E_p}\big) - d_E(S_{E_p(t)})$

From Figure 26 we can see that the Simple Immune Model is very similar in terms of sensitivity resulting from changes in the parameters, specifically for β, δ, and p, to the target-cell-limited model. This is illustrated by the fact that during the viral production phases of infection the value of the virus remains relatively constant for all three of the parameters. During the viral decay phase, there is variation in the population of the virus, however, it is most pronounced for the parameters δ and β. Also similar to the target-cell-limited model, increasing the death rate of the infected cells decreases the slope for the rate of viral decay, however the differences are smaller in magnitude for the simple immune model than the target-cell-limited. Most of the variation due to changes in the parameters results in small variation during the steady state, as is consistent with the target-cell-limited model.

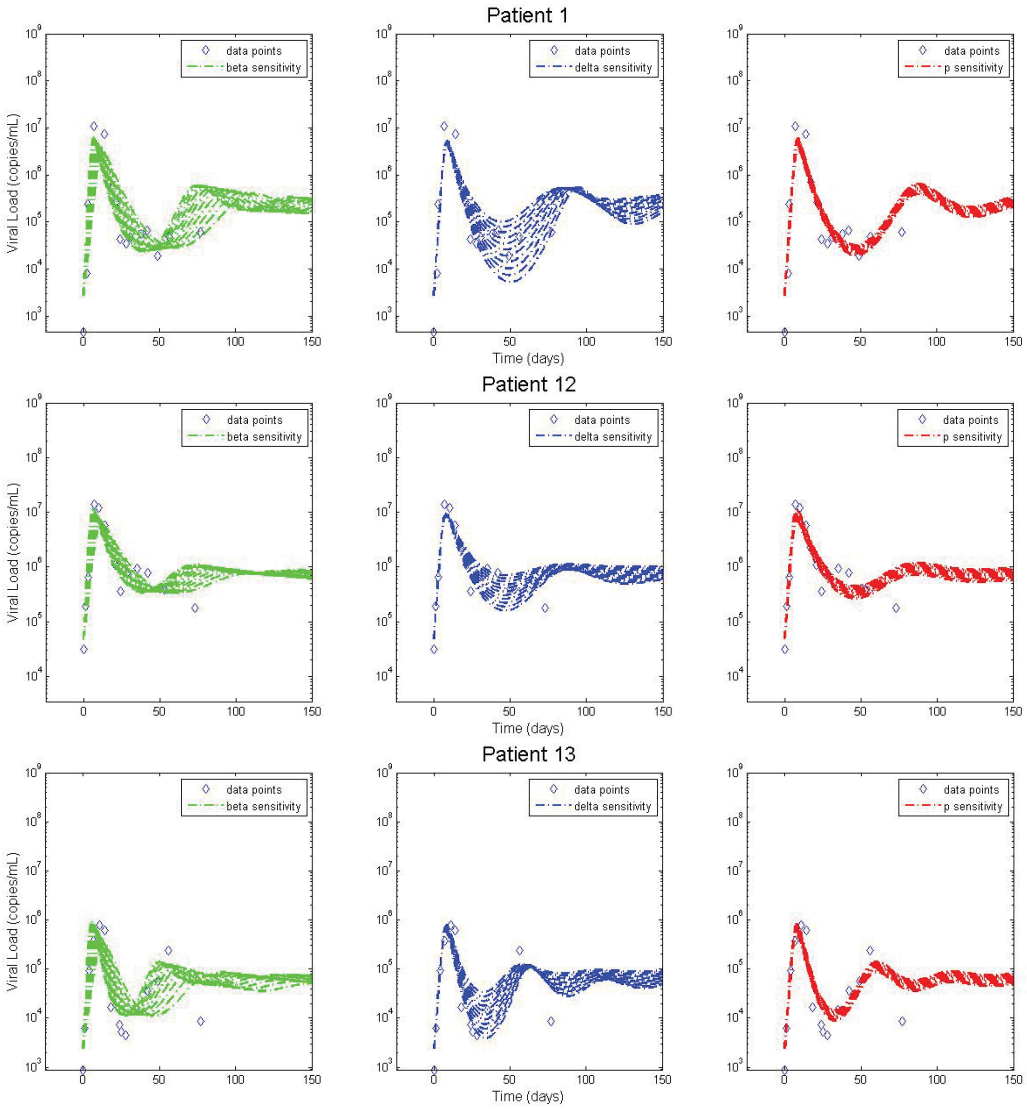

Figure 26: The effect of varying the parameters β, δ, and p.

Yet, a closer examination of the sensitivity with regards to the infected cell death rate δ reveals

that when compared with the standard target-cell-limited model, the value of the infected cell death rate for the simple immune model seems to have a smaller effect on the rate of viral decay. This suggests that we would not necessarily expect the real rate of viral decay to be much larger than our estimate, 0.60 $days^{-1}$, which corresponds to the value found in the literature. However, the value of δ does have a very large impact on the magnitude of the oscillations. For instance, for larger values of δ, the viral load achieves a much smaller value at the end of the decay phase before returning to the steady state equilibrium.

7 Extended Model with Immune Control

The Extended Model with Immune control was proposed by D. Burg et. al [3] in order to include the effects of a cell-mediated immune response. The model extends the target-cell-limited model by accounting for the loss of infected cells during the viral transient peak similar to the simple immune model, but exhibits more complex dynamics than the simple model. The response is dependent upon the infected cell frequency via a saturation function and allows for the possible early control of the virus. The model considers four distinct populations which are denoted:

$T(t)$: concentration of target cells at time t,
$I(t)$: concentration of infected cells at time t,
$V(t)$: concentration of free virus at time t,
$E(t)$: concentration of immune effector cells at time t.

The model is a system of four nonlinear ordinary differential equations denoted:

$$\text{(6a)}\quad \frac{dT}{dt} = \lambda - \beta V(t)T(t) - dT(t)$$
$$\text{(6b)}\quad \frac{dI}{dt} = \beta V(t)T(t) - \big(\alpha d + k_0 E(t)\big)I(t)$$
$$\text{(6c)}\quad \frac{dV}{dt} = pI(t) - cV(t)$$
$$\text{(6d)}\quad \frac{dE}{dt} = a_E \frac{I(t)}{I(t)+\theta} - d_E E(t)$$

With initial conditions $T(0) = T_0$, $I(0) = I_0$, $V(0) = V_0$, $E(0) = E_0$. Here effector cells can serve to represent short-lived cells which have cytopathic effects (for example, $CD8^+$ T-cells or Cytotoxic T-lymphocytes, CTLs). In this model a_E is the constant rate at which immune effector cells are stimulated, θ is the half-maximal stimulation threshold, and d_E is the death rate of the effector cells. All of the other parameters remain the same as previously defined in the other models.

7.1 Model Development

Equation 6a models the dynamics of the uninfected cellular population. The development of this equation is synonymous with that for the standard target-cell-limited model.

Equation 6b represents the dynamics of infected cells. The equation for the rate of change of the infected cell population is dictated by both the rate of infection and death rate. The equation can be represented as:

Rate of change of infected cell population = (Infection rate) - (Immune Interaction rate) - (Death rate)

Infection rate: This term is the same as we previously defined in the other models.

Interaction rate: Immune effector cells are activated when contact between a effector cell and an infected cell is made within the infected host. This interaction causes the infected cell to be removed from the infected cell population since it no longer maintains the ability to infect previously uninfected target cells. As mentioned previously, the interaction rate for the activated effector cells, k_0, can be assumed to be proportional to the product of the CTL and infected cell populations

which is consistent with Michaelis-Menten interaction dynamics [27].

Death rate: Similar to target cell death, infected cells are cleared by the immune system at a rate, proportional to the infected cell population [14].

Equation 6c mathematically describes the dynamics of the virus cell population. The development of this equation is synonymous with that for the standard Target-cell-limited model, however, the parameter δ is replaced by the expression αd.

Equation 6d highlights the dynamics of immune effector cells. The effector cell population is composed of production rate and death rate. The overall equation is:

Rate of change of Effector cell population = (Production rate) - (Death rate)

Production rate: Effector cells are activated when contact between the effector cell and an infected cell is made within the infected host. However, the dynamics for the production of effector cells is much more complicated in the extended immune model than the simple immune model. This is because the development of an immune response (and the production of effector cells) is dependent upon the infected cell frequency via a saturation function $\frac{I(t)}{I(t)+\theta}$.

Death rate: Similar to target cell death, effector cells are cleared by the immune system at a rate, d_E, proportional to the effector cell population.

It is important to note that all of the model parameters are presumed to be positive. In addition, there are two biologically reasonable assumptions we are able to make with regard to the values of parameters in relation to one another. Notably, it is biologically reasonable to assume that infected cells have a higher death rate than target cells, namely $\alpha \geq \mu$. Furthermore, we are also able to assume that the death rate of infected cells is greater than the natural death rate of CTLs, and thus $\alpha \geq \delta$.

7.2 Existence and Uniqueness

7.2.1 Positivity and Boundedness

Lemma (*Positivity*)**.** *Let $t_0 > 0$. In the model, if the initial conditions satisfy $T(0) > 0$, $I(0) > 0$, $V(0) > 0$, $E(0) > 0$ then for all $t \in [0, t_0]$, $T(t)$, $I(t)$, $V(t)$, $E(t)$ will remain positive in $\mathbb{R}^4_+$.*

Proof: Positivity. We must prove that for all $t \in [0, t_0]$, $T(t)$, $I(t)$, $V(t)$, $E(t)$ will be positive in $\mathbb{R}^4_+$. We know that all of the parameters used in the system are positive. Thus, we can place lower bounds on each of the equations given in the model. Thus,

$$\frac{dT}{dt} = \lambda - dT(t) - \beta V(t)T(t) \geq -dT(t) - \beta V(t)T(t)$$

$$\frac{dI}{dt} = \beta V(t)T(t) - \delta I(t) - k_E I(t)E(t) \geq -\delta I(t) - k_0 I(t)E(t)$$

$$\frac{dV}{dt} = pI(t) - cV(t) \geq -cV(t)$$

$$\frac{dE}{dt} = a_E \frac{I(t)}{I(t)+\theta} - d_E E(t) \geq -d_E E(t)$$

Through basic differential equations methods we can resolve the inequalities and produce:

$$T(t) \geq e^{-dt-\beta \int V(t)dt} \geq 0$$

$$I(t) \geq e^{-\delta t-k_0 \int E(t)dt} \geq 0$$

$$V(t) \geq e^{-ct} \geq 0$$

$$E(t) \geq e^{-d_E t} \geq 0$$

Thus, for all $t \in [0, t_0]$, $T(t)$, $I(t)$, $V(t)$, $E(t)$ will be positive and remain in $\mathbb{R}^4_+$. □

Lemma (Boundedness)**.** *There exists an* $T_M, I_M, V_M, E_M > 0$ *such that for* $T(t)$, $I(t)$, $I(t)$, $E(t)$ $\limsup_{t\to\infty}\Big(X(t)\Big) \leq T_M$, $\limsup_{t\to\infty}\Big(I(t)\Big) \leq I_M$, $\limsup_{t\to\infty}\Big(V(t)\Big) \leq V_M$, $\limsup_{t\to\infty}\Big(E(t)\Big) \leq E_M$ *for all* $t \in [0, t_0]$.

Proof: Boundedness. We must prove that for all $t \in [0, t_0]$, $T(t)$, $I(t)$, $V(t)$, $E(t)$ will be bounded. We know that all of the constants used in the system are positive. In addition, we can assume that $\theta > 1$ []. Thus, we know that $a_E I(t) > a_E \frac{I(t)}{I(t)+\theta}$.
As a result,

$$\frac{dT}{dt} + \frac{dI}{dt} + \frac{dE}{dt} + k_0 E(t)I(t) = \lambda - dT(t) - \alpha d I(t) - d_E E(t) \geq \frac{dT}{dt} + \frac{dI}{dt} + \frac{dE}{dt}$$

Since all of the constants are positive,

$$\frac{d(T+I+E)}{dt} \leq \lambda - \min\{d, \alpha d, d_E\}(T+I+E)(t)$$

which implies,

$$(T+I+E)(t) \leq \frac{\lambda}{\min\{d, \alpha d, d_E\}} + c_0 e^{-\min\{d,\alpha d,d_E\}t}$$

taking the limsup of both sides,

$$\limsup_{t\to\infty}(T+I+E)(t) \leq \limsup_{t\to\infty}\Big(\frac{\lambda}{\min\{d, \alpha d, d_E\}} + c_0 e^{-\min\{d,\alpha d,d_E\}t}\Big) = \frac{\lambda}{\min\{d, \alpha d, d_E\}}$$

So, choose

$$T_M = I_M = E_M = \frac{\lambda}{\min\{d, \alpha d, d_E\}}$$

Thus, $(T+I+E)(t)$ is bounded, so $T(t), I(t)$, and $E(t)$ are all bounded since

$$T(t), I(t), E(t) \leq (T+I+E)(t).$$

So,

$$T(t) \leq T_M,\ I(t) \leq I_M,\ \text{and } E(t) \leq E_M \text{ for all } t \in [0, t_0]$$

Furthermore, since all of the constants are positive, we can place an upper bound on $\frac{dV}{dt}$ so,

$$\frac{dV}{dt} = pI(t) - cV(t) \leq pI(t)$$

Therefore, we can choose

$$V_M = pI_M$$

Thus,

$$V(t) \leq pI_M = V_M.$$

Hence, since $I(t)$ is bounded for all $t \in [0, t_0]$, we know that $V(t)$ is bounded for all $t \in [0, t_0]$. □

Theorem 10 (Existence)**.** *Let $t_0 > 0$. In the model, if the initial conditions satisfy $T(0) > 0$, $I(0) > 0$, $V(0) > 0$, $E(0) > 0$ then $\forall t \in \mathbb{R}$ $T(t)$, $I(t)$, $V(t)$, $E(t)$ will exist in $\mathbb{R}^4_+$.*

Proof: Existence and Uniqueness. In the case of our model we have:

$$\mathbf{x} = \begin{bmatrix} T(t) \\ I(t) \\ V(t) \\ E(t) \end{bmatrix} \text{ and } \mathbf{f}(\mathbf{x}) = \begin{bmatrix} \lambda - dT(t) - \beta V(t)T(t) \\ \beta V(t)T(t) - \Big(\alpha d + k_0 E(t)\Big)I(t) \\ pI(t) - cV(t) \\ a_E \frac{I(t)}{\theta + I(t)} - d_E E(t) \end{bmatrix}$$

Note that f has a continuous derivative on $\mathbb{R}^5$ and thus, f is locally Lipschitz in $\mathbb{R}^5$. Hence, by the Fundamental Existence and Uniqueness Theorem located in the appendix as well as the lemmas proved on positivity and boundedness of solutions, we know that there exists a unique, positive, and bounded solution to the ordinary differential equations given in $6(a) - 6(d)$. □

7.3 Simplified Extended Model

Since data on the number of effector cells is not available, there are a large number of parameters that are currently not estimated. Thus, we adopt the approach from D. Burg et al. [3] and simplify the extended model (equations 6a - 6d) by using a quasi steady state approximation over the Immune Effector cell population. This assumption assumes that the dynamics of the effector cell population is faster than the time course of acute HIV resolution [3] and that the population of effector cells is proportional to the infected cell population. The result is the simplified extended model (equations 7a - 7c) shown below.

Using a quasi-steady state approximation for $\frac{dE}{dt}$,
$\frac{dE}{dt} = 0 \implies a_E \frac{I}{\theta + I} = d_E E \implies E = \frac{a_E}{d_E}\frac{I}{\theta + I} \implies \frac{dI}{dt} = \beta VT - \Big(\alpha d + k_0 \frac{a_E}{d_E}\frac{I}{\theta + I}\Big)I.$

Let $k = k_0 \frac{a_E}{d_E}$.

Then,

$$\text{(7a)} \quad \frac{dT}{dt} = \lambda - dT(t) - \beta V(t)T(t)$$
$$\text{(7b)} \quad \frac{dI}{dt} = \beta V(t)T(t) - [\alpha d + k\frac{I(t)}{I(t) + \theta}]I(t)$$
$$\text{(7c)} \quad \frac{dV}{dt} = pI(t) - cV(t)$$

With initial conditions $T(0) = T_0$, $I(0) = I_0$, $V(0) = V_0$. By employing the extended model, we reduce the number of parameters that need to be estimated. Note that the infected cell death rate in the Target-Cell-Limited Model, δ, has been replaced with the function $\delta(I(t)) = \alpha d + k\frac{I(t)}{I(t)+\theta}$. In addition, the Target-Cell-Limited Model appears as the special case where $k = 0$, $\theta = 0$,and $\delta = d\alpha$.

The asterisk in Tables 14 and 15 denotes estimations that we carried our for the Target-cell-limited model using the data from the patients from Section 2.

Table 14: Parameters for the Extended Immune Model

Parameter	Biological Interpretation	Units	Known Value
λ	Target cell production rate	$(Cells)mL{-}1days^{-1}$	dT_0
β	Rate of infection	$(mL)Cells^{-1}days^{-1}$	$(r+d)\frac{c}{pT_0}$
d	Target cell death rate	day^{-1}	Estimated*
α	Rate of Viral Decay	$days^{-1}$	Estimated*
p	Viral production rate	$days^{-1}$	Estimated*
c	Viral clearance rate	$days^{-1}$	23
k	Maximum Value of Activity Potential	$(mL)Cells^{-1}days^{-1}$	Estimated*
θ	Half-maximal Simulation Threshold	$(Cells)mL^{-1}$	Estimated*

Table 15: Initial Conditions for the Extended Immune Model

Initial Conditions	Value	Units
T_0	5.9×10^5	$(Cells)mL^{-1}$
I_0	$\frac{c}{p}V_0$	$(Cells)mL^{-1}$
V_0	Estimated*	$(Cells)mL^{-1}$

Since we know that solutions to the Extended Immune Model exist, and are positive, unique, and bounded, we know that the solutions to the simplified model also have these characteristics. Thus, we do not need to prove existence for this simplified model.

7.4 Parameter Estimates and Numerical Simulations

The final model that we used in order to analyze the data was the simplified extended immune model as developed in [3] as described in section 7.3. Table 16 highlights the estimates for the parameter values for the extended immune model. Upon examination of the parameter values, we find that the estimate for δ, 0.62 $days^{-1}$, is very close to what we expect as well as extremely consistent with our results from the simple immune model. Furthermore, our estimates for the initial viral population has been extremely consistent across all of the models, the extended immune included.

However, there are several of the parameters which are very different from estimates that we achieved with the simple immune model. For example, the rate of viral production p is nearly twice as large as the rate of viral production estimated for the simple immune model and four times as large as that estimated for the standard target-cell-limited model. This again may reflect the notion that the immune response is much more powerful in the extended immune model and so the rate at which the virus is produced must be larger in order to have the same amount of viral growth occur in the presence of a significantly more effective immune response. Additionally, Table 16 illustrates that the natural death rate for the target cells, d, is several orders of magnitude smaller than we expect $(O(10^{-3}) - O(10^{-2}))$ as well as many orders of magnitude smaller than in any of the other models.

While several of the values for rse for the individual parameters suggests that there is a lot of individual variability within the data, we can see that the variability is much smaller than that for the simple immune model. The parameter which has the most variability is the death rate for the target cells, d, which also happens to be the parameter that is significantly smaller; thus, any

minute change will greatly effect the value for the residual square error.

Table 16: Parameter Estimates for the Extended Immune Model

Parameter	Value	$s.e._{lin}$	$r.s.e._{lin}$
p_{pop}	2589.19	937.00	36.19
d_{pop}	0.00002	0.00005	280.91
δ_{pop}	0.618	0.0932	15.07
$V_{0_{pop}}$	3.48	0.338	9.72
θ_{pop}	1029.96	534.50	51.9
k_{pop}	0.712	0.0920	12.91

Figure 27 illustrates that the extended immune model appears to effectively capture the dynamics of the viral expansion phase, viral decay phase, as well as the steady state. We can clearly see that compared to the standard target-cell limited model, as well as the constrained Target-Cell-Limited model, which was the most effective model to this point, the extended immune model seems to do the best job at capturing the dynamic behavior of the virus. For instance, in the two of the three patients, the model effectively captures the peak viral load, something that many of the other models struggled to do. The only exception is Patient 9 where the model underestimated the expected peak viral load. However, the extended immune model also had the highest estimation of the peak viral load in Patient 9 for any of the models. Furthermore, the model does a fantastic job capturing the dynamics of the viral growth and decay phases without any need to constrain the model to do so. In addition, the estimate for the death rate of infected cells is 0.61 which is similar to that of the simple immune model and similar to what we expect. Yet, unlike in the simple immune model, the rate of viral decay seems to be accurately estimated as there is no apparent under or over estimation. This is likely the result of a more effective modeling of the immune dynamics and their interaction with the natural death of the infected cells.

However, the model is not without a few minor flaws. Figure 27 suggests that the extended immune model is not very sensitive to the small variations that occur within the data after the virus achieves the steady state. As illustrated in Patient 9, the viral load may not remain entirely constant after the virus reaches its steady state. Small deviations in an individuals behavior may even result in changes in the viral load. Furthermore, the immune system is not considered "perfect" and at times its strength may vary. We see from Figure 27 that the model does not exhibit the same type of oscillatory behavior that is illustrated by the target-cell-limited and simple immune models and may struggle to capture any dynamics where the patient's viral load changes post steady state. In addition, the model seems to overestimate the initial value of the steady state. This is likely due to the fact that the model desires to account for the changes in the population after the steady state and as a result tests to overestimate the value of the viral load during that time period. Yet, even with these flaws the extended immune model does a wonderful job at capturing and illustrating the overall dynamics of the system

In addition to the simplified extended immune model, we ran a simulation with the standard extended immune model to examine the behavior of the immune effector cells, E, during the course of the infection. This was done in order to determine how realistic our assumption of a quasi-steady state solution was for the system. By utilizing a stead state approximation, we assumed

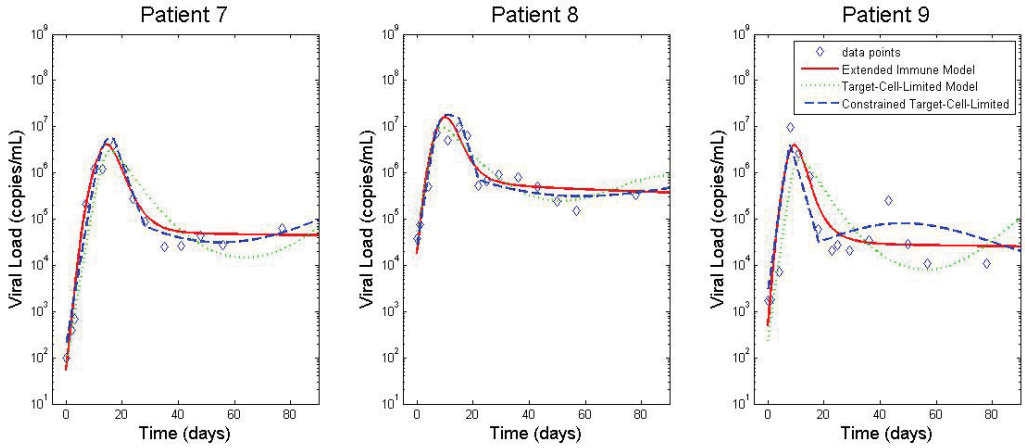

Figure 27: All three Models applied to Patients 7 - 9.

that $\frac{dE}{dt} = 0$. As we can see in Figure 28, the immune response does change during the course of the infection. There is the immune response, which begins on approximately day 2 and reaches a max of $1.8\frac{copies}{mL}$ at approximately day 13. The immune response then decays until it ultimately reaches a steady state of approximately $0.15\frac{copies}{mL}$. However, relative to the other populations that we have in the system the change in the immune response is minimal during the course of infection. Furthermore, after approximately day 40, the population remains entirely constant as the virus reaches the steady state and the viral population is controlled.

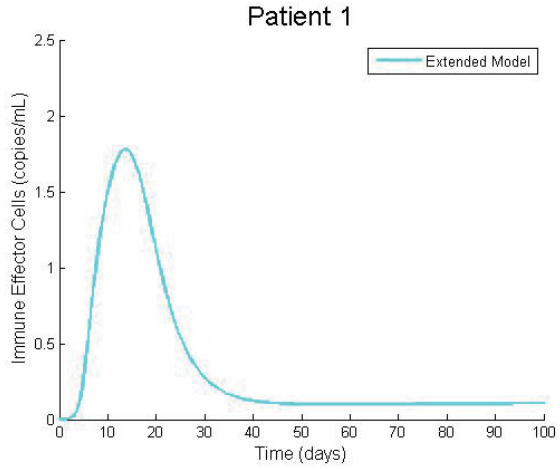

Figure 28: The dynamics of the Immune Effector Cell population with $\frac{dE}{dt} \neq 0$.

7.5 Sensitivity Analysis

As with the previous models, we examined how small changes in the parameters impact the dynamics of the system in order to determine how sensitive or robust the model is to changes in its inputs. The corresponding sensitivity systems with respect to β, δ, and p are shown below.

For β:

(6e) $S'_{T_\beta(t)} = -\big(V(t)S_{T_beta(t)} + S_{V_\beta(t)}\big) - dS_{T_\beta(t)}$

(6f) $S'_{I_\beta(t)} = \big(V(t)S_{T_\beta(t)} + S_{V_\beta(t)}\big) - \big((\alpha d + k_0 E(t)) + I(t)k_0 S_{E_\beta(t)}\big)$

(6g) $S'_{V_\beta(t)} = pS_{I_\beta(t)} - cS_{V_\beta(t)}$

(6h) $S'_{E_\beta(t)} = \dfrac{a_E(I(t)+\theta)S_{I_\beta(t)} - I(t)S_{I_\beta(t)}}{(I(t)+\theta)^2} - d_E S_{E_\beta(t)}$

For δ:

(6i) $S'_{T_\delta(t)} = -\beta\big(V(t)S_{T_\delta(t)} + S_{V_\delta(t)}\big) - dS_{T_\delta(t)}$

(6j) $S'_{I_\delta(t)} = \beta\big(V(t)S_{T_\delta(t)} + S_{V_\delta(t)}\big) - \big((\alpha d + k_0 E(t)) + I(t)k_0 S_{E_\delta(t)}\big)$

(6k) $S'_{V_\delta(t)} = pS_{I_\delta(t)} - cS_{V_\delta(t)}$

(6l) $S'_{E_\delta(t)} = \dfrac{a_E(I(t)+\theta)S_{I_\delta(t)} - I(t)S_{I_\delta(t)}}{(I(t)+\theta)^2} - d_E S_{E_\delta(t)}$

For p:

(6m) $S'_{T_p(t)} = -\beta\big(V(t)S_{T_p(t)} + S_{V_p(t)}\big) - dS_{T_p(t)}$

(6n) $S'_{I_p(t)} = \beta\big(V(t)S_{T_p(t)} + S_{V_p(t)}\big) - \big((\alpha d + k_0 E(t)) + I(t)k_0 S_{E_p(t)}\big)$

(6o) $S'_{V_p(t)} = S_{I_p(t)} - cS_{V_p(t)}$

(6p) $S'_{E_p(t)} = \dfrac{a_E(I(t)+\theta)S_{I_p(t)} - I(t)S_{I_p(t)}}{(I(t)+\theta)^2} - d_E S_{E_p(t)}$

From Figure 29 we can see that while the extended immune model is most sensitive to the rate of infection, β, overall, the model is much less sensitive to changes in the parameters relative to the other model we have examined up to this point for β, δ, and p. Furthermore, we can see that the changes in the parameters do not impact the behavior of the virus population after the steady state, a problem that persisted in all of the other models we examined.

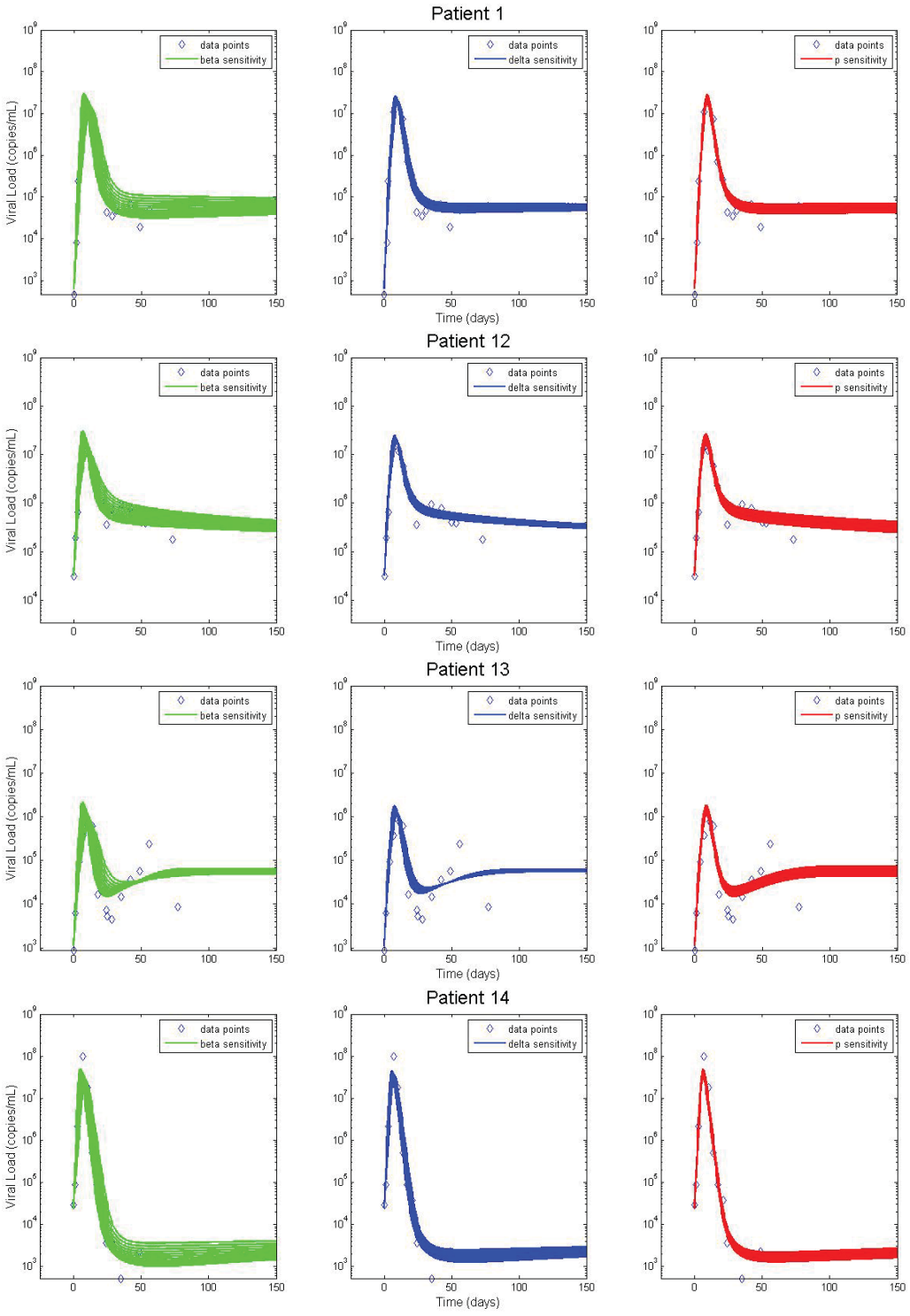

Figure 29: The effect of varying the parameters β, δ, and p.

8 Model Comparison and Results

We used three primary methods in order to compare the fits of the three models. We focused on three metrics commonly used to measure the quality of statistical models for a given set of data. Each one of these metrics provides a quantitative estimate of the quality of each model in relation to the others and thus allows s to determine which model is the best fit of the data. In comparing the models, the model with the lowest value for any of the criteria means that the model is the best fit of the data. This is because the value is essentially the logarithm of the residual sum of square errors, thus when both positive and negative the lower value suggests a positive fit. First, we considered the log-likelihood, Akaike Information Criteria (AIC) and Bayesian Information Criteria (BIC) derived from Monolix. In addition to the calculations in Monolix, we calculated the residuals of the various fits using MATLAB in order to compute the sum of squares. We then used the known formulas for AIC and BIC in order to compare the three model fits.

8.1 Akaike Information Criterion

(8a) $$AIC = n \log\left(\frac{L}{n}\right) + 2k$$

(8b) $$AIC_c = AIC + \frac{2k(k+1)}{n-k-1}$$

Table 17: Parameters for the Akaike Information Criteria

Parameter	Interpretation
k	Number of Parameters
L	Residual Sum of Squares
n	Total number of Observations

In our first model comparison, we used the corrected AIC test, which is an AIC test that accounts for a finite number of sample sizes, which is the case in our analysis. As a result of accounting for finite sample sizes, the model tends to account more for changes in the number of parameters relative to the other models. Thus, in the corrected AIC test, the number of parameters has a much larger impact on the AIC value (and hence impacts the quantitative quality) of the fit. For instance, with the standard target-cell-limited model we fit five parameters, whereas with the extended immune model we fit an extra parameter (totaling 6), and the constrained target-cell-limited model we fit two extra parameters (totaling 7). These number of parameters have a large impact of the AIC value and thus in determining which model is the best fit for the data. Therefore, there may be cases when one model is technically more accurate (has a lower residual sum of square errors, however, due to the model having additional parameters, may not appear to be the overall best fit of the data.

The AIC_C values listed in Table 18 for patients 1 - 14 suggest that the Extended Immune model is most accurate in describing the dynamics over the first 95 days of infection. Again, the lowest number suggests the best fit for that specific model. Thus, if we examine Patient 1, the AIC_C value for the target-cell-limited model was -5.48, for the extended immune it was -32.322. Thus, the extended immune model was a better fit of the data than the target-cell-limited model. As we can see in the table, for 13 of the 14 patients, the corrected AIC value for

Table 18: Akaike Information Criteria Values

Patient	$AIC_{(c,TCL)}$	$AIC_{(c,Extended)}$	$AIC_{(c,constTCL)}$	$AIC_{(c,SimpleImmune)}$
1	-5.4822	-32.331	-11.4176	5.19
2	-5.7999	-22.621	-16.7554	1.3545
3	-18.5493	-18.7395	-17.473	-6.9006
4	-11.8164	-16.1279	-9.0006	-1.7777
5	-8.6837	-33.4409	-12.5796	1.8669
6	9.894	-16.8676	4.7287	20.7795
7	-16.9918	-35.2786	-27.8071	-13.3892
8	-26.9879	-33.5626	-27.1607	-14.4744
9	8.2402	-5.0845	2.1027	15.8091
10	21.6822	-4.3086	20.5935	35.0533
11	-21.0187	-32.0683	-11.4072	-9.06
12	-0.7421	-9.5161	-1.5145	12.3056
13	15.7057	3.5286	1.9273	16.2128
14	6.7216	-7.1624	12.6372	31.5652

the extended model was less than those for the Target-Cell-Limited and constrained Target-Cell-Limited models. The constrained target-cell-limited model appeared to be the next best fit of the data, and actually eclipsed the extended immune model in 1 of the 14 patients. However, since the number of parameters impacts the value of the AIC for a specific model, we expect that part of the reason that the constrained Target-Cell-Limited model achieves a lower corrected AIC value is due to the estimation of a smaller number of parameters.

8.2 Bayesian Information Criterion

(9) $$BIC = n \log\left(\frac{L}{n}\right) + k \log n$$

Table 19: Parameters for the Bayesian Information Criteria

Parameter	Interpretation
k	Number of Parameters
L	Residual Sum of Squares
n	Total number of Observations

In addition to the AIC criteria, we implemented the Bayesian Information Criterion in order to help determine which model was the best fit of the data. The BIC, like the AIC, accounts for the number of estimated parameters. In addition, the BIC values listed in Table 20 support the same conclusion made from the AIC values in table 18: the extended immune model does the best job of fitting the data. As we can see from Table 20, again 13 of the 14 patients have the lowest BIC value given by the extended immune model; the corrected AIC value of patient 13 was lower for the Constrained Target-Cell-Limited model.

Furthermore, Monolix provides estimates for the Log-likelihood, AIC, and BIC for the individual fits. The results from Monolix again suggest that the extended immune model is the most

Table 20: Bayesian Information Criteria Values

Patient	BIC_{TCL}	$BIC_{Extended}$	$BIC_{constTCL}$	$BIC_{SimpleImmune}$
1	49.1288	22.28	43.1934	49.0823
2	58.4022	41.5811	47.4467	53.5357
3	50.3999	50.2097	51.4761	57.6582
4	32.9475	28.636	35.7633	41.4297
5	55.5184	30.7613	51.6225	57.7115
6	64.505	37.7434	59.3396	65.2285
7	42.4357	24.1489	31.6204	37.6119
8	32.4396	25.8649	32.2668	38.2582
9	57.9727	44.6481	51.8352	57.616
10	66.4461	40.4553	65.3574	71.0238
11	33.5922	22.5426	43.2038	49.0927
12	48.9904	40.2165	48.2181	53.9988
13	60.4696	48.2925	46.6912	52.3577
14	29.4556	15.5716	35.3713	40.5012

appropriate for modeling the dynamics of primary infection in these patients: all three of the measurements were lowest for the extended immune model.

Table 21: Comparison of the Models

Measure	TCL	Constrained TCL	Simple Immune	Extended Immune
Log-Likelihood	425.87	397.59	405.05	337.01
AIC	443.87	415.59	431.05	363.01
BIC	449.63	421.34	438.39	371.32

9 Tumor Dynamics Models

Prior to integrating the dynamics of cancerous tumor development in with our study of HIV, it is first important to explore the dynamics of tumor growth alone, without immune interaction or viral interference. The two most commonly used platforms for examining cancerous tumor development are the exponential growth and the logistic growth tumor models. In our preliminary study of tumor dynamics models, we will examine both the exponential power growth tumor model as well as the logistic growth tumor model. We will then choose a single model to be the basis of our tumor-immunodeficiency model which will allow us to examine the tumor's interaction with an HIV compromised immune system. The decision for which model to use depends on several factors including the type of tumor, location of the tumor, however the most important characteristics to consider are the stage of tumor growth as well as the time frame that we will be examining.

There are two primary stages of tumor growth, early and late stage growth. Early stage growth is highlighted by simple exponential growth where the tumor proliferates uncontrollably as a result of cellulate mutation as described in section 1.1.3. Therefore, if the tumor is in it's early stages, there is not a significant distinction between the power growth and logistic growth models [9]. The distinction between the two models is amplified in the later stages where the behavior of the tumor is characterized by one of two scenarios: the limiting of growth, either by immune mediated suppression, achievement of the carrying capacity, or ultimately the termination of the host. As opposed to power growth, logistic growth during this late stage is self limiting, meaning that the tumor grows until it reaches the carrying capacity.

Ultimately our decision between the logistic growth and power growth models hinges on whether or not we are attempting to examine the long term behavior of the tumor. We will explore the differences between the two models, discuss which model is best for our study, and ultimately use the model we choose as the basis for our further study with HIV interaction.

9.1 Power Growth Tumor Model

The Power Growth Tumor Model includes the effects of cell growth as a result of genetic mutations within cells and tumor suppressing genes. The model is the most basic model for examining tumor growth and is often applied more generally to study population dynamics in simple systems. It is important to note that the Power Growth Tumor Model does not include the dynamics of any sort of response, nor does it include any self limited growth. Therefore, we expect that the population will continue to proliferate indefinitely since there is no mechanism to impede growth. The Power Growth Tumor Model considers only one population $C(t)$, which denotes the concentration of cancerous tumor cells at time t and is represented by the following differential equation:

$$\frac{dC}{dt} = aC(t)^b \tag{10}$$

where a is the tumor cell growth rate, $\frac{1}{b}$ represents the carrying capacity for the tumor, and $C(0) = C_0$ is the initial condition for the tumor population. In our case we assume that a mutation occurs in a single cell, and thus that $C(0) = 1$. Since the power growth model is relatively simple,

we are able to explicitly solve the model and derive an expression for the population of tumor cells for all time. For the Power Growth Tumor Model, we solve equation 10 such that:

$$C(t) = \Big((1-b)(at + \frac{C_0^{1-b}}{1-b})\Big)^{\frac{1}{1-b}}$$

.

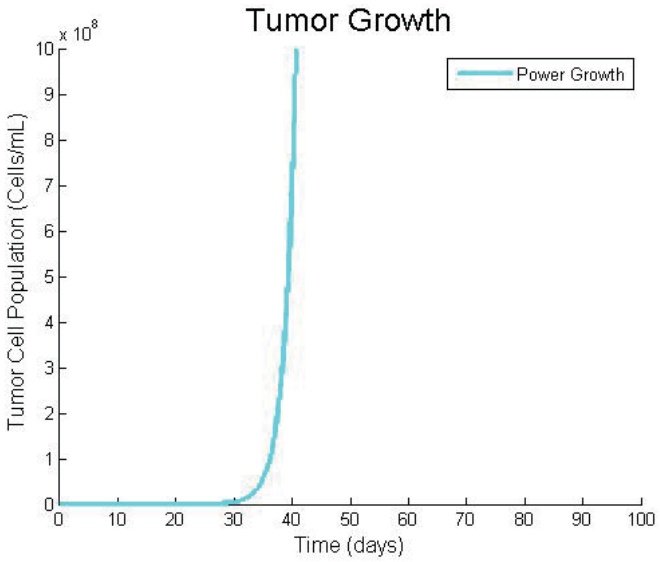

Figure 30: A numerical simulation illustrating the dynamics of the power growth tumor.

We can clearly from this expression that the solution is positive, however that the population of tumor cells is not bounded for all time. Figure 30 is a numerical simulation representing the behavior of the Tumor in the absence of any sort of response where the parameters were estimated from [9]. As we can clearly see, the Tumor begins uncontrolled exponential growth that is never checked at any point, thus confirming our theory that the system was not bounded since the population approaches a vertical asymptote. Furthermore, unchecked growth suggests that the model is not appropriate for all time, since the population will simply approach infinity as time increases which is not realistic for our system. Yet, although we cannot use the model for all time, the power growth model is extremely effective at representing the initial dynamics of tumor growth, which has been characterized as exponential in nature [9].

However, in our study of tumor dynamics, we are not only trying to examine the initial growth phase of the tumor; we are also interested in the long term behavior of the system. Furthermore, we are interested in more complex system dynamics seen during the introduction of HIV. The exponential growth phase which will only be good at representing the initial growth and will remain unaffected by any sort of immune response or viral propagation. Thus, the power growth tumor model will likely not be the best model for our analysis. However, there are several additional tumor models which examine the growth and include more complex dynamics which are better for examining the long term behavior. In the next section we will introduce the Logistic Growth Model and examine its feasibility as the basis for our tumor-immune model.

9.2 Logistic Growth Tumor Model

The Logistic Growth Tumor Model, like the Power Growth Model, includes the effects of cancerous tumor development. However, unlike the Power Growth Model, the Logistic Growth Model includes self containing logistic growth properties that are characteristic for cancer cell development and the long term behavior of a cancerous tumor. While the model includes self

limited growth, the Logistic Growth Model does not include any sort of immune mediated response, and thus, the Logistic Growth Tumor Model, like the Power Growth Model, only considers one population, $C(t)$ which is the concentration of cancerous tumor cells at time t. The model can be represented by the single ordinary differential equation:

$$(11)\quad \frac{dC}{dt} = aC(t)(1 - bC(t))$$

where again a is the tumor cell growth rate, $\frac{1}{b}$ represents the carrying capacity for the tumor, and $C(0) = C_0$ is the initial condition for the cancerous cell population. As with the Power Growth Model, we are able to find an explicit solution for the number of tumor cells. In the case of the logistic growth tumor model, we find that

$$C(t) = \frac{1}{b + \left(\frac{1-bC_0}{C_0}\right)e^{-at}}$$

By examining this expression, we can see that $C(t)$ will be both positive and bounded for all time. This is incredibly important, because, as discussed previously, we know that the cellular population in the body is finite. In addition, we know that the long term growth dynamics of the tumor can be characterized by exponential growth followed by the where it will approach a carrying capacity. This carrying capacity will either be determined by the location and amount of resources that are available for the tumor's consumption, which can control the growth, or by the terminal capacity of the patient, whereby the patient (and thus the tumor) will not survive the when the tumor grows past a specific population. From Figure 31 we can see a numerical simulation of the logistic growth of a tumor with estimates obtained from [9]. As is characteristic of cancerous cell development, the tumor assumes an exponential like form during the initial growth, however, as the tumor cells exhaust the resources promoting their growth, the tumor's growth rate begins to subside and the tumor population approaches the carrying capacity, which in this case is approximately 1×10^9 $\frac{cells}{mL}$. In total, the entire growth process, from a mutation in a single cell takes approximately 50 days with the most dynamic portion of the life cycle occurring between days 30 and 50. It is important to note that this life cycle is almost twice as long as the cycle for HIV and that the dynamic behavior occurs much later. This notion will become more important when we characterize immune responses to cancerous cell development.

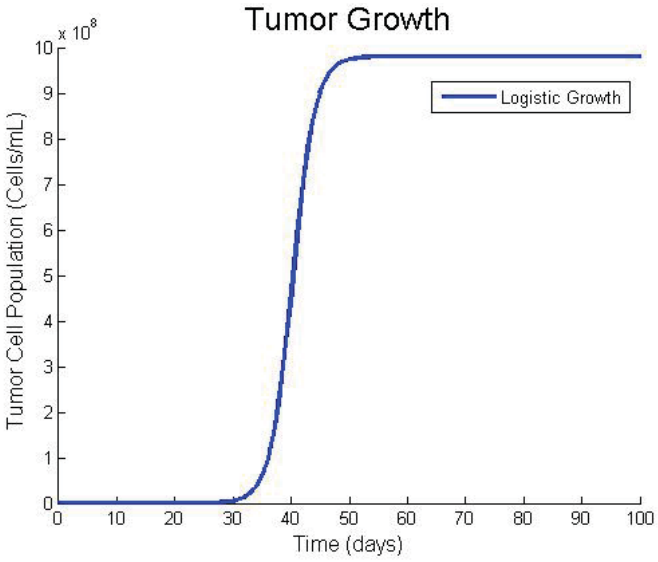

Figure 31: A numerical simulation highlighting the dynamics of a logistic growth tumor model.

In Figure 32 we can see the comparison between the Exponential Growth and Logistic Growth Models. From days 0 to approximately day 38, during what is known as the exponential growth phase (shown in black on the graph) of the cancer cell development, both the logistic and power growth models are extremely similar and even overlap. However, at approximately day 38, the two models begin to diverge as the proliferation rates for the logistic growth begins to slow. This stage is denoted as the Slowing Growth stage (shown in orange), however, this stage only occurs for the logistic growth model. Furthermore, by day 50 when the logistic growth has reached its maximum value (what is known as the carrying capacity), the exponential growth (shown in green) continues, and the curves have diverged significantly.

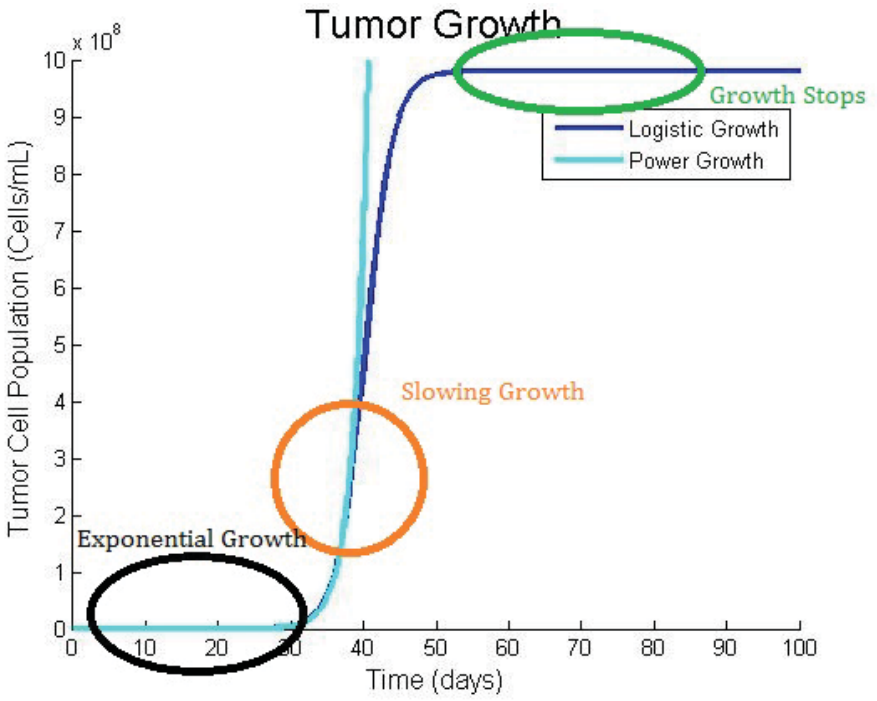

Figure 32: A comparison of the Logistic and Power Growth Tumor Models.

9.3 Tumor Immune Model

Since we are going to be examining the long term behavior of the system in an attempt to see how the tumor will interact with HIV and the immune system, it is much more appropriate to use the logistic growth tumor model as the basis for developing a tumor-immune model and ultimately a tumor-immunodeficiency model. As discussed in Section 1.1.3, we know that Cytokines, which are secreted by Helper-T cells, play an extremely larger role in the development and proliferation of a immunosuppressive response and ultimately in cancer immunity. Furthermore, they can encourage innate anti-cancer responses including the proliferation of cytotoxic T-lymphocytes or CD8 T-cells which are able to attack and kill tumor cells making them a primary component of the immune response. Thus, when we examine the impact of an immune response and the interaction between

a developing tumor and the immune system, we will highlight and model the interaction of the tumor with CD4 T-cells. Thus, the model considers two distinct populations which are denoted:

$T(t)$: concentration of target cells (CD4 T-cells) at time t,
$C(t)$: concentration of cancerous tumor cells at time t.

The model assumes that the CD4 T-cells mature at a constant rate in the thymus and experience the same death behavior as in the HIV models. Thus, equation 12a of this model is the same as equation 2a from the standard Target-Cell-Limited model where the viral population is zero. Furthermore, it supposes that the cancer cells grow logistically and that the interaction between the cancer and the CD4 T-cells abides by the mass action principle. Given these assumptions, the model can be defined such that:

$$\text{(12a)} \quad \frac{dT}{dt} = \sigma - dT(t)$$

$$\text{(12b)} \quad \frac{dC}{dt} = aC(t)(1 - bC(t)) - a_C C(t)T(t)$$

The parameters for which are provided in the table below.

Table 22: Parameters for the Tumor-Immune Model

Parameter	**Biological Interpretation**	**Units**	**Estimate**
a	Growth rate	$(mL)^{-1}days^{-1}$	0.514
b	1/Carrying capacity	$mL(cells)^{-1}$	1.02×10^{-9}
λ	Immune production rate	$(cells)(mL)^{-1}days^{-1}$	1.30×10^{4}
a_c	Immune-tumor interaction rate	$(cells)(mL)^{-1}days^{-1}$	1×10^{-6}
d	Death rate of immune cells	$days^{-1}$	4.12×10^{-2}

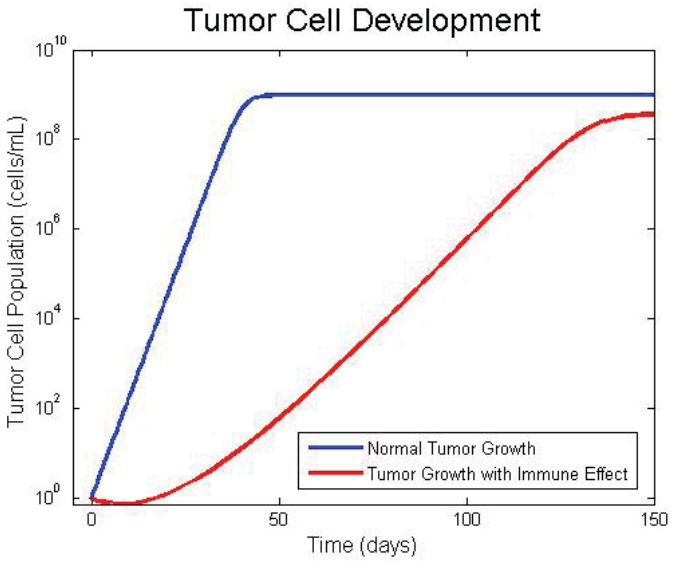

Figure 33: A simulation of the Tumor-Immune Model and Comparison to Logistic Growth Tumor Model.

Figure 33 illustrates the dynamics of the tumor-immune model. The blue line represents the normal tumor growth without an activated immune response and the red line represents the system dynamic with immune activation. Clearly, the immune system has a major impact on cancerous cell development, primarily in pace, however, also in magnitude. We can see that the immune response clearly slows cancerous cell growth; whereas the normal tumor is a carrying capacity near day 35, the tumor with immune response does not reach full strength until $\approx$ day 145. This delay of tumor cell proliferation is extremely important as it would allow

for doctors to more easily and quickly identify tumor development and treat it much more effectively with therapies (whose effects are not included in this model). It has been shown that early identified cancerous and tumor development is crucial in mounting effective responses [9]. Furthermore, the immune system response results in a lower steady state tumor population; for instance, the long term steady state for the normal tumor growth model is $\approx 10^9$ whereas, the steady state for the tumor growth with immune effect is $\approx 5 \times 10^8$, or roughly half. Overall, this simulation suggests that the immune system has a very large impact on the proliferation and progression of cancerous cell development by highlighting the immune system's ability to slow cancer cell development and even limit its growth.

In addition, we used a sensitivity analysis to analyze the effects of varying the Immune-tumor interaction parameter, a_c.

For a_c:

$$S'_{T_{a_c}(t)} = -d(S_{T_{a_c}(t)}) \tag{12c}$$

$$S'_{C_{a_c}(t)} = aC(t)\big(-bS_{C_{a_c}(t)}\big) + \big(1 - bC(t)\big)aS_{C_{a_c}(t)} - a_c\big(C(t)S_{T_{a_c}(t)} + S_{C_{a_c}(t)}\big) \tag{12d}$$

In Figure 34 we notice that as the interaction rate between the tumor and the target cells increases, the delay of the tumor increases, causing the time at which the tumor reaches the carrying capacity to also increase. This gives the doctors even more time to recognize the cancerous tumor development and prescribe therapies to cease further growth. In addition, the minimum value of tumor cells that is achieved is effected by the interaction rate; as the interaction rate increases, the minimum number of cancerous tumor cells decreases. This is important because treatment implemented at this time would likely be extremely effective at combating future tumor growth and ultimately leading to the clearance of the cancer.

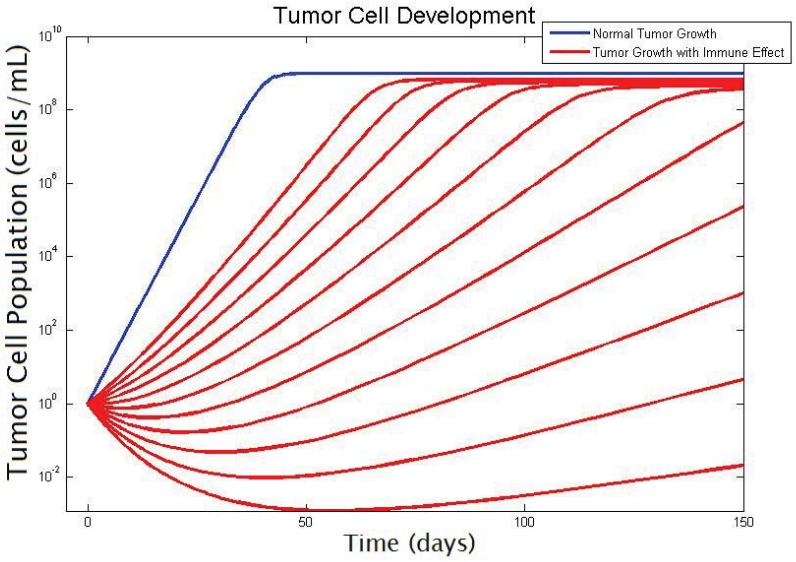

Figure 34: The effect of varying the tumor-immune interaction rate, a_C.

10 Tumor-Immunodeficiency Model

10.1 Model Development

We use the Extended Immune Model as well as the Tumor-Immune Model as the basis for developing our Tumor-Immunodeficiency Model. However, before we proceed with the model development and analysis, it is important for us to note one change between the Tumor-Immunodeficiency Model and the previous models we base this new model on. One of the original assumptions we made with regard to the Extended Immune Model was the quasi steady state approximation when analyzing the dynamics of the immune effector cells. The details of this approximation are provided in Section 7. We made this assumption due to the short duration of HIV infection prior to the steady state. As we saw in Section 7, by approximately day 25, the patients had all arrived at the steady state, and most of the dynamic interaction had already taken place within the system. Thus, the immune system's ability to proliferate a vast amount of effector cells is somewhat limited. However, when we examine the dynamics of the more complex tumor-immune interaction this assumption will no longer hold. This results from the much longer time frame in which cancerous cell development occurs. For instance the dynamic portion of the tumor life cycle (until the tumor population reaches the steady state) is usually between 50 and 150 days [9]. This time period is significantly longer that the ≈ 25 days in which the viral dynamic occur. Thus, we must remove the quasi-steady state approximation we utilized earlier in this paper. In developing the model, we integrate the entire Extended Immune Model from Section 7 with the cancerous tumor cells equation Tumor-Immune Model from Section 8, where the population of the target cells (CD4 T-cells) is held consistent across both models. The resulting model is a system of five nonlinear ordinary differential equations which are detailed in the next section.

10.2 The Model

The Tumor-Immunodeficiency Model examines the interaction between cancer and HIV within the immune system. As mentioned previously, the model considers five distinct populations:

$T(t)$: concentration of target cells at time t,
$I(t)$: concentration of infected cells at time t,
$V(t)$: concentration of free virus at time t,
$E(t)$: concentration of immune effector cells at time t,
$C(t)$: concentration of cancerous tumor cells at time t.

The resulting model is a system of five nonlinear ordinary differential equations where:

$$\text{(13a)}\quad \frac{dT}{dt} = \lambda - \beta V(t)T(t) - dT(t)$$

$$\text{(13b)}\quad \frac{dI}{dt} = \beta V(t)T(t) - \Big(\alpha d + k_0 E(t)\Big)I(t)$$

$$\text{(13c)}\quad \frac{dV}{dt} = pI(t) - cV(t)$$

$$\text{(13d)}\quad \frac{dE}{dt} = a_E \frac{I(t)}{\theta + I(t)} - d_E E(t)$$

$$\text{(13e)}\quad \frac{dC}{dt} = aC(t)(1 - bC(t)) - a_C C(t)T(t)$$

Table 23: Parameters for the Tumor-Immunodeficiency Model

Parameter	Biological Interpretation	Units	Known Value
λ	Target cell production rate	$(Cells)mL^{-1}days^{-1}$	dT_0
β	Rate of infection	$(mL)Cells^{-1}days^{-1}$	$(r+\delta)\frac{c}{pT_0}$
d	Target cell death rate	$days^{-1}$	Estimated*
α	Rate of viral decay	$days^{-1}$	Estimated*
p	Viral production rate	$days^{-1}$	Estimated*
c	Viral clearance rate	$days^{-1}$	23
k_0	Maximum value of activity potential	$(mL)Cells^{-1}days^{-1}$	Estimated*
θ	Half-maximal simulation threshold	$(Cells)mL^{-1}$	Estimated*
a	Growth rate	$mL^{-1}days^{-1}$	0.514
b	1/Carrying capacity	$mL(cells)^{-1}$	1.02×10^{-9}
a_c	Immune-tumor interaction rate	$(cells)(mL)^{-1}days^{-1}$	1×10^{-6}
d_E	Death rate of immune cells	$days^{-1}$	4.12×10^{-2}

Table 24: Initial Conditions for the Tumor-Immunodeficiency Model

Initial Conditions	Value	Units
T_0	5.9×10^5	$(Cells)mL^{-1}$
I_0	$\frac{c}{p}V_0$	$(Cells)mL^{-1}$
V_0	Estimated*	$(Cells)mL^{-1}$
E_0	0	$(Cells)mL^{-1}$
C_0	1	$(Cells)mL^{-1}$

The asterisk in Tables 21 and 23 denotes estimations that we carried our for the Tumor-Immunodeficiency model using the data from the patients from Section 2.

10.3 Existence and Uniqueness

10.3.1 Positivity and Boundedness

Lemma (*Positivity*)**.** *Let $t_0 > 0$. In the model, if the initial conditions satisfy $T(0) > 0$, $I(0) > 0$, $V(0) > 0$, $E(0) > 0$, $C(0) > 0$ then for all $t \in [0, t_0]$, $T(t)$, $I(t)$, $V(t)$, $E(t)$, and $C(t)$ will remain positive in $\mathbb{R}^5_+$.*

Proof: Positivity. We must prove that for all $t \in [0, t_0]$, $T(t)$, $I(t)$, $V(t)$, $E(t)$, and $C(t)$ will be positive in $\mathbb{R}^5_+$. We know that all of the parameters used in the system are positive. In section 6.2.1 we proved the positivity of the Extended Immune Model. For the Tumor-Immunodeficiency Model, the equations for $T(t)$, $I(t)$, $V(t)$, $E(t)$, remain the same. Thus, we do not need to go through the proofs for these equations since they are done above. However, we need to show that $C(t)$ remains positive.

We can place lower bounds on the differential equation for $C(t)$ and thus,

$$\frac{dC}{dt} = aC(t)(1 - bC(t)) - a_C C(t)T(t) \geq -a_C C(t)T(t)$$

Through basic differential equations methods we can resolve the inequalities and produce:

$$C(t) \geq e^{-a_C \int T(t)dt} \geq 0$$

Thus, for all $t \in [0, t_0]$, $T(t)$, $I(t)$, $V(t)$, $E(t)$, and $C(t)$ will be positive and remain in $\mathbb{R}^5_+$. □

Lemma (Boundedness)**.** *There exists an* $T_M, I_M, V_M, E_M, C_M > 0$ *such that for* $T(t)$, $I(t)$, $I(t)$, $E(t)$, $C(t)$ $\limsup_{t\to\infty}\Big(X(t)\Big) \leq T_M$, $\limsup_{t\to\infty}\Big(I(t)\Big) \leq I_M$, $\limsup_{t\to\infty}\Big(V(t)\Big) \leq V_M$, $\limsup_{t\to\infty}\Big(E(t)\Big) \leq E_M$, $\limsup_{t\to\infty}\Big(C(t)\Big) \leq C_M$ *for all* $t \in [0, t_0]$.

Proof: Boundedness. We must prove that for all $t \in [0, t_0]$, $T(t)$, $I(t)$, $V(t)$, $E(t)$, and $C(t)$ will be bounded. We know that all of the constants used in the system are positive. In addition, we have shown that $T(t)$, $I(t)$, $V(t)$, and $E(t)$ are bounded in section 6.2.
As a result, we only need to show that $C(t)$ is bounded.

We can place an upper bound on $\frac{dC}{dt}$ such that

$$\frac{dC}{dt} = aC(t)(1 - bC(t)) - a_C C(t)T(t) \leq aC(t)(1 - bC(t))$$

Furthermore, we know that $\frac{dC}{dt} = aC(t)(1 - bC(t))$ implies that $C(t) = \frac{1}{b+\left(\frac{1-bC_0}{C_0}\right)e^{-at}}$. Thus, we can choose $C_M = \frac{1}{b}$ such that $C(t) \leq C_M$ for all $t \in [0, t_0]$. □

Theorem 11 (Existence)**.** *Let* $t_0 > 0$. *In the model, if the initial conditions satisfy* $T(0) > 0$, $I(0) > 0$, $V(0) > 0$, $E(0) > 0$, $C(0) > 0$ *then* $\forall t \in \mathbb{R}$ $T(t)$, $I(t)$, $V(t)$, $E(t)$, *and* $C(t)$ *will exist in* $\mathbb{R}^5_+$.

Proof: Existence and Uniqueness. In the case of our model we have:

$$\mathbf{x} = \begin{bmatrix} T(t) \\ I(t) \\ V(t) \\ E(t) \\ C(t) \end{bmatrix} \text{ and } \mathbf{f}(\mathbf{x}) = \begin{bmatrix} \lambda - dT(t) - \beta V(t)T(t) \\ \beta V(t)T(t) - \Big(\alpha d + k_0 E(t)\Big)I(t) \\ pI(t) - cV(t) \\ a_E \frac{I(t)}{\theta + I(t)} - d_E E(t) \\ aC(t)(1 - bC(t)) - a_C C(t)T(t) \end{bmatrix}$$

Note that f has a continuous derivative on $\mathbb{R}^5$ and thus, f is locally Lipschitz in $\mathbb{R}^5$. Hence, by the Fundamental Existence and Uniqueness Theorem located in the appendix as well as the lemmas proved on positivity and boundedness of solutions, we know that there exists a unique, positive, and bounded solution to the ordinary differential equations given in $13(a) - 13(e)$. □

10.4 Numerical Simulations

We used these parameter estimates to simulate the dynamics of the five populations within the system. Furthermore, we examined and analyzed the behavior of the three most critical populations, the Target Cells (CD4 T-cells), Virus, and Cancerous Tumor cells.

As we can see in Figure 35, the viral population is exactly the same as when we simulated it for the extended immune model and the Tumor-Immunodeficiency model does a really nice job at representing the dynamics of the system. The projected viral population is extremely similar to the data we received from our study patients. Figure 35 also illustrates that the proliferation of cancer has no impact on the dynamics of the virus or the target cell populations. This is because the tumor cell's only interaction with the populations from the Extended Immune system is with the target cells, and this interaction does not promote production or death within the target cell population.

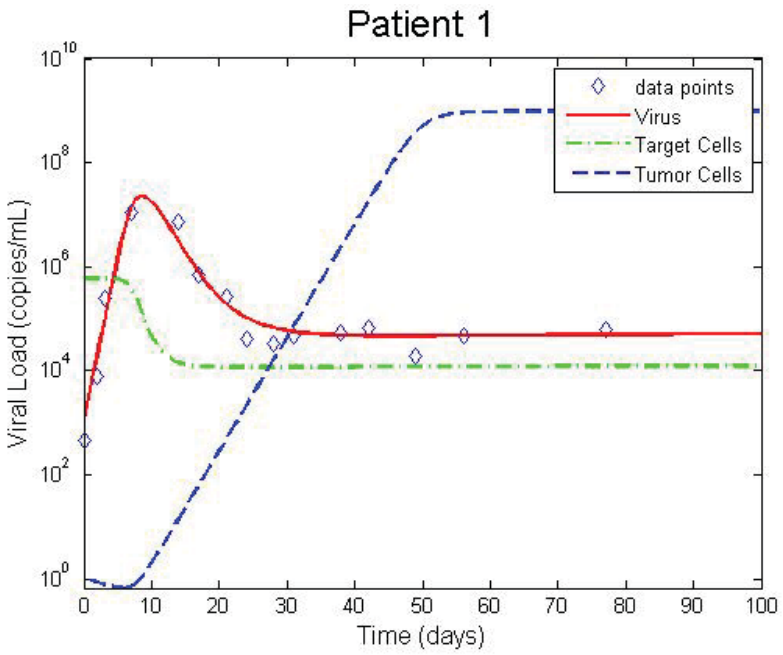

Figure 35: Simulations of the Tumor-Immunodeficiency Model for Patient 1.

Biologically, when target cells interact with the cancerous tumor cells, they are able to recognize the tumor as foreign and release cytokines that ultimately lead to the activation of cytotoxic T-lymphocytes as stated in section 1.1.3. These cells, once activated, are able to kill the cancerous tumor cells. Yet, the cancerous cells' interaction with the target cells does not promote T-cell growth or death, and thus the viral, Target, and infected cell populations remain unaffected by the growth of the cancer.

Yet, while it initially appears as though the cancerous tumor population is not affected by the introduction of the virus and the cancer is simply abiding by the logistic growth, a closer examination reveals that this is not the case. In fact, the tumor cell population is greatly impacted by the immune system and subsequent development of an immune response. However the effectiveness of the immune system is greatly impacted upon the introduction of the virus and viral production, hence the notion of an immunodeficiency.

Figure 36 reveals a magnified illustration of the dynamics of the system during the first 20 days, which is the most dynamic portion of the HIV infection cycle. The Figure shows that introduction of the virus at day zero results in a significant amount of viral growth during the first 8 days of infection where the viral population grows from approximately $1000\frac{virions}{mL}$ to $3 \times 10^7 \frac{virions}{mL}$ by day 8. While the population of the target cells remains relatively consistent for the first few days of infection, over time, the growth of the virus drastically impacts the population of the Target cells.

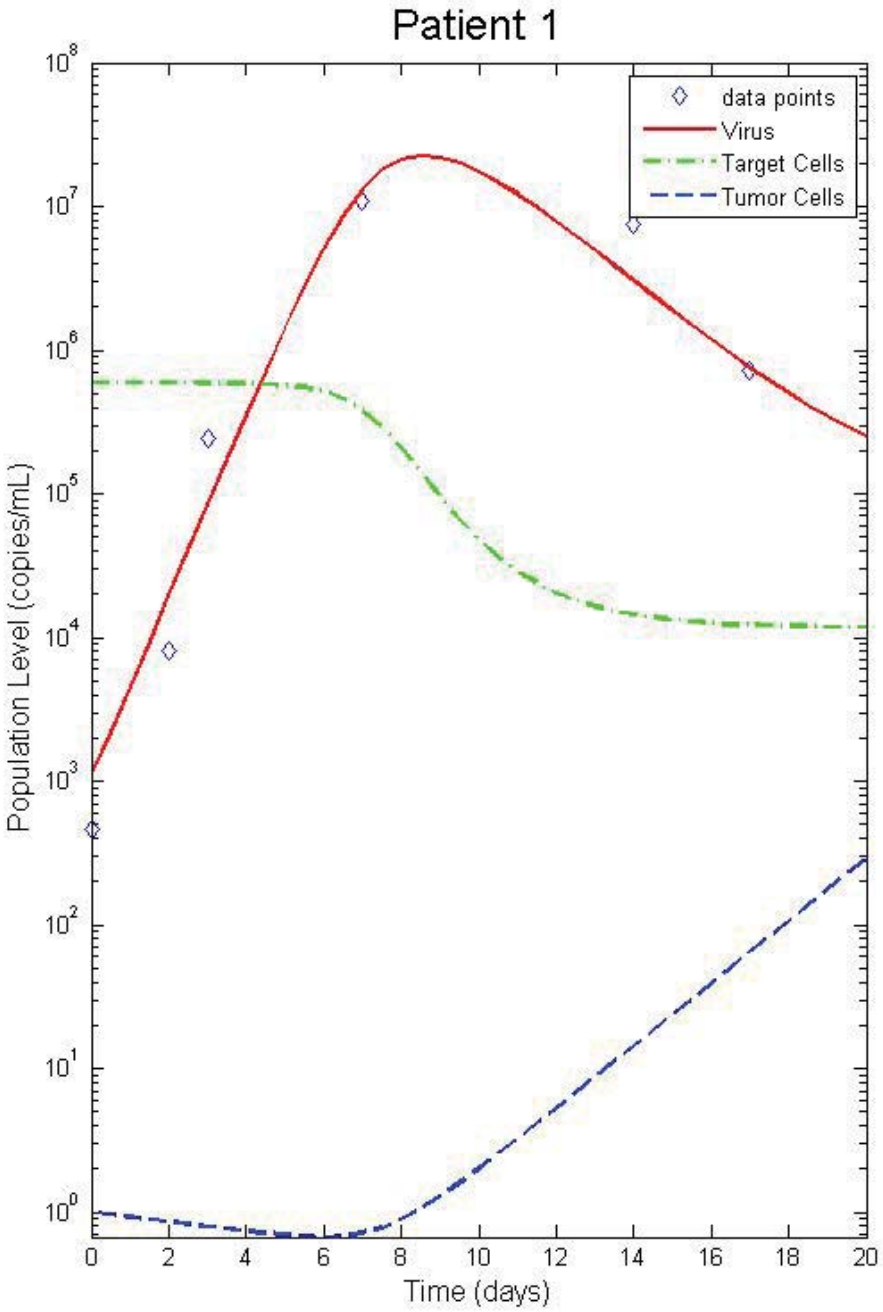

Figure 36: A closer look at the Dynamics of the Tumor-Immunodeficiency Model which highlights system behavior during the most dynamic portion of the viral life cycle.

For instance, by day 6 the target cell population begins to decrease, until it reaches a steady state at approximately day 14. What's more important is that the population of target cells decreases from $5.9 \times 10^5 \frac{cells}{mL}$ to $1 \times 10^4 \frac{cells}{mL}$. This decrease has a extremely large impact on the dynamics of the tumor population. As stated previously, the Target cells serve as a means of recognizing the existence of cancerous tumor development and are ultimately a crucial component for the initiation of an immune response. Thus, the death of a significant portion of the population of Target-cells drastically effects the ability of the tumor to evade, or be unaffected by an immune response. Figure 36 highlights the ability of the tumor to grow during this immunodeficient stage that occurs after the proliferation of the viral population. In addition, we can see that the target-cell population begins to decrease at exactly the same time in which the cancerous tumor resurges.

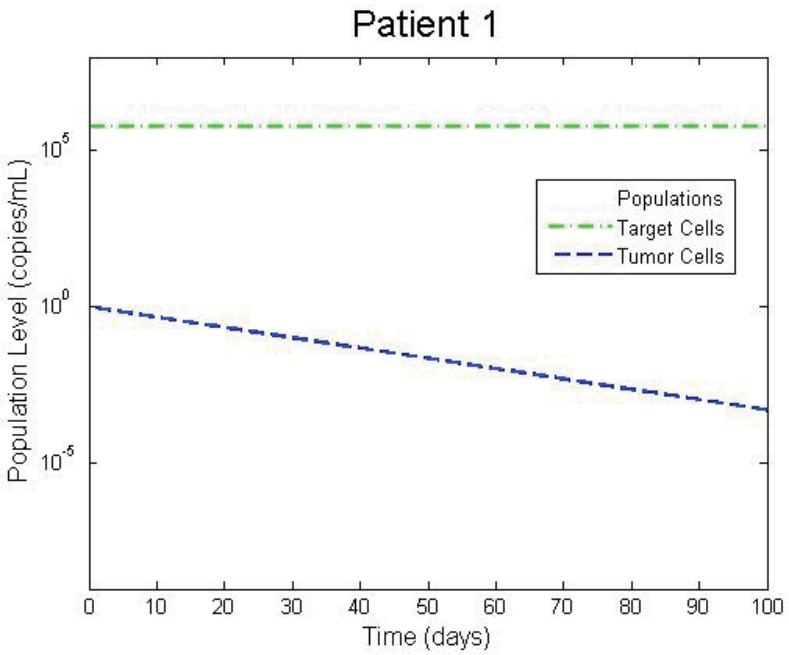

Figure 37: This figure shows the dynamics of the Tumor-Immunodeficiency Model with no HIV infection.

From Figure 36, we can see that during the initial portion of the viral production stage the tumor population is decreasing. For Patient 1, the tumor population decreases from day 0 until approximately day 6 when we see a resurgence of tumor cell growth and the tumor begins to grow logistically as though unaffected by an immune response. Thus, there seems to be a relationship between the population of target cells and the initiation of cancerous cell growth. Furthermore, when the population of the target cells remains constant, we see that the cancerous tumor population decreases. This notion is highlighted in Figure 36, where from day 0 to day 6, during which time the Target cell population remains relatively constant, the population of cancerous tumor cells decreases. Figure 37 is a simulation of the Tumor-Immunodeficiency system where infection is not present ($\beta = 0$ and $V_0 = 0$) and we can see that the cancerous cells ultimately reach levels which are undetectable, and thus the cancerous tumor growth is stopped and the tumor is effectively eliminated. This suggests that the immune system plays a crucial role in controlling cancerous cell development. However, this also suggests that, as soon as the immune system's ability to detect and destroy the tumor population as a result of HIV infection occurs, the tumor resurges.

Figure 38 is a system phase portrait which illustrates the dynamics between the cancerous tumor cell and virus populations. We can see that during viral growth phase, prior to the peak viral

load point, the population of the cancer cells actually decreases. Yet, as soon as the peak viral load is achieved, the population of tumor cells begins to proliferate significantly, and ultimately the population approaches the carrying capacity. This again suggests that the tumor population is being initially controlled during the proliferation of the virus, however, that the tumor population resurges sometime around the point where the peak viral load occurs.

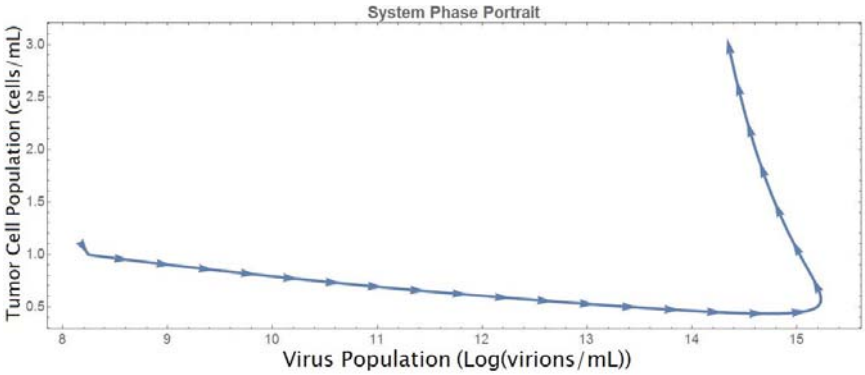

Figure 38: System Phase Portrait comparing the Tumor and Viral Populations.

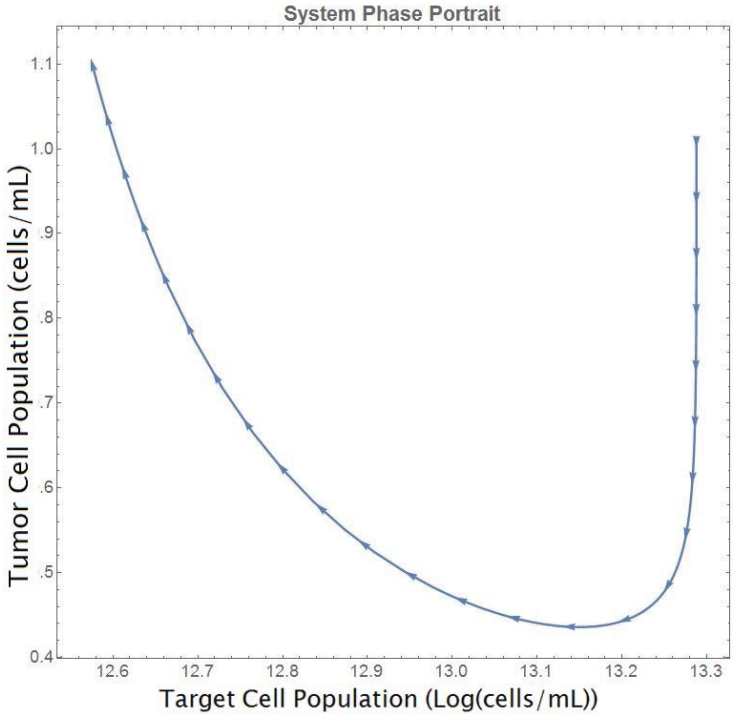

Figure 39: System Phase Portrait comparing the Tumor and Target Cell Populations.

Figure 39 highlights the relationship between the Target cells and cancerous tumor cells. We can see from the Figure that initially the population of cancer cells decreases while the target cell

population remains relatively constant. This again is reflective of the period of time between days 0 and 6 where the virus and resulting infection has not yet significantly decreased the population of target-cells. However, after the target cell population begins to decrease as a result of the infection, the cancerous cell population resurges. This figure is extremely important because it highlights the central role that the Target cells play in the control of cancer and how their population, when impacted is very significant with regards to cancerous cell growth. For instance, even small changes in the target cell population drastically change the dynamics of the tumor.

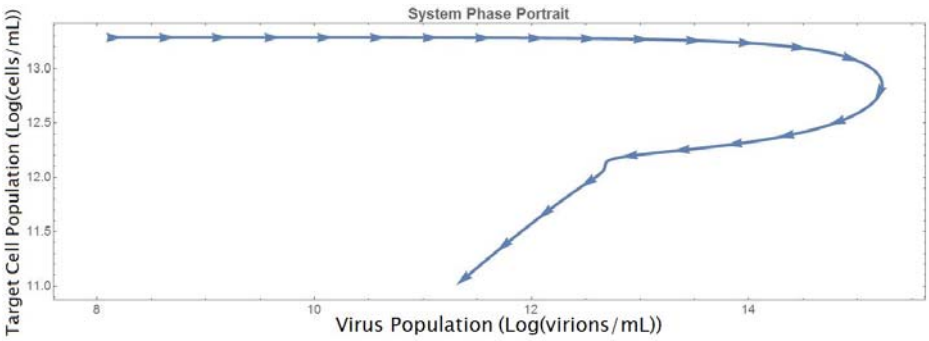

Figure 40: System Phase Portrait comparing the Target Cell and Viral Populations.

Figure 40 is a system phase portrait which examines the relationship between the target cells and virus. As we expect, the target cell population remains relatively constant as the viral population begins to increase, until approximately the peak viral load point, at which time the population of target cells begins to decrease significantly. This Figure shows how the virus and target cells interact. We can clearly see that the virus has a very substantial effect on the population of target cells, however, that a lag exists between the proliferation of the infection and the negative effects the infection has on the population of target cells.

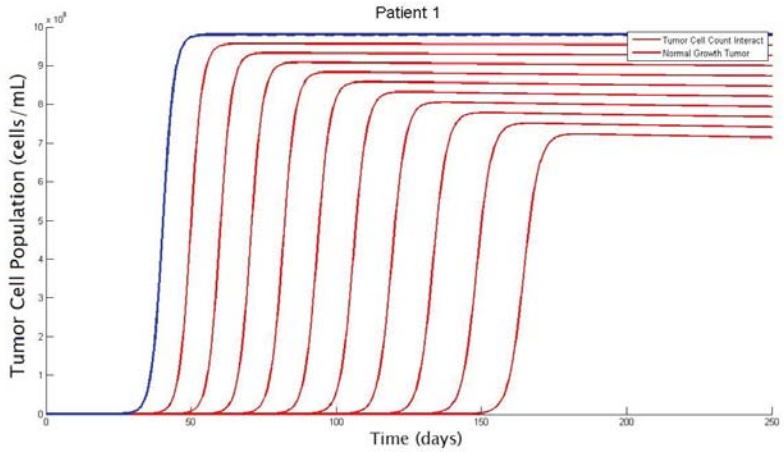

Figure 41: The effect of varying the tumor-immune interaction rate, a_C.

Figure 41 and Figure 42 illustrate simulations in which we vary the rate at which the cancerous tumor cells interact with the target cell populations. We can see from Figure 41 that the rate at which the new cells interact impacts two characteristics of the tumor cells behavior, namely, the time at which the cancerous cell proliferation begins as well as the final

steady-state population. More specifically, as the rate at which the tumor and immune cells interact increases, the time at which the tumor begins to experience logistics growth increases. This means that the immune system maintains the ability to delay the proliferation of cancer. This notion is extremely important within a treatment context as it can provide doctors addition time to recognize and ultimately prescribe treatments for effectively controlling the spread and growth of the cancer. Additionally, we can see that from Figure 41 that as we increase the rate of interaction between the target and tumor cells, the final steady state population of the tumor decreases. This highlights that the immune system not only can delay the growth, but can also result in some limited amount of control. Figure 42 is a magnification of Figure 41 and highlights the delay phase of cancerous cell development. Figure 42 reveals that not only does the increase in interaction delay the growth of the tumor, it also results in a lower population during this initial phase making the cancer easier to treat during this time period.

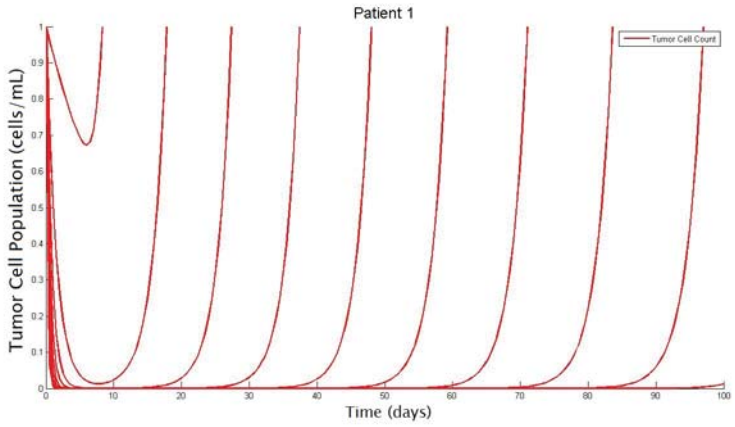

Figure 42: A magnified visualization of effect of varying the tumor-immune interaction rate, a_C.

The following figures are simulations for all 14 of the patients that were infected with HIV. The figure highlights that the growth of HIV impacts the proliferation of cancer uniquely in each patient, specifically focusing on the phase of infection from day 0 to approximately day 10 during which the cancerous tumor population is controlled by the immune system. However, in each case, after the virus reaches the peak viral load, the cancer beings to grow logistically and approaches the steady state.

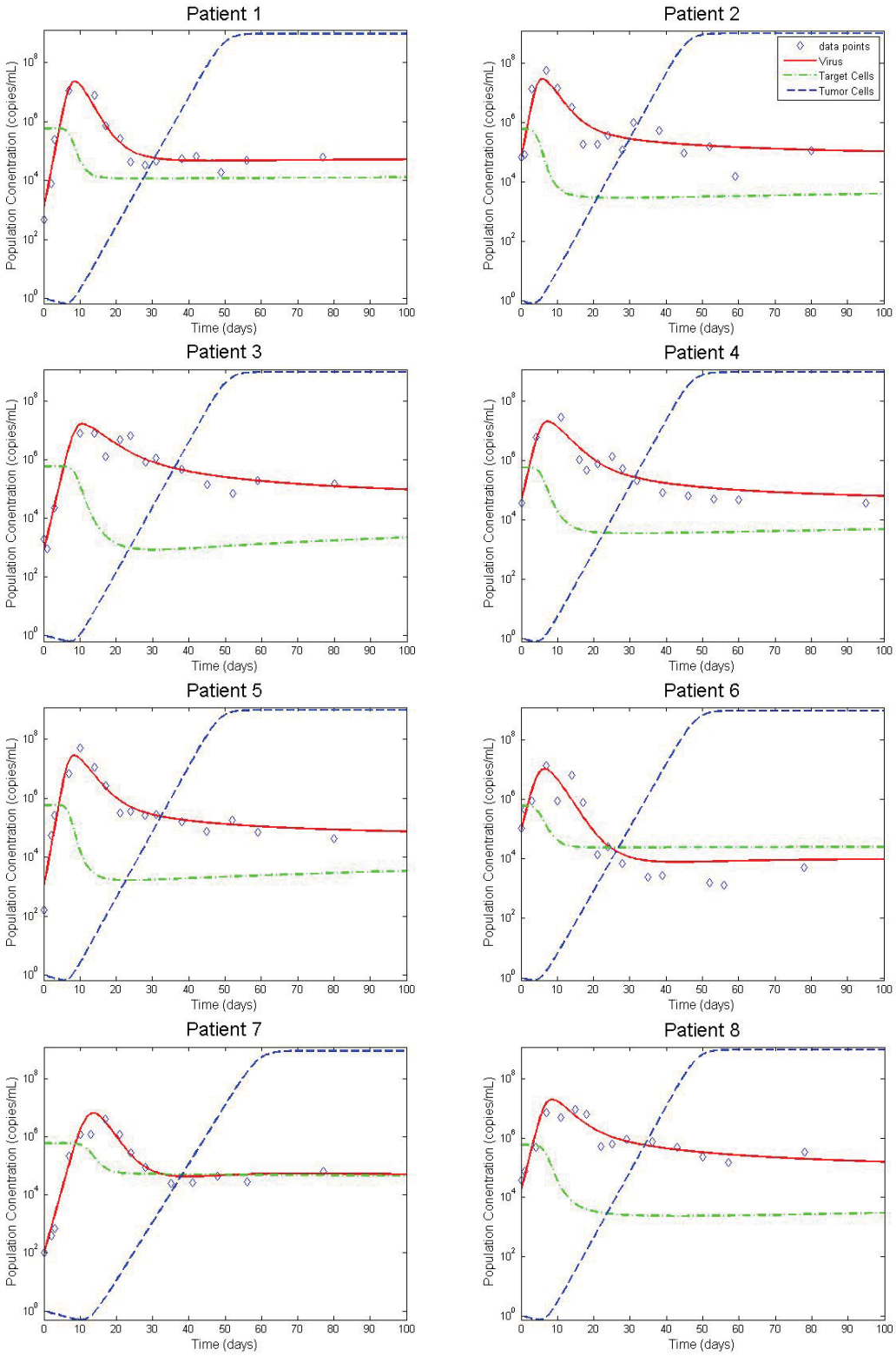

Figure 43: Simulations of the Tumor-Immunodeficiency Model

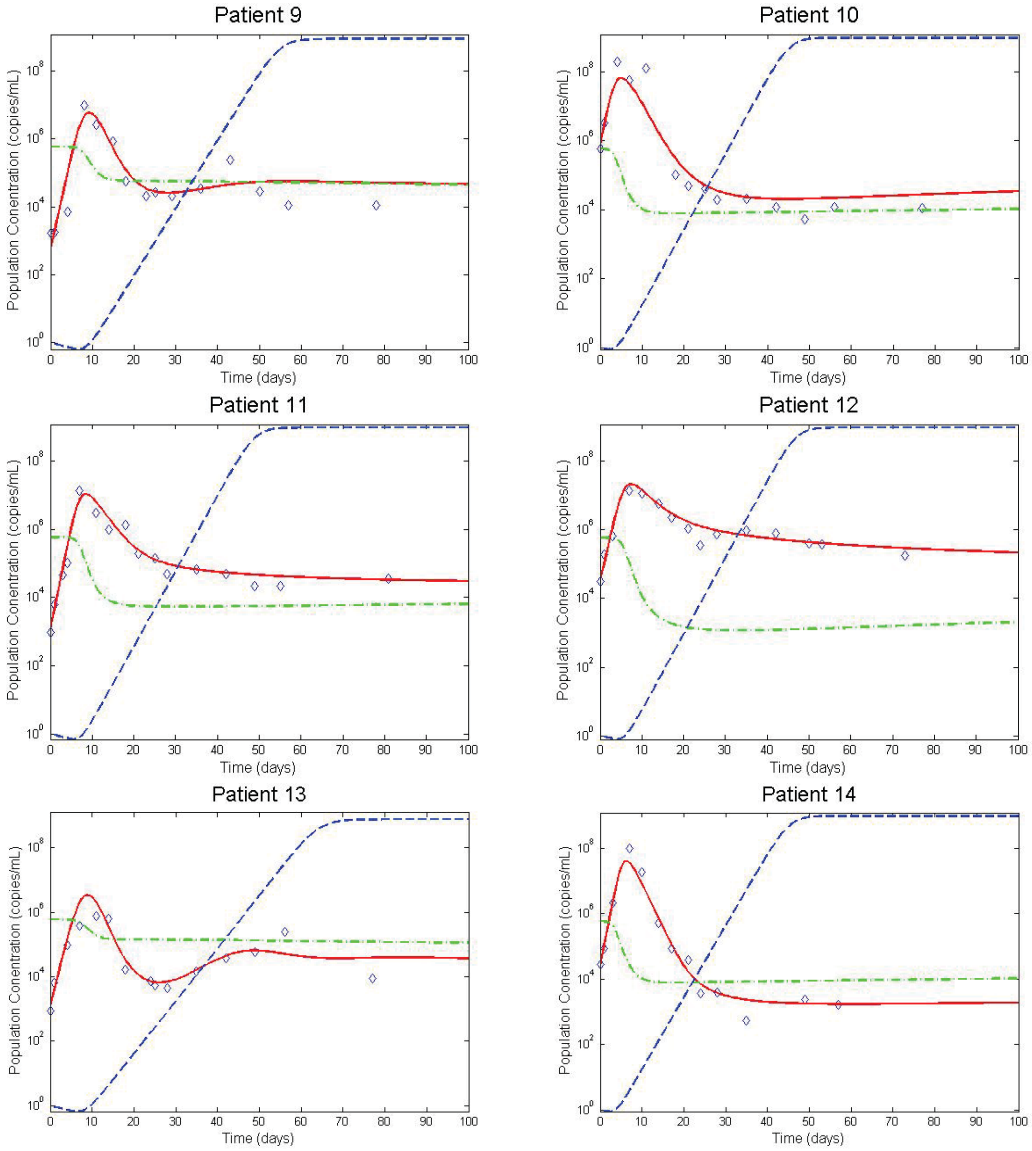

Figure 44: Simulations of the Tumor-Immunodeficiency Model

11 Proposed Treatment Model

In this section we will introduce the background for the treatment model that we will develop during the project. We will integrate treatments from a mathematical, rather than biological perspective and our integration will be based on biological assumptions as well as an understanding of how the treatments impact the viral life cycle. Our analysis will yield insights in optimal treatment techniques and allow for the precise calculation of individual treatment needs and requirements.

11.1 Biological Background

Essentially the treatment model incorporates drug efficacies and results in a pseudo parameter modification which changes the behavior of the standard Target-Cell-Limited model to accommodate the effects of treatment. Our goal is to see how these changes imparted by the treatment impact the system and determine what their impact means from a biological perspective.

11.1.1 Highly Active Antiretroviral Therapy

The management and treatment of HIV normally includes the use of multiple types of medication to attempt to control HIV from growing and multiplying. There are several different types of therapies which target different stages of the viral life cycle. These include Reverse Transcriptase Inhibitors as well as Protease Inhibitors. This usage of multiple forms of antiretroviral agents is often known as Highly Active Antiretroviral Therapy (HAART) and is a common type of therapy used to address patient's suffering from HIV. HAART decreases a patients total burden of HIV, maintains the functionality of the immune system to a much greater extent, and prevents many opportunistic infections which can often lead to death in non-treated patients.

11.1.2 Reverse Transcriptase Inhibitors

As developed previously, HIV is a RNA virus. This means that when it infects a cell, the enzyme reverse transcriptase (RT) allows for the creation of a DNA copy of the virus RNA genome, which is essential for virus replication. Current drug therapies incorporate RT inhibitors. By inhibiting the reverse transcription process, HIV can enter a cell but will not successfully infect it; a DNA copy of the viral genome will not be made and the cell will not make viral proteins or new virus particles. Thus, the viral RNA that enters the cell will not be stable and will degrade, leaving the cell uninfected.

In terms of the model, a reverse transcriptase inhibitor blocks infections and hence the infectivity of the virus. We use ϵ_{RT} to denote the efficacy, or effectiveness, of reverse transcriptase inhibitors. A perfect reverse transcriptase inhibitor is defined such that ($\epsilon_{RT} = 1$). However, reverse transcriptase inhibitors, like other drugs, are not perfect, yet their overall effect on the dynamics of the model is significant enough to include in our analysis [26].

11.1.3 Protease Inhibitors

The viral enzyme protease cleaves the viral protein chains, called polyproteins, into individual proteins. This ultimately allows for the production of virus particles [25]. However, protease inhibitors cause infected cells to produce non-infectious virus particles. Therefore, when considering the implementation of protease inhibitors it is essential to consider two separate populations of virus particles, those infected, V_I, and those non-infected, V_{NI} [26]. More specifically, V_I denotes the population of virus particles that have not been influenced by a protease inhibitor and thus their polyproteins have been cleaved. In contrast, V_{NI} represents the population of virus particles with uncleaved polyproteins. Therefore, we will let $V = V_I + V_{NI}$ where V is the total virus population [26].

11.2 Model

A model for treatment of HIV infection was developed based on the Target-Cell-Limited Model and describe the viral dynamics of primary infection. The model considers four distinct populations which are denoted:

$T(t)$: concentration of target cells at time t,
$I(t)$: concentration of infected cells at time t,
$V_I(t)$: concentration of free virus at time t,
$V_{NI}(t)$: concentration of free virus at time t.

Thus, we consider the mathematical model of HIV-1 infection given by the nonlinear system of ordinary differential equations:

$$\text{(14a)}\quad \frac{dT}{dt} = s - (1-\epsilon_{RT})\beta V_I(t)T(t) - dT(t)$$

$$\text{(14b)}\quad \frac{dI}{dt} = (1-\epsilon_{RT})\beta V_I(t)T(t) - \delta I(t)$$

$$\text{(14c)}\quad \frac{dV_I}{dt} = (1-\epsilon_{PI})pI(t) - cV_I(t)$$

$$\text{(14d)}\quad \frac{dV_{NI}}{dt} = \epsilon_{PI}pI(t) - cV_{NI}(t)$$

With initial conditions $T(0) = T_0$, $I(0) = I_0$, $V_I(0) = V_0$, and $V_{NI} = 0$.

11.3 Model Development

Equation 14a models the dynamics of the target cell population. The equation can be represented by production rate, infection rate, and death rate. The equation is determined to be:

Rate of change of target cell population = (Production rate) - (Infection rate) - (Death rate)

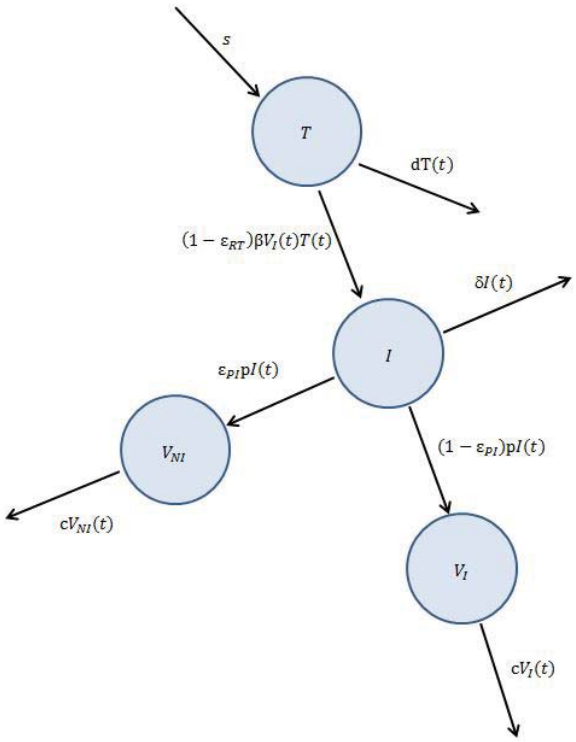

Figure 45: A visual representation of the dynamics that govern the interactions as mathematically described in the Treatment Model.

Production rate: Just as in the standard Target-Cell-Limited model, we assume that target cells are produced at a constant rate, the target cell production rate, s [11, 14, 25].

Infection rate: As stated previously, Reverse Transciptase Inhibitors block infection reducing the parameter β. We use the expression $(1 - \epsilon_{RT})$ to account for the effect of the Reverse Transciptase Inhibitors since the infection will result from the proportion of time where the Reverse Transcriptase inhibitor is ineffective. As previously denoted, ϵ_{RT} is the efficacy of the inhibitor.

Death rate: The target cell death rate term is the same as for the Target-Cell-Limited model.

Equation 14b represents the dynamics of infected cells. The equation for the rate of change of the infected cell population is dictated by both the rate of infection and death rate. The equation can be represented as:

Rate of change of infected cell population = (Infection rate) - (Death rate)

Infection rate: This term is the same as the infection rate term in the target cell differential equation with a reversal in sign.

Death rate: Similar to target cell death, infected cells are cleared by the immune system at a rate, δ, proportional to the infected cell population [14].

Equation 14c mathematically describes the dynamics of the infectious virus cell population. This equation consists of the virus production rate and viral clearance rate and is:

Rate of change of virus population = (Growth rate) - (Clearance rate)

Production rate: While the infectious virus production rate varies from cell to cell and individual to individual, when considering the aggregate population this model assumes the rate of proliferation is constant and that new infectious viruses are produced at a rate, p, proportional to the infected cell population [14]. Additionally, only the virions that are not impacted by the protease inhibitors will become infectious. Thus, we multiply the growth rate by the expression $(1 - \epsilon_{PI})$ to adjust for the impact of the treatment since infectious virus will be produced at a rate proportional to the ineffectiveness of the inhibitor.

Clearance rate: The clearance rate remains the same as for the Target-Cell-Limited model.

Equation 14d mathematically describes the dynamics of the non-infectious virus cell population. This equation consists of the non-infectious virus production rate and non-infectious viral clearance rate and is:

Rate of change of virus population = (Growth rate) - (Clearance rate)

Production rate: This expression is the same as the infectious virus with the exception that the non-infectious virus is produced by interacting with the protease inhibitors. However, unlike the infectious virus production rate the growth of the non-infectious virus is multiplied by (ϵ_{PI}) which corresponds to the proportion of time where the inhibitor is effective.

Clearance rate: The non-infectious virus clearance rate is the same as the infectious virus with the exception that the clearance rate is proportional to the population of the non-infectious virus.

It is important to note that all of the model parameters are presumed to be positive. In addition, there are two biologically reasonable assumptions we are able to make with regard to the

Table 25: Parameters for the Treatment Model.

Parameter	Biological Interpretation	Units	Known Value
s	Target cell production rate	$(Cells)mL^{-1}days^{-1}$	dT_0
β	Rate of infection	$(mL)Cells^{-1}days^{-1}$	Estimated*
d	Target cell death rate	$days^{-1}$	Estimated*
δ	Infected cell death rate	$days^{-1}$	Estimated*
p	Viral production rate	$days^{-1}$	Estimated*
c	Viral clearance rate	$days^{-1}$	23
ϵ_{RT}	Reverse Transciptase Inhibitor Efficacy	N/A	N/A
ϵ_{PI}	Protease Inhibitor Efficacy	N/A	N/A

Table 26: Initial Conditions for the Treatment Model

Initial Conditions	Value	Units
T_0	5.9×10^5	$(Cells)mL^{-1}$
I_0	$\frac{c}{p}V_0$	$(Cells)mL^{-1}$
V_0	Estimated*	$(Cells)mL^{-1}$

values of parameters in relation to one another. Notably, it is biologically reasonable to assume that infected cells have a higher death rate than target cells, namely $\delta \geq d$. Furthermore, in early HIV infection, before the peak in viral load, we assume that the total number of target cells remains approximately constant (i.e. at equilibrium). Thus, the equilibrium number of target cells is given by:

$\frac{dT}{dt} = 0 \implies 0 = s - \beta TV - dT$, where V=0, $\implies s = dT_0$. Thus, $s = dT_0$.

Furthermore, as with the Target-Cell-Limited model, estimates of c made during HIV chronic infection indicate that $c \approx 23day^{-1}$ [27]. While this value is estimated from chronic infection, clinical studies have determined that viral clearance may have the same magnitude during early infection. Additionally, we know that T_0, the initial number of target cells is fixed. Additionally, perfect drugs are the special case where ϵ_{RT} or ϵ_{PI} are equal to one. The asterisk in Tables 23 and 24 denotes estimations that we carried our for the Treatment model using the data from the patients from Section 2.

11.4 Positivity and Boundedness

In order to retain the biological validity of the model, we must prove that solutions to the system of differential equations are positive and bounded for all values of time. For example, concluding that a population is negative is not biologically feasible. Furthermore, the populations must remain finite since the human body can only be composed of a finite number of cells. In addition, boundedness and positivity illustrate that once infected, it is possible that the population of the virus will continue to exist beneath the detectable threshold without doing significant damage [25]. The next step in analyzing our model will be to prove positivity and boundedness for the system of differential equations. We will do so by proving the following theorems.

Lemma (*Positivity*)**.** *Let $t_0 > 0$. In the model, if the initial conditions satisfy $T(0) > 0$, $I(0) > 0$,*

$V_I(0) > 0$, $V_{NI}(0) > 0$ *then for all* $t \in [0, t_0]$, $T(t)$, $I(t)$, $V_I(t)$, $V_{NI}(t)$ *will remain positive in* $\mathbb{R}^4_+$.

Proof: Positivity. We must prove that for all $t \in [0, t_0]$, $T(t)$, $I(t)$, $V_I(t)$, $V_{NI}(t)$ will be positive in $\mathbb{R}^4_+$. We know that all of the parameters used in the system are positive. Thus, we can place lower bounds on each of the equations given in the model. Thus,

$$\frac{dT}{dt} = s - dT(t) - (1 - \epsilon_{RT})\beta V_I(t)T(t) \geq -dT(t) - (1 - \epsilon_{RT})\beta V_I(t)T(t)$$

$$\frac{dI}{dt} = (1 - \epsilon_{RT})\beta V_I(t)T(t) - \delta I(t) \geq -\delta I(t)$$
$$\frac{dV_I}{dt} = (1 - \epsilon_{PI})pT(t) - cV_I(t) \geq -cV_I(t)$$
$$\frac{dV_{NI}}{dt} = \epsilon_{PI}pT(t) - cV_{NI}(t) \geq -cV_{NI}(t)$$

Through basic differential equations methods we can resolve the inequalities and produce:

$$T(t) \geq e^{-\mu t - (1-\epsilon_{RT})\beta \int V_I(t)dt} > 0$$

$$I(t) \geq e^{-\delta t} > 0$$
$$V_I(t) \geq e^{-ct} > 0$$
$$V_{NI}(t) \geq e^{-ct} > 0$$

Thus, for all $t \in [0, t_0]$, $T(t)$, $I(t)$, $V_I(t)$, $V_{NI}(t)$ will be positive and remain in $\mathbb{R}^4_+$. □

Lemma (Boundedness)**.** *There exists an* $T_M, I_M, V_{I,M}, V_{NI,M} > 0$ *such that for* $T(t)$, $I(t)$, $V_I(t)$, $V_{NI}(t)$ $\limsup_{t\to\infty}\Big(T(t)\Big) \leq T_M$, $\limsup_{t\to\infty}\Big(I(t)\Big) \leq I_M$, $\limsup_{t\to\infty}\Big(V_I(t)\Big) \leq V_{I,M}$, $\limsup_{t\to\infty}\Big(V_{NI}(t)\Big) \leq V_{NI,M}$ *for all* $t \in [0, t_0]$.

Proof: Boundedness. We must prove that for all $t \in [0, t_0]$, $T(t)$, $I(t)$, $V_I(t)$, V_{NI} will be bounded. We know that all of the constants used in the system are positive.

$$\frac{dT}{dt} + \frac{dI}{dt} = s - dT(t) - \delta I(t)$$

Since all of the constants are positive,

$$\frac{d(T+I)}{dt} \leq s - \min\{d, \delta\}(T + I)(t)$$

which implies,

$$(T + I)(t) \leq \frac{s}{\min\{d, \delta\}} + c_0 e^{-\min\{d,\delta\}t}$$

taking the limsup of both sides,

$$\limsup_{t\to\infty}(T + I)(t) \leq \limsup_{t\to\infty}\Big(\frac{s}{\min\{d, \delta\}} + c_0 e^{-\min\{d,\delta\}t}\Big) = \frac{s}{\min\{d, \delta\}}$$

So, choose

$$T_M = I_M = \frac{s}{\min\{d, \delta\}}$$

Thus, $(T + I)(t)$ is bounded, so $T(t)$ and $I(t)$ are all bounded since

$$T(t), I(t) \leq (T + I)(t).$$

So,

$$T(t) \leq T_M, \text{ and } I(t) \leq I_M \text{ for all } t \in [0, t_0]$$

In addition, since all of the constants are positive, we can place an upper bound on $\frac{dV_I}{dt}$ so,

$$\frac{dV_I}{dt} = (1 - \epsilon_{PI})pI(t) - cV_I(t) \leq (1 - \epsilon_{PI})pI(t)$$

Therefore, we can choose

$$V_{I,M} = (1 - \epsilon_{PI})pI_M$$

Thus,

$$V_I(t) \leq pI_M = V_{I,M}.$$

Hence, since $I(t)$ is bounded for all $t \in [0, t_0]$, we know that $V_I(t)$ is bounded for all $t \in [0, t_0]$. Additionally, we can place an upper bound on $\frac{dV_{NI}}{dt}$ so,

$$\frac{dV_{NI}}{dt} = (\epsilon_{PI})pI(t) - cV_{NI}(t) \leq (\epsilon_{PI})pI(t)$$

Therefore, we can choose

$$V_{NI,M} = (\epsilon_{PI})pI_M$$

Thus,

$$V_{NI}(t) \leq pI_M = V_{NI,M}.$$

Hence, since $I(t)$ is bounded for all $t \in [0, t_0]$, we know that $V_{NI}(t)$ is bounded for all $t \in [0, t_0]$. □

Theorem 12 (Existence)**.** *Let $t_0 > 0$. In the model, if the initial conditions satisfy $T(0) > 0$, $I(0) > 0$, $V(0) > 0$ then $\forall t \in \mathbb{R}$ $T(t)$, $I(t)$, $V_I(t)$, V_{NI} will exist in $\mathbb{R}^4_+$.*

Proof: Existence and Uniqueness. In the case of our model we have:

$$\mathbf{x} = \begin{bmatrix} T(t) \\ I(t) \\ V_I(t) \\ V_{NI}(t) \end{bmatrix} \text{ and } \mathbf{f}(\mathbf{x}) = \begin{bmatrix} s - dT(t) - (1 - \epsilon_{RT})\beta V_I(t)T(t) \\ (1 - \epsilon_{RT})\beta V_I(t)T(t) - \delta I(t) \\ (1 - \epsilon_{PI})pI(t) - cV_I(t) \\ (\epsilon_{PI})pI(t) - cV_{NI}(t) \end{bmatrix}$$

Note that f has a continuous derivative on $\mathbb{R}^4$ and thus, f is locally Lipschitz in $\mathbb{R}^4$. Hence, by the Fundamental Existence and Uniqueness Theorem located in the appendix as well as the lemmas proved on positivity and boundedness of solutions, we know that there exists a unique, positive, and bounded solution to the ordinary differential equations given in $1(a) - 1(d)$. □

11.5 Optimal Control

11.5.1 Objective Function

In this model, the single-objective cost function to be minimized is given by

$$J(\epsilon_{PI}, \epsilon_{RT}) = \int_0^{t_f} [mI(t) + n\epsilon_{RT}^2 + q\epsilon_{PI}^2]dt$$

where $m, n, q > 0$ are positive weights to balance the factors and t_f is the final time. The term $mI(t)$ represents the cost of the infection. In the case of vaccinations, it is commonly assumed that

the cost of control is usually nonlinear with the quadratic form, $n\epsilon_{RT}^2$ and $q\epsilon_{PI}^2$ [1]. Our goal is to minimize the infected cell population, thus the cost of the infection, while also keeping the cost of treatment small. This is because high doses of treatment can often have harmful effects. We can achieve this goal by finding an optimal control for ϵ_{RT}^* and ϵ_{PI}^* such that

$$J(\epsilon_{PI}^*, \epsilon_{RT}^*) = min\{J(\epsilon_{PI}, \epsilon_{RT}) | \epsilon_{PI}, \epsilon_{RT} \in U\}$$

with the control set

$$U = \{(\epsilon_{PI}, \epsilon_{RT}) | \epsilon_i : [0, t_f] \to [0, 1], \text{ lebesgue measurable } i = PI, RT\}$$

The necessary conditions that an optimal control satisfy result from Pontryagin's Maximum Principle.

11.5.2 Pontryagin's Maximum Principle

Assume we have an objective function that has a control $u(t)$ and an associated state $x(t)$, we want to optimize the cost functional, $J[x(t), u(t)]$.

If $u^*(t)$ and $x^*(t)$ are optimal for the problem

$$max\{J[x(t), u(t)]\}, \text{ where } J[x(t), u(t)] = max\{\int_{t_0}^{t_f} f(t, x(t), u(t))dt\}$$

subject to $\frac{dx}{dt} = g(t, x(t), u(t))$ and $x(t_0) = x_0$ then there exists a piecewise differential adjoint variable $\lambda(t)$ such that

$$H(t, x^*(t), u(t), \lambda(t)) \leq H(t, x^*(t), u^*(t), \lambda(t))$$

for all controls u at each time t, where the Hamiltonian, H, is given by

$$H(t, x(t), u(t), \lambda(t)) = f(t, x(t), u(t)) + \lambda(t)g(t, x(t), u(t))$$

and

$$\frac{\lambda(t)}{dt} = -\frac{\partial H(t, x^*(t), u^*(t), \lambda(t)}{\partial x} \text{ where } \lambda(t_f) = 0$$

Thus, Pontryagin's Maximum Principle gives the necessary conditions for the existence of an optimal solution. However, in order to determine the sufficient conditions we must reference the following theorem [15].

Theorem. *For the optimal control problem, the conditions of the maximum principle are sufficient for the global minimization of $J[x(t), u(t)]$, if the minimized Hamiltonian function H, defined above is convex in the variable x for all t in the time interval $[t_0, t_f]$ for a given λ [1].*

11.5.3 Analysis

Pontrayagin's Maximum Principle applied to our objective function $J(\epsilon_{PI}, \epsilon_{RT}) = \int_0^{t_f} [mI(t) + n\epsilon_{RT}^2 + q\epsilon_{PI}^2]dt$ results in minimizing a Hamiltonian H where

$H = mI(t) + n\epsilon_{RT}^2 + q\epsilon_{PI}^2 + \lambda_T\{s - (1-\epsilon_{RT})\beta V_I(t)T(t) - dT(t)\} + \lambda_I\{(1-\epsilon_{RT})\beta V_I(t)T(t) - \delta I(t)\} + \lambda_{V_I}\{(1-\epsilon_{PI})pI(t) - cV_I(t)\} + \lambda_{V_{NI}}\{\epsilon_{PI}pI(t) - cV_{NI}(t)\}$

where $\lambda_T, \lambda_I, \lambda_{V_I}, \lambda_{V_{NI}}$ are the adjoint variables (also sometimes referred to as co-state variables).

Applying Pontryagin's Maximum Principle results in the following theorem.

Theorem 13 (Optimal Control for the Treatment Model)**.** *There exists an optimal control ϵ_{PI}^* and ϵ_{RT}^* and the corresponding solutions $(T^*, I^*, V_I^*, V_{NI}^*)$ that minimizes $J(\epsilon_{PI}, \epsilon_{RT})$ over U. Furthermore, there exists adjoint variables $\lambda_T, \lambda_I, \lambda_{V_I}, \lambda_{V_{NI}}$ which satisfy*

(15a) $$-\frac{d\lambda_T}{dt} = \lambda_T[-(1-\epsilon_{RT})\beta V_I(t) - d] + \lambda_I[(1-\epsilon_{RT})\beta V_I]$$

(15b) $$-\frac{d\lambda_I}{dt} = m - \lambda_I d + \lambda_{V_I}[(1-\epsilon_{PI})p] + \lambda_{V_{NI}}[\epsilon_{PI}p]$$

(15c) $$-\frac{d\lambda_{V_I}}{dt} = \lambda_T[-(1-\epsilon_{RT})\beta T(t)] + \lambda_I[(1-\epsilon_{RT})\beta T(t)] - \lambda_{V_I}c$$

(15d) $$-\frac{d\lambda_{V_{NI}}}{dt} = -\lambda_{V_{NI}}c$$

with transversality conditions $\lambda_T(t_f), \lambda_I(t_f), \lambda_{V_I}(t_f), \lambda_{V_{NI}}(t_f) = 0$

and the controls ϵ_{RT}^* and ϵ_{PI}^* which satisfy the optimality conditions,

$$\epsilon_{RT}^* = \frac{\beta V_I^* T^*(\lambda_T + \lambda_I)}{2n} \text{ and } \epsilon_{PI}^* = \frac{pI^*(\lambda_{V_I} - \lambda_{V_{NI}})}{2q}$$

Proof. The differential equations governing the adjoint variables are obtained by differentiation of the Hamiltonian function, evaluated at the optimal control [1]. Thus, the adjoint system can be written as

(15a) $$-\frac{d\lambda_T}{dt} = \frac{\partial H}{\partial T} = \lambda_T[-(1-\epsilon_{RT})\beta V_I(t) - d] + \lambda_I[(1-\epsilon_{RT})\beta V_I]$$

(15b) $$-\frac{d\lambda_I}{dt} = \frac{\partial H}{\partial I} = m - \lambda_I d + \lambda_{V_I}[(1-\epsilon_{PI})p] + \lambda_{V_{NI}}[\epsilon_{PI}p]$$

(15c) $$-\frac{d\lambda_{V_I}}{dt} = \frac{\partial H}{\partial V_I} = \lambda_T[-(1-\epsilon_{RT})\beta T(t)] + \lambda_I[(1-\epsilon_{RT})\beta T(t)] - \lambda_{V_I}c$$

(15d) $$-\frac{d\lambda_{V_{NI}}}{dt} = \frac{\partial H}{\partial V_{NI}} = -\lambda_{V_{NI}}c$$

with transversality conditions $\lambda_T(t_f), \lambda_I(t_f), \lambda_{V_I}(t_f), \lambda_{V_{NI}}(t_f) = 0$.

On the interior to the control set, where $0 < \epsilon_{RT}, \epsilon_{PI} < 1$, we have

$$0 = \frac{\partial H}{\partial \epsilon_{RT}} = 2n\epsilon^*_{RT} - \beta V^*_I T^* \lambda_T - \lambda_I \beta V^*_I T^*$$
$$0 = \frac{\partial H}{\partial \epsilon_{PI}} = 2q\epsilon^*_{PI} - \lambda_{V_I} pI^* + \lambda_{V_{NI}} pI^*$$

which can be simplified such that

$$2n\epsilon^*_{RT} = \beta V^*_I T^*(\lambda_T + \lambda_I) \text{ and } 2q\epsilon^*_{PI} = (\lambda_{V_I} + \lambda_{V_{NI}})pI^*$$

and hence we obtain

$$\epsilon^*_{RT} = \frac{\beta V^*_I T^*(\lambda_T + \lambda_I)}{2n} \text{ and } \epsilon^*_{PI} = \frac{(\lambda_{V_I} + \lambda_{V_{NI}})pI^*}{2q}$$

and thus,

$$\epsilon^*_{RT} = max\{0, min\Big(1, \frac{\beta V^*_I T^*(\lambda_T + \lambda_I)}{2n}\Big)\} \text{ and } \epsilon^*_{PI} = max\{0, min\Big(1, \frac{(\lambda_{V_I} + \lambda_{V_{NI}})pI^*}{2q}\Big)\}$$

□

11.6 Numerical Simulations

Table 27: Parameter estimates of the Treatment Model

Parameter	**Value**	$s.e._{lin}$	$r.s.e._{lin}$
p_{pop}	374.756	121.466	32.41
d_{pop}	0.00728	0.00098	13.39
δ_{pop}	0.24168	0.033	13.66
$V_{0_{pop}}$	3.844	0.295	7.68

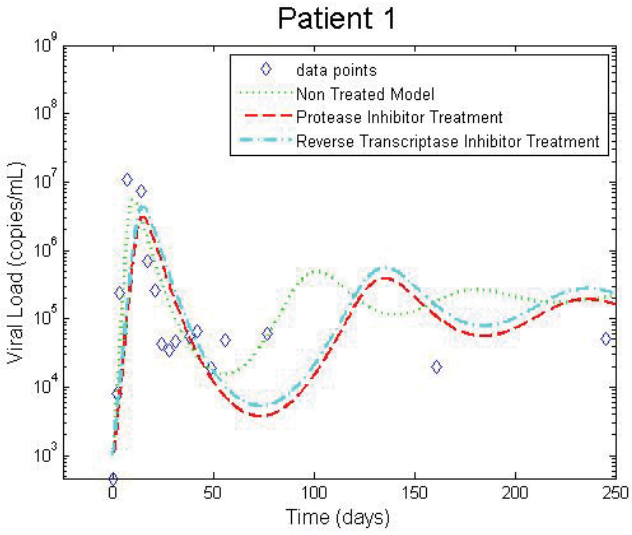

Figure 46: A numerical simulation of Protease Inhibitors and Reverse Transciptase Inhibitors at $\epsilon_{PI} = \epsilon_{RT} = 0.3$.

In this section, we utilize the data as discussed in section 2 to simulate the impact of treatment on the dynamics of HIV primary infection. We explore the Treatment Model as derived in section 4 to study the effects of both reverse transciptase inhibitors and protease inhibitors on the proliferation of the viral and infected cell populations within the host. Using various combinations of the two treatment, one at a time and combined, we investigate and compare the numerical results from simulations. In doing so, we are able to numerically illustrate how the efficacy of each one of the treatments effects the level of infection, as well as consider the application

of HAART therapy in order to ultimately achieve viral clearance.

Our analysis yielded parameter estimates for both the population fit as well as individual fit parameters; Table 25 illustrates the estimates obtained for the population parameters. In addition, Table 25 provides the standard errors (se) and residual standard errors (rse) for both the population fixed and random parameters. The standard error measure indicates the extent to which an estimate deviates from the true population. The rse is the standard error expressed as a percentage of the estimate. In general, rse of 25% or higher should be used with caution. As we can see, the rse values for the population parameters are less than 25 with the exception of p_{pop} which is 32.41; however, we will proceed with the estimates we obtained.

Furthermore, we can use these estimates to run simulations of the model at various levels of treatment, in order to visualize how treatment impacts the dynamics of the system. As we can see in Figure 46, both the reverse transcriptase and protease inhibitors impact the behavior of the virus as well as the characteristics of viral infection. For instance, the rate of viral production appears to decrease, as visualized by the decrease in the slope from the initiation of infection to the peak viral load under treatment. Additionally, the virus achieves a peak viral load that is approximately 20% smaller for the reverse transcriptase inhibitor and 40% lower for the protease inhibitor. In addition to a smaller peak viral load, the time at which the peak viral load is achieved is also delayed by several days with both treatments. This decrease in peak viral load can be explained due to the decrease in the rate of viral production which is likely giving the immune system more time to respond to the infection. As a result of this increased horizon, we are seeing a smaller peak viral load as a result.

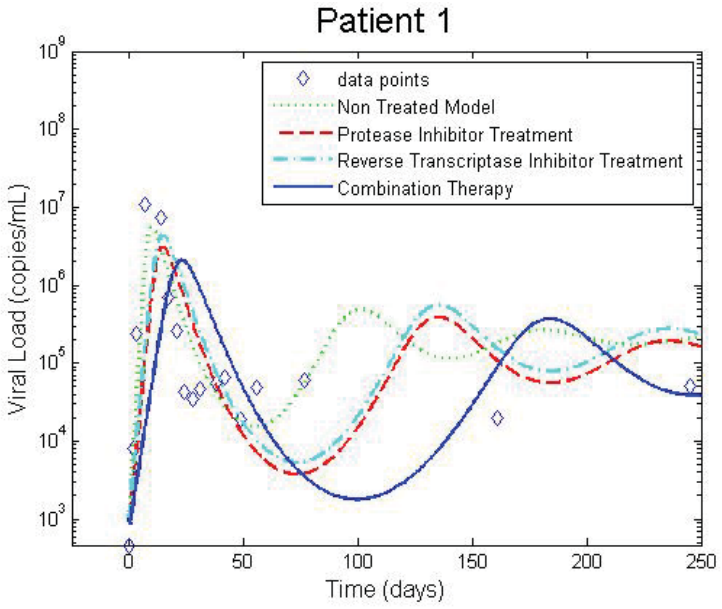

Figure 47: The increased impact of combination therapy with both inhibitors at 0.3.

Figure 47 illustrates the impact of combination HAART treatment protocol. As we can see, combining both the reverse transcriptase inhibitor and protease inhibitor therapies, at the same levels as previously determined simulated in Figure 47 results in the decrease in the rate of viral production, a peak viral load that is approximately 80% smaller than the non-treated patient, as well as a delay in the time at which the peak is achieved. However, even at this level of combination treatment, the virus persists and we do not see viral decrease or the elimination of infection.

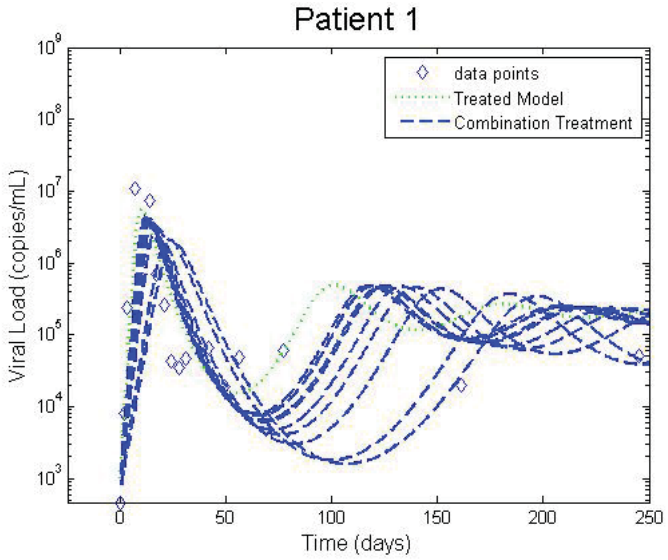

Figure 48: An illustration of the sensitivity of the combination therapy in the Treatment Model.

In Figure 48, we simulate the effect of a combination therapy at various levels. In this figure, we increase the treatment effectiveness of the combination therapy by 10% each new simulation from 0 until 0.7, or 70% effective combination therapy. The figure suggests that changes in the treatment effectiveness at lower levels (i.e. the change from 10% effective to 20% effective) do not drastically change the behavior of the model, however, as the treatment becomes more effective the subsequent change on the behavior of the virus becomes more pronounced. In addition, this figure highlights the impact that changes in treatment effectiveness have on the behavior of the virus. For instance, we can clearly see that more effective treatment results in a smaller rater of viral production, lower peak viral load, as well as a continued delay of the peak viral load point which is consistent with the behavior that was exhibited with the individual protease and reverse transcriptase treatments.

11.7 Discussion

As completed in section 4, we can derive the viral reproduction number for our system of equations. The notion of a viral reproduction number was initially developed for the field of epidemiology in order to mathematically characterize the volatility of an infectious disease. In an epidemiological setting, R_0 represents the number of people that an infected individual will infect during their lifetime. However, this notion can be applied to the study of viral dynamics in vivo. In fact, the viral reproduction number is an extremely important quantity in our analysis of our models. Biologically, in an in vivo model, R_0 represents the average number of infected cells produced by an initially infected cell over its lifetime [24]. As stated previously, the value of R_0 is a well established norm when discussing viral infections and is commonly discussed when approaching modeling problems [24].

The literature which focuses on HIV typically characterizes the R_0 value for HIV to be between 3 and 6. This means that for every cell that is infected with HIV, three to six more cells will be infected. This suggests that the infection will tend to persist within the immune system. However, from section 4, we can determine that treatment impacts the value of the viral reproduction number and thus, $R_{0,Treated} = \frac{(1-\epsilon_{RT})(1-\epsilon_{PI})\beta p\lambda}{\delta dc} = R_0(1-\epsilon_{RT})(1-\epsilon_{PI})$ where R_0 is the non-treated viral

reproduction number. In order to eliminate infection, the viral reproduction number must be less than one. Thus, we need $R_{0,Treated} < 1$. This is because, when the viral reproduction number is less than one, the viral clearance equilibrium will always be stable as seen in section 4. Therefore in order to achieve viral clearance, $R_0(1-\epsilon_{RT})(1-\epsilon_{PI}) < 1$, and thus, $(1-\epsilon_{RT})(1-\epsilon_{PI}) < \frac{1}{R_0}$. We can interpret this as the following theorem.

Theorem 14. *In order to achieve viral clearance, for each individual patient* $(1-\epsilon_{RT})(1-\epsilon_{PI}) < \frac{1}{R_0}$.

Essentially, this means that for each patient the combined effectiveness of the combination therapy must be greater than or equal to $1-\frac{1}{R_0}$. Thus, on average, in order to completely eliminate the virus, we need a combined therapy treatment which is approximately 80.12% effective as illustrated in Table 5.

Table 28: Individual Treatment Efficacies Required for Viral Clearance

Patient	R_0	Efficacy of Treatment to Eliminate Infection
1	5.326	0.8122 or 81.22%
2	5.872	0.8297 or 82.97%
3	5.914	0.8309 or 83.09%
4	5.310	0.8117 or 81.17%
5	6.043	0.8345 or 83.45%
6	3.574	0.7202 or 72.02%
7	4.532	0.7793 or 77.93%
8	6.213	0.8390 or 83.90%
9	4.994	0.7998 or 79.98%
10	3.965	0.7478 or 74.78%
11	5.766	0.8266 or 82.66%
12	6.442	0.8448 or 84.48%
13	3.940	0.7462 or 74.62%
14	2.559	0.6092 or 60.92%
Mean	5.032	0.8013 or 80.13%
Median	5.318	0.8120 or 81.20%
Standard Deviation	1.157	0.0646 or 6.46%

Figure 49 illustrates the notion of the required level of treatment in order to achieve viral clearance, and thus eliminate the infection. The graph on the left shows treatment which is 80% effective. Even with a treatment at is 80% effective, we do not see an elimination of the virus in Patient 11. However, while viral clearance does not occur, there is a very notable change in the behavior of the virus. The peak viral load for the reverse transcriptase treatment is just 3% of the non-treated patient, and less than 0.5% of the non treated for the protease inhibitor treatment. Furthermore, the peak viral load occurs at approximately day 143, which is significantly later than in the non-treated patient. Yet, while the treatment clearly has drastic effects on the behavior of the infection, it fails to eliminate the infection entirely. According to our table above, Patient 11 is required to have at least an 82.66% effective treatment in order to achieve viral clearance.

Figure 49 illustrates the effects of both protease inhibitor treatment as well as reverse transcriptase treatment when they are both individually 83% effective, holding the other to be 0% effective

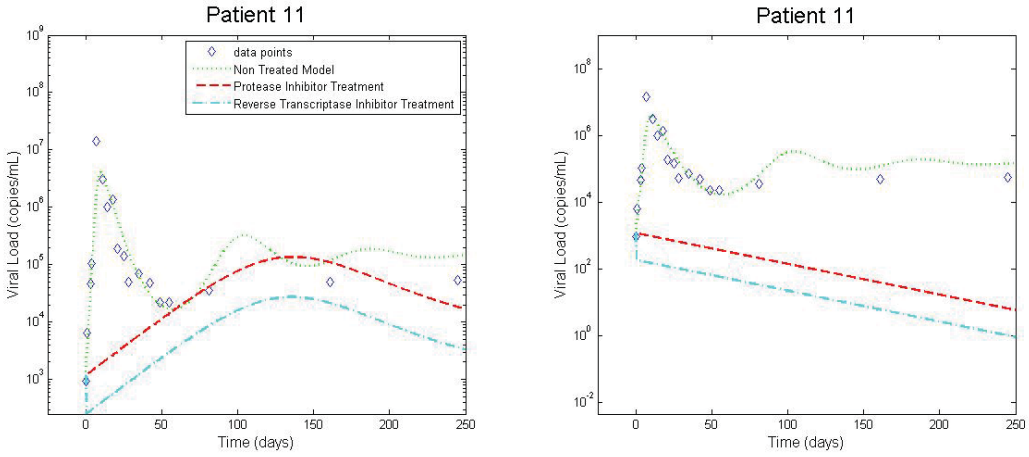

Figure 49: Simulation of the Treatment model at varying efficacies for the therapies for Patient 11. We can see that our estimation of efficacy of treatment to eliminate infection results in viral clearance.

(or not in use). We can see that the more effective treatment drastically changes the behavior of the virus. From the initiation of infection, the virus population decays until it reaches levels low enough to be considered undetectable; there is never an increase in the viral population. Thus, the figure illustrates that our estimate provided in Table 26 was correct.

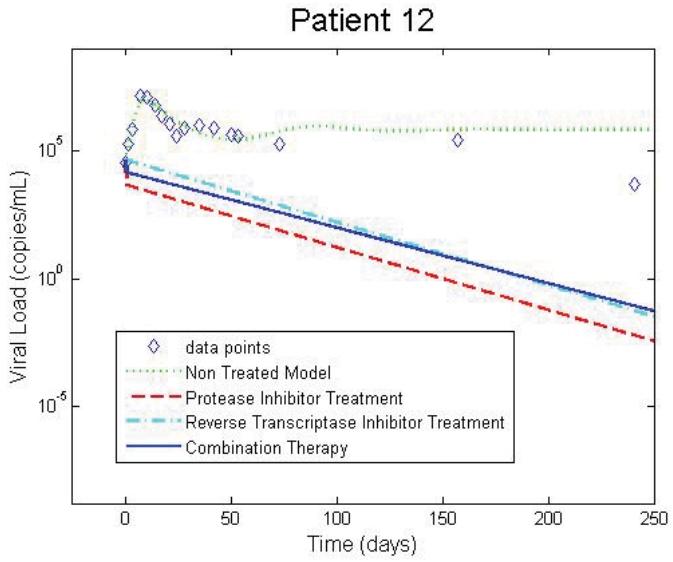

Figure 50: The impact of treatment that causes viral clearance versus combination therapy.

Figure 50 highlights the effectiveness of the HAART combination therapy treatment. In Figure 50, both the reverse transcriptase and protease inhibitor treatments are individually conducted at an effectiveness level of 90% and, as predicted, the virus is cleared from the system. By day 100, the population of the virus was approximately 100, which would be undetectable, however, the virus may remain latent. Yet, we can see that the viral population continues to decay over time, eventually approaching the 0 limit. The solid blue line represents the combination therapy where both the reverse transcriptase and protease inhibitors are held at 67.5% effective treatment. Clearly, the combination therapy follows a similar functional form to the 90% effective individual therapies as the virus population continues to decay over time. Thus, despite the fact that each individual treatment is less effective (and hence less potent) 67.5% compared to 90%, the same

results hold. This is because a 67.5% combination therapy treatment results in the same effect as an 89.43% effective non-combination therapy treatment. Thus, this figure illustrates how a less potent dose of both treatments, when combined, can produce the same effect as higher doses of the individual therapies.

12 Conclusions

In this paper, we sought to learn more about the relationship between cancer and HIV within the immune system by introducing and analyzing mathematical models of immune system dynamics in the presence of cancer and immunodeficiency. We began by developing and analyzing several models for HIV infection and, using data from HIV infected individuals, compared the models to determine which best fit the data. We proved existence, uniqueness, positivity, and boundedness for the models and derived the conditions that guarantee the asymptotic stability of the equilibria. Next, we explained some basic tumor growth models as well as a tumor-immune model which integrated an immune response to cancerous tumor cell development. Then using insights from our analysis of both the HIV and tumor models, as well as our determination of best fit from the patient data, we developed a novel model which integrated the effects of HIV and cancer within the immune system. Through our analysis of the models, we gained valuable insights into the behavior of the immune system as well as the dynamics of infection and cancerous cell growth.

During primary infection, the mechanism which causes the virus to reach a peak value prior to decaying to the lower steady state population is still unknown. One hypothesis is that the peak is Target-Cell-Limited, meaning that the virus runs out of possible hosts to infect, while another suggests that the immune system plays a key role in controlling the infection. We sought to explore these two schools of thought by examining four models to represent the dynamics of the infection, two that were Target-Cell-Limited and two that included an immune response.

Using both qualitative and quantitative techniques, we determined that the immune system plays a key role in characterizing HIV infection. The Extended Immune model, which included a complex immune response mechanism, maintained the lowest corrected Akaike Information Criterion, Bayesian Information Criterion, and Log-likelihood values which suggests that the Extended model was the best at capturing the overall dynamic and behavior of the infection. This suggests that the immune system plays an important role in defining the dynamics of the infection. However, additional study could be conducted to better investigate this hypothesis. For instance, we assumed a quasi-steady state approximation for the immune effector cells, which simplified the model. This simplification could be removed, and the more complex model can be compared to the simplified model to determine which was more accurate. In addition, we could advance the model to break down individual populations of immune cells which we did not explore in our study. For instance, one could distinguish between CD8 T-cells, Cytotoxic T-lymphocytes, and Natural Killer Cells, all which likely play a significant role, but would exhibit different dynamics and interactions with the infected cells. Yet, by making the models more complex to account for the additional populations, the ability to conduct more advanced analysis will be limited.

Since the Extended Immune model was the best for characterizing the infection, we utilized it as the basis of our Tumor-Immunodeficincy model. In addition, during our study we investigated several tumor growth models. Through simulations studying long-term dynamics of cancerous cell growth and examining the positivity and boundedness of the populations within these models, we determined that it is much better to utilize a logistic or other form of self-limiting growth to model the dynamics of cancerous tumor cell growth. In addition to uncontrolled tumor growth, we in-

cluded the interaction of T-cells and tumor within the immune system based on the CD4 T-cell (Target) cells present in the HIV models. We then combined the Extended Immune and Tumor-Immune models and developed a novel Tumor-Immunodeficiency model which included populations for characterizing both the infection of HIV as well as cancerous tumor cell development.

Through our analysis of this new model we gleaned several results. First, we were able to see that CD4 T-cells play a role in the immune system's interaction with cancer, and ultimately have the ability to control cancerous cell development. Additionally, we noted that the immune system loses this ability to control cancer upon infection by HIV, thus validating, from a mathematical perspective, the notion that HIV greatly impacts the proliferation of cancer.

By examining the dynamics of the model, we were able to determine that our immune system is constantly eliminating early cancerous cell development through normal immune function, and that our models suggest that the CD4 T-cells play a crucial role in doing so. Through simulation of the mathematical models, we determined that each patient in our study would be able to stop the cancerous cell development through normal function. In each case, we saw an immediate decrease in the population of tumor cells and either control or elimination of the cancerous cell population. This likely involves CD4 T-cells recognizing the beginning stages of development and proliferating a robust immune response. Furthermore, when we removed HIV from our Tumor-Immunodeficiency Model, by setting the population of the virus equal to zero, we saw that the tumor was eliminated. While there are instances in which a more prolific tumor will trump any normal immune response, our analysis of the immune system's ability to ward off tumor development under normal conditions suggests that CD4 T-cells play a crucial role in that ability. Yet, our analysis also highlights that the CD4 T-cells are very vulnerable upon initiation of HIV infection.

In our analysis, we showed that while the immune system has the ability to control cancerous cell development through normal function of the CD4 T-cells, HIV infection greatly impacts the systems capabilities and has a huge impact on the dynamics of the tumor. Upon the initiation of infection, there is a massive proliferation of the virus. However, immediately following the viral production, the population of target cells remains steady. There is an apparent "lag" before the target cell population decreases as a result of infection. During this time period, which typically lasts seven days, the cancer is controlled by the immune system via the same mechanism as discussed in the previous paragraph. This is illustrated by the fact that the cancerous tumor population is decreasing despite the proliferation of the virus. However, after approximately seven days, the target cell population begins to be affected by the proliferation of the virus and the concentration of CD4 T-cells decreases rapidly. During this time, the cancer population begins to proliferate uncontrollably and assumes uncontrolled growth once again. Thus, while the immune system previously maintained the ability to control the cancer, shortly after the proliferation of HIV, the immune system loses this functionality. During our study, we primarily considered that the proliferation of cancer and initiation of infection occurred at day zero. Additional exploration should be conducted to see if a simulated delay might be possible to examine the behavior of HIV and cancer initiation at different points at time and the impact that delay has on the dynamics of the system.

In addition to examining untreated systems, we also examined how treatment impacts the pro-

liferation of HIV. In doing so, we used asymptotic stability analyses to define treatment thresholds in order to eliminate the virus and clear the infection. Additionally, we were able to estimate necessary efficacies of treatment for individual patients and apply optimal control theory to prove the existence of the optimal treatment solution. This would allow doctors to estimate a few basic parameters, and then prescribe an optimal treatment for the patient in order to clear the virus while limiting the negative side effects associated with treatment therapies. Furthermore, our findings illustrate that combination therapy can provide the same level of effectiveness as individual treatments with much lower levels of toxicity. In our study, we included only two of several treatment variants that are prescribed to patients suffering from HIV. Future work may include additional therapies that we did not include in our study and may consider including novel treatment such as immuotherapy, where the immune system is trained to identify the virus and eliminate the infection. In addition, one may be able to examine the timing in which treatment occurs and how that impacts the viral dynamics and optimal solution.

Also, we determined that when considering treatments, it is extremely important to account for any sort of natural delay that may occur as a result of treatment. We analyzed a delay differential equation model which included a time delay as a result of normal viral cytopathic effects. Our stability analysis revealed that a bifurcation occurs in both of the equilibria (viral clearance and viral persistence). As a result, even though we may reduce the viral reproduction number below one via effective treatment, the viral clearance equilibrium may not be a stable equilibrium if the treatment causes massive viral cytopathic effects. This is extremely important when considering treatment since the appropriate efficacy may not be sufficient to eliminate infection. Additional analysis must be done on the impact that the treatment has with regard to delay prior to using the models to prescribe treatment to an infected individual.

Furthermore, our review of the literature and several personal experiences revealed some important conclusions beyond the scope of this work. During the year, I volunteered at the AIDS Medical Resource Center of Wisconsin, an HIV clinic located in his home-town of Milwaukee. While at the clinic, I spent time working with patients who were being treated for and struggled with HIV related general and chronic health conditions. In speaking with the patients, as well as the doctors at the clinic, I came to the conclusion that the most important study that needs to be conducted is not necessarily the dynamics of the virus and treatment in vivo, but rather how to get medications and treatments to populations that need it the most. It is well known that the treatment for HIV is extremely effective. Many patients who take medications see a significant decrease in viral load and negative side effects; however, this only occurs as long as they remain consistently on the medication. For many of them, that requires them to take numerous pills, every day, for the rest of their lives. In short, a major problem is understanding how to get that treatment to patients, and this should be explored.

However, treating patients necessitates developing the ability to effectively develop solutions to combat the threat posed by the infection. While several other infectious diseases currently endanger millions of people across the globe, little is understood about the dynamics of many of these threats. For instance, the manner in which Zika virus as well as numerous other infectious diseases interact with the immune system is not well understood. Models like the ones we described in our study, when applied to these infections, may yield insights into the behavior and lead to the development

of treatment protocols. Developments in computing, mathematics, biology, and immunology have created an environment yearning for advanced mathematical analysis and insights gleaned from integrating these areas together may lead to the development of innovative approaches to both address and solve some of the world's most perplexing biological problems.

13 Appendix

To prove the existence and uniqueness of solutions, we must prove the following theorem, referred to in Section 3.1.

Theorem (*Fundamental Existence and Uniqueness Theorem*)**.** *Suppose the function $f : \mathbb{R}^n \to \mathbb{R}^n$ is continuously differentiable. Then $x(t)$ is a solution of the differential equation $\frac{dx}{dt} = f(x)$ on an interval I if $x(t)$ is differentiable on I and if $\forall t \in I, x(t) \in \mathbb{R}^n$ and $\frac{dx}{dt} = f(x(t))$ and given $x_0 \in \mathbb{R}^n, x(t)$ is a solution of the initial value problem*

$$\frac{dx}{dt} = f(x)$$
$$x(t_0) = x_0$$

Remark: The above is a well known theorem and ensures that the solutions exists and is unique in the neighborhood of x_0, i.e., the function is locally Lipschitz [25]. The proof for this theorem can be found in [19].

Definition (*Locally Lipschitz Functions*)**.** *A function is locally Lipschitz if for each $x_0 \in \mathbb{R}^n$ there is a ϵ neighborhood of x_0, $N_\epsilon(x_0) \subset \mathbb{R}^n$, and a constant $k_0 > 0$, such that $\forall x, y \in N_\epsilon(x_0)$*

$$|f(x) - f(y)| \leq k_0|x - y|$$

In our analysis for P_3 from section 6.3.6 we also need to show that $a_1a_2a_3 - (a_3^2 + a_1^2a_4) > 0$.

We know for P_3, which is given by $(T, I, V, E) = (\frac{c\lambda k_E}{p\beta d_E + cdk_E}, \frac{d_E}{k_E}, \frac{pd_E}{ck_E}, \frac{-p\delta\beta c + p\beta\lambda k_E - \delta c k_E d}{k_E(p\beta d_E + cdk_E)})$:

$$a_1a_2a_3 - (a_3^2 + a_1^2a_4) = \frac{1}{c^3k_E^2(\beta pd_E + cdk_E)^3}\Big(\beta pd_E\lambda(\delta c^5d^2k_E^5(c+d)(\delta d_E - d^2) + \beta^5p^5d_E^3(d_E(\lambda k_E - \delta d_E) + c^2d_E + c\lambda k_E) + \beta^4p^4cd_Ek_E(d_E(\lambda k_E(4d_Ed + \lambda k_E) - \delta d_E(5d_Ed + \lambda k_E)) + c^3d_E^2 + c^2d_E(4d_Ed + \lambda k_E) + c\lambda k_E(3d_Ed + \lambda k_E)) + \beta^3p^3c^2k_E^2(\delta^2d_E^4 + \delta d_E^2(c^2d_E - c(d_Ed + \lambda k_E) - 2d_E(\lambda k_E + 5d^2) - 3\lambda dk_E) + 3c^3d_E^2d + c^2d_E(-d_E\lambda k_E + 6d_Ed^2 + 3\lambda dk_E) + c\lambda k_E(d_E^2d + d_E\lambda k_E + 3d_Ed^2 + \lambda dk_E) + d_E\lambda k_E(d_E\lambda k_E + 6d_Ed^2 + 2\lambda dk_E)) + \beta^2p^2c^3k_E^3(\delta^2d_E^3(c+3d) + \delta d_E(2c^2d_Ed - c(2d_E\lambda k_E + 3d_Ed^2 + \lambda dk_E) - d(4d_E\lambda k_E + 10d_Ed^2 + 3\lambda dk_E)) + 3c^3d_Ed^2 + c^2d(-d_E\lambda k_E + 4d_Ed^2 + 2\lambda dk_E) + c\lambda k_E(d_E\lambda k_E + 2d_Ed^2 + d^3) + \lambda dk_E(d_E\lambda k_E + 4d_Ed^2 + \lambda dk_E)) + \beta pc^4dk_E^4(\delta^2d_E^2(2c + 3d) + \delta(c^2d_Ed - cd_E(2\lambda k_E + 3d^2) - d(2d_E\lambda k_E + 5d_Ed^2 + \lambda dk_E)) + d^2(c+d)(c^2 + \lambda k_E))\Big)$$

thus, since $p\beta > \delta k_E, p\beta\lambda > \delta d_E c, R_1 > 1, R_0 > 1$, and $\lambda k_E(c + d_E) > d_E^2\delta$ we can simplify the expression to show that $a_1a_2a_3 > (a_3^2 + a_1^2a_4)$ and thus we have shown $a_1a_2a_3 - (a_3^2 + a_1^2a_4) > 0$.

Below we provided the numerical simulations for all four of the HIV models (the Target-Cell-Limited, Constrained Target-Cell-Limited, Simple Immune, and Extended Immune).

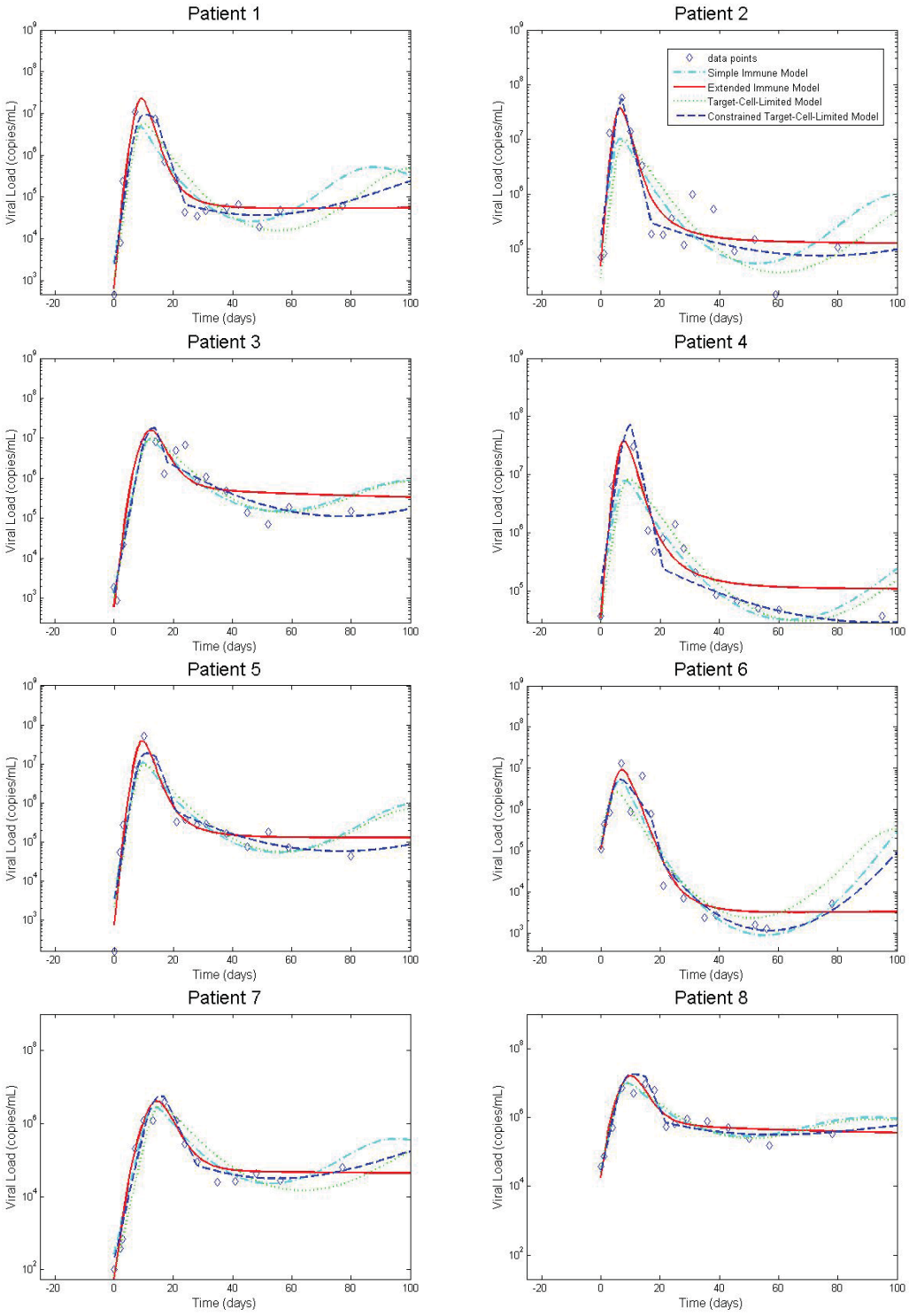

Figure 51: Simulations of the Tumor-Immunodeficiency Model

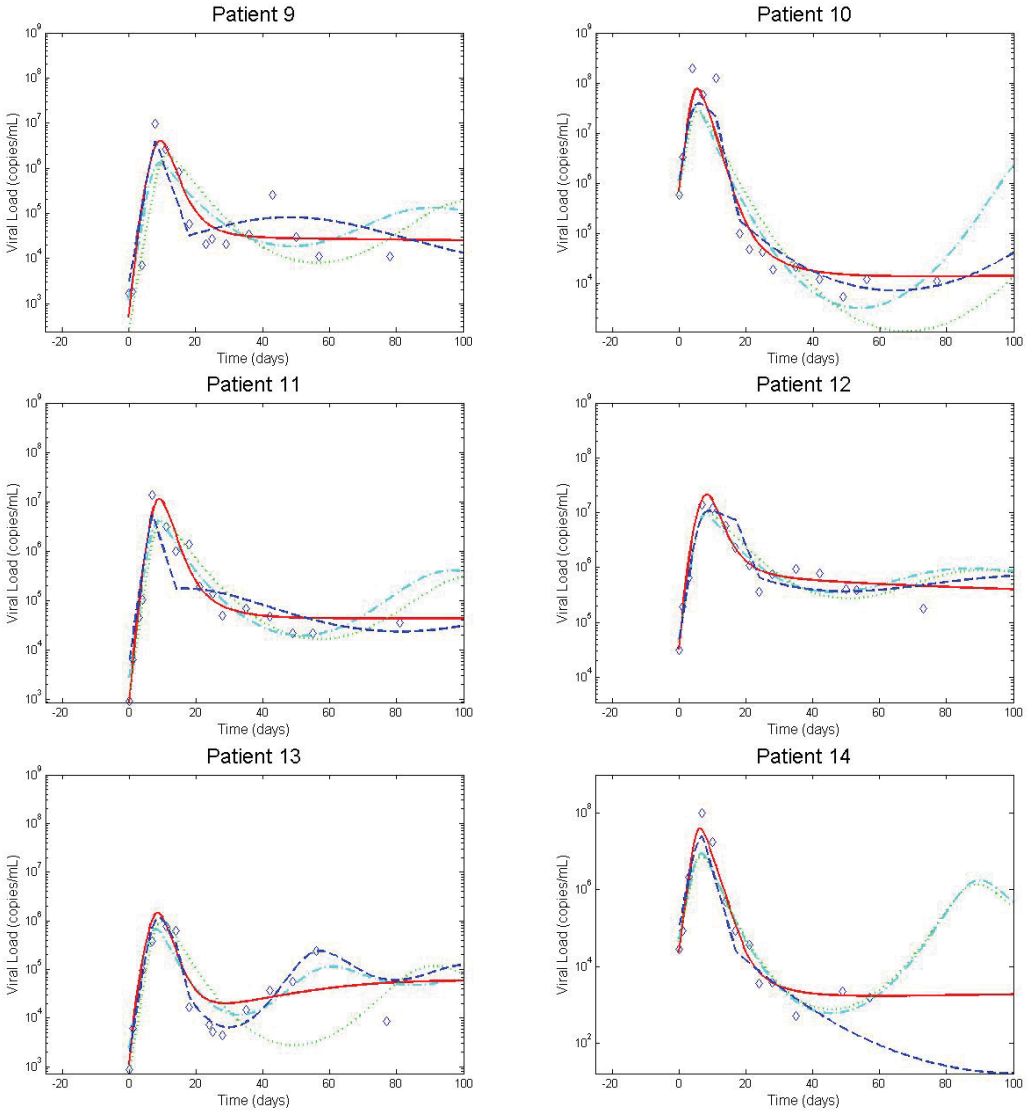

Figure 52: Simulations of the Tumor-Immunodeficiency Model

References

[1] Agusto, Folashade B., Nizar Marcus, and Kazeem O. Okosun. "Application of optimal Control to the Epidemiology of Malaria." *Electronic Journal of Differential Equations* 2012, no. 81 (May 22, 2012): 1-22.

[2] Audet, J., and G. P. Kobinger. "Immune Evasion in Ebolavirus Infection." *Viral Immunology* 28, no. 1 (February 28, 2015): 10-18.

[3] Burg, David, Libin Rong, Avidan U. Neumann, and Harel Dahari. "Mathematical Modeling of Viral Kinetics Under Immune Control During Primary HIV-1 Infection." *Journal of Theoretical Biology*, no. 259 (April 2009): 751-59.

[4] Carter, John, and Venetia Saunders. *Virology: Principles and Applicaitons.* 2nd ed. N.p.: John Wiley and Sons, 2013.

[5] Chowell, G., N. Hengartner, C. Castillo-Chavez, P. Fenimore, and J. Hyman. "The basic reproductive number of Ebola and the effects of public health measures: the cases of Congo and Uganda." *Journal of Theoretical Biology* 229, no. 1 (July 7, 2004): 119-26.

[6] "Course of Infection with HIV and SIV." In *Retroviruses*, edited by J. M. Coffin, S. H. Hughes, and H. E. Varmus. New York, NY: Cold Spring Harbor Laboratory Press, 1997.

[7] Culshaw, Rebecca V., and Shigui Ruan. "A delay-differential equation model of HIV infection of CD4+ T-cells." *Mathematical Biosciences* 165 (February 2000): 27-39.

[8] de Pillis, Lisette G., Ami E. Radunskaya, and Charles L. Wiseman. "A Validated Mathematical Model of Cell-Mediated Immune Response to Tumor Growth." Last modified June 9, 2005.

[9] Eladdadi, Amina, Peter Kim, and Dann Mallet, eds. *Springer Proceedings in Mathematics and Statistics.* Vol. 107 of *Mathematical Models of Tumor-Immune System Dynamics.* New York, NY: Springer, 2014.

[10] Feizabadi, Mitra, and Tarynn Witten. "Modeling the Effects of a Simple Immune System and Immunodeficiency on the Dynamics of Conjointly Growing Tumor and Normal Cells." *International Journal of Biological Sciences* 7, no. 6 (2011): 700-07.

[11] Hubbard, J. H., and B. H. West. *Differential Equations: A Dynamical Systems Approach.* Texts in Applied Mathematics 18. New York, NY: Springer-Verlag, 1995.

[12] Jordan, D. W., and P. Smith. *Nonlinear Ordinary Differential Equations.* 4th ed. New York, NY: Oxford University Press, 2007.

[13] Lakshmanan, M., and D. V. Senthilkumar. *Dynamics of Nonlinear Time-Delay Systems.* Berlin, Germany: Springer, 2010.

[14] Lentz, and Feezor. "Principles of Immunology." *Nutrition in clinical practice: official publication of the American Society for Parenteral and Enteral Nutrition 18*, no. 6 (December 2003).

[15] Lenhart, Suzanne, and John T. Workman. *Optimal Control Applied to Biological Models.* Mathematical and Computational Biology Series. London, UK: Taylor and Francis Group, 2007.

[16] Lindstrom, Mary J., and Douglas M. Bates. "Nonlinear Mixed Effects Models for Repeated Measures Data." *Biometrics* 46, no. 3 (September 1990): 673-87.

[17] Lynch, Steven. *Dynamical Systems with Applications Using Mathematica.* Boston, MA: Birkhauser, 2007.

[18] Movellan, J. R. "Tutorial on Stochastic Differential Equations." MPLab Tutorials Version 06.1. Last modified 2011.

[19] Murray, John D. *An Introduction*. 3rd ed. Vol. I of *Mathematical Biology*. Berlin: Springer, 2003.

[20] National Institute of Health. "Accelerating Medicines Partnership." Accelerating Medicines Partnership. Last modified August 15, 2014. Accessed December 6, 2014. http://nih.gov/science/amp/index.htm.

[21] National Institute of Health. "Biology of HIV." National Institute of Allergy and Infectious Diseases. Last modified April 3, 2012. Accessed April 17, 2014. http://www.niaid.nih.gov/topics/HIVAIDS.

[22] "HIV Infection and Cancer Risk." National Cancer Institute. Last modified May 16, 2011. Accessed April 17, 2014. http://www.cancer.gov/cancertopics/factsheet/Risk/hiv-infection.

[23] Ndhlouv, Zaza M., Philomena Kamya, Thumbi Ndung'u, and Bruce D. Walker. "Magnitude and Kinetics of CD8+ T Cell Activation during Hyperacute HIV Infection Impact Viral Set Point." *Immunity* 43 (September 15, 2015): 591-604.

[24] Nowak, Martin A., and Robert M. May. *Virus Dynamics: Mathematical Principles of Immunology and Virology*. New York, NY: Oxford University Press, 2000.

[25] Owen, Judy, Jenni Punt, and Sharon Stranford. *Kuby Immunology*. 7th ed. N.p.: W.H. Freeman, 2013.

[26] Perelson, Alan. "Modelling Viral and Immune System Dynamics." *Nature Reviews*, January 2002, 28-36.

[27] Perelson, Alan, and Patrick Nelson. "Mathematical Analysis of HIV-1 Dynamics in Vivo." *Society for Industrial and Applied Mathematics* 41, no. 1 (March 2001): 3-43.

[28] Perko, Lawrence. *Differential Equations and Dynamical Systems*. Texts in Applied Mathematics 7. New York, NY: Springer, 2006.

[29] Reece, Jane, Lisa Urry, Michael L. Cain, Steven A. Wasserman, Peter V. Minorsky, and Robert B. Jackson. *Campbell Biology*. 9th ed. New York: Benjamin Cummings, 2010.

[30] Ribeiro, Ruy M., Li Qin, Leslie L. Chavez, Dongfeng Li, Steven G. Self, and Alan S. Perelson. "Estimation of the Initial Viral Growth Rate and Basic Reproductive Number During Acute HIV-1 Infection." *Journal of Virology* 84, no. 12 (June 2010): 6096-102.

[31] Rihan, Fathalla A., and Duaa H. Abdel Rahman. "Delay differential model for tumor-immune dynamics with HIV infection of CD4+ T-cells." *International Journal of Computer Mathematics* 90, no. 3 (2013): 594-614.

[32] Rihan, F. A., D. Abdel Rahman, S. Lakshmanan, and A. S. Alkhajeh. "A Time Delay Model of Tumor-Immune System Interactions: Global Dynamics, Parameter Estimation, Sensitivity Analysis." *Applied Mathematics and Computation*, no. 232 (2014): 606-23.

[33] Roemer, Peter A. "Stochastic Modeling of the Persistence of HIV: Early Population Dynamics." Trident Scholar Project Report. Last modified 2013.

[34] Stafford, Max A., Lawrence Corey, Yunzhen Cao, Eric S. Daar, David D. Ho, and Alan S. Perelson. "Modeling Plasma Virus Concentration during Primary HIV Infection." *Journal of Theoretical Biology*, no. 203 (December 2000): 285-301.

[35] Sharomi, Oluwaseun, and Tufail Malik. "Optimal Control in Epidemiology." *Operations Research*, March 20, 2015.

[36] Smith, Hal. *An Introduction to Delay Differential Equations with Applications in the Life Sciences*. Texts in Applied Mathematics 57. New York, NY: Springer, 2010.

[37] Strogatz, Steven H. *Nonlinear Dynamics and Chaos with Applications to Physics, Biology, Chemistry, and Engineering*. 2nd ed. Philadelphia, PN: Westview Press, 2015.

[38] University of Vermont College of Engineering and Mathematical Sciences. "Routh-Hurwitz Criteria." Math 295: Systems Theory. Accessed December 6, 2014. http://www.cems.uvm.edu/t̃lakoba/08_fall/EE_295/.

[39] Wilson, David P., Matthew G. Law, Andrew E. Grulich, David A. Cooper, and John M. Kaldor. "Relation between HIV Viral Load and Infectiousness: A Model-based Analysis." *The Lancet* 372.9635 (2008): 314-20. Web. 18 Apr. 2016.

[40] Yang, Junyuan, Xiaoyan Wang, and Fengquin Zhang. "A Differential Equation Model of HIV Infection of CD4+ T-cells with Delay." *Discrete Dynamics in Nature and Society* 2008 (October 2008): 1-16.

[41] Zhuang, Kejun, and Hailong Zhu. "Stability and Bifurcation Analysis for an Improved HIV Model with Time Delay and Cure Rate." *Transactions on Mathematics* 12, no. 8 (August 2013): 860-69.